STUDIES ON THE EFFECT OF SELF FIELDS ON THE PROPAGATION OF RELATIVISTIC ELECTRON BEAMS

by

M.K.VIJAYA SANKAR

A THESIS

SUBMITTED FOR THE DEGREE OF

DOCTOR OF PHILOSOPHY

OF THE

GUJARAT UNIVERSITY

JANUARY 1988

PHYSICAL RESEARCH LABORATORY

AHMEDABAD 380 009

INDIA

CERTIFICATE

I hereby declare that the work presented in this thesis is original and has not formed the basis for the research of any degree or diploma by any University or Institution.

Vijay Sankar

M.K. Vijaya Sankar

Certified by:

P.I. John

P.I. John
Professor-in-Charge

Place: Ahmedabad

Date : January, 1988

ACKNOWLEDGEMENTS

I take this opportunity to thank my Ph.D. Supervisor Professor P.I. John for the encouragement and enthusiastic support throughout the period of my doctoral work.He has been always a great source of inspiration.I express my sincere gratitude to him for his affection.

It is a pleasure to acknowledge the help and encouragement given by Dr. A.S. Sharma. I have had many fruitful discussions with him in the context of numerical modelling. I would like to thank Professors P.K. Kaw,A. Sen, A.K. Sundaram, Y.C. Saxena and Dr. Chitra Natarajan for having taken keen interest in my progress.

I would like to thank my senior colleagues Drs. K.K. Jain and Sekhar for their cooperation and the discussions I had with them. I thank the other academic staff of IPR for the encouragement shown.

I express my thankfulness to the PRL authorities for having allowed me to continue my thesis work at PRL after the Plasma Physics group shifted to IPR.I thank the staff of Workshop, Glass Blowing Section, Maintenance, Computer Centre and Library of PRL for their cooperation during the thesis period.

My thanks are due to Messrs Pathak,Lali,Pujara,Bhatt and Shaikh for their technical assistance during the initial stages of my experiment. I thank the staff of Workshop, Library, Drafting Section and the other office

staff of IPR for various helps during the course of my work.

A thank you goes to Sengupta, Usha, Chitra, Chenna, Vinod, Bhaskaran, Sunil, Debi, Asok, Pande, Kanchan, Sarkar, Krishnakumar, Maqbool, Sishir, Banerjee, Sharadini, Jitesh, Janardhan, Mathew, Tripathy, Sarangi, Vijay Kumar and Durga for the friendly atmosphere provided by them. Thanks are due to Subramanian, Puravi, Ajay and Raju for their help in proof-reading.

This thesis work was prepared on DEC-1091 Computer with the help of Word Processing Software developed by Dr. B.R. Sitaram and Mr. Amarendra Narayan. My thanks are due to them. I sincerely thank Mr. V.T. Viswanathan for his assistance in storing the manuscript in the computer files and for editing and processing it neatly.

Finally, I thank all my friends and well wishers who have directly and indirectly helped me in completing this work successfully.

M.K. Vijay Sankar

Ahmedabad

January, 1988

STATEMENT

This thesis reports studies on the effect of self fields on the propagation of rotating relativistic electron beams, formed by injecting a laminar relativistic electron beam through a cusp magnetic field in a neutral gas background. For currents larger than the space charge limiting current, the propagation characteristics will be influenced by the self electric fields until effective charge neutralisation takes place. As the beam current increases, the self magnetic fields of the beam will begin to exert significant influence on the beam dynamics.The present set of experiments and numerical analysis were motivated to gain a better understanding of the deviations from the single particle description due to the effect of self electric and magnetic fields.

A long pulse rotating relativistic electron beam of about 800 nsec duration and peak energy of about 200 KeV, injected through neutral gas (~100m Torr),has been used for the study. The rise time of the beam (~ 500 nsec) is long compared to the charge neutralisation time (< 100 nsec).For the long duration beam,the beam self magnetic fields become significant after the beam is charge neutralised,and hence provides temporal seperation of the phases when the propagation is influenced by self electric and magnetic fields. A variety of diagnostics were used for the measurement of plasma,beam and magnetic field parameters.

The beam propagating through neutral gas has been shown to be stable against the microscopic instabilities like diocotron and filamentation. For a rotating beam, radial equilibrium has been shown to be possible for a value of charge neutralisation factor low compared to that required for a laminar beam.

The net beam potential was seen to be minimum at the central region of the chamber. The charge neutralisation factor has been estimated from a measurement of the beam potential. Charge neutralisation of the beam, which involves expulsion of the plasma electrons, was seen to be influenced by the external axial magnetic field. For magnetic field above the value required for magnetic insulation for the plasma electrons against radial loss, the plasma electrons were seen, in the numerical calculations, to escape to the axial walls. Here, the inductive axial electric field was seen to cause electron avalanche in the region between the position of potential minimum and the far end wall. This was seen to result in a faster charge neutralisation, creating an axial asymmetry in the beam potential structure. The charge netralisation time has been observed to decrease inversely proportional to pressure. Oscillatory decay of the beam potential was observed in certain parameter range.

External cusp magnetic field was seen to be drastically modified by the beam self magnetic fields. The diamagnetism produced by the rotating beam of the postcusp side has been found to result in a shift of the cusp plane towards the post cusp side.

Trajectories were obtained for the beam electrons in the numerical calculation using a model for the self fields based on measurements. Self magnetic fields were seen to reduce the radial extent of the beam.The beam diamagnetic field, radial loss at the cusp etc as given by the single particle description were also obtained in the numerical calculations done with the external fields alone present.

A measurement of the radial loss of beam electrons in the cusp region showed the peak to occur along the shifted cusp plane.Total radial loss in the cusp region was seen to depart from the value given by single particle description for self fields comparable to the external field.Radial loss saturated at external field comparable to single particle critical field for cusp cutoff.

The diamagnetic field produced by the rotating beam in the post cusp region was also observed to be enhanced over the value estimated from single particle description in the range of beam self fields comparable to and larger than the external field. The enhancement is partly explained by the density enhancement caused by the reduction in parallel velocity due to the energy lost by the beam in setting up the self magnetic fields. Addititional enhancement comes from the increase in the ratio of number of axis non encircling to the axis encircling electrons transmitted through the cusp.

CONTENTS

CHAPTER I

INTRODUCTION

Intense relativistic electron beams (REB) have been used for a variety of applications like plasma heating and confinement, microwave generation, collective ion acceleration etc. A typical REB machine consists of a Marx generator which is used to produce high voltage pulses, intermediate storage line (transmission line or Blumlein) for pulse compression to nanosecond time scale and a diode for converting the electrical energy into electron beam energy. The diode typically consists of a cold field emission cathode and a thin foil anode through which the REB emerges. The typical parameters for a REB are energy in the range 100 KeV to 10 MeV, current in the range 1 KA to 1 MA, and pulse length 10 nsec to 1 μsec. For such an intense REB, the strong self electric and magnetic fields will have great influence on the propagation characteristics.

1.1. Propagation Characteristics of REB

For an intense REB injected into a conducting cylindrical cavity of radius r_w, the space charge of the beam front decelerates the electrons following the front. If the current is large enough, this leads to the formation of a large negative potential (virtual cathode) of the same

order as that of the accelerating voltage.This will cause reflection of a part of the beam.This limiting current is called space charge limiting current.Its value is obtained by equating the beam kinetic energy to the electrostatic energy and is given by Bogdankevich & Rukhadze (1971) as

$I_{\perp} = m c^3/e \times (\gamma^{2/3}-1)^{3/2} [1+2\ln(r_w/r_b)]^{-1}$

γ = relativistic mass factor, r_w = wall radius,and r_b = beam radius.

Injection of the beam into a plasma will provide compensation for the space charge of the beam. The transportable beam current is then enhanced by a factor $(1-f_e)^{-1}$, where f_e is the charge neutralisation factor.For f_e = 1,a fully charge neutralised beam,space charge effects are taken care of.But there still exists the effect of the self magnetic fields.The electrons execute cyclotron motion about B_θ,the self field of the beam.If the cyclotron radius of an electron at the edge of the beam is greater than half the beam radius, the beam turns around and a propagating beam will not exist.The critical current for this to happen is called the Alfven-Lawson magnetic stopping current and is given by $I_A = 17\beta\gamma$ KA [Alfven,1939].In addition,other critical currents based on instabilities caused by the beam streaming through a charge and/or current neutralising plasma background, can be defined,that may also effect beam propagation. These critical currents define the existence for a linear propagating REB.

With regard to the stability of a REB for an unneutralised hollow beam, the major instability is of the diocotron type [Buneman et al,1966].This essentially arises from the perturbations in charge density on the inner and outer edges of the beam.This instability is most serious for very hollow beams with radii substantially smaller than the drift tube radius.An essential condition for stability is f_e, the charge neutralisation factor greater than γ^{-2}, where γ is the relativistic mass factor.A beam propagating through a plasma can be subject to macroscopic instabilities such as hose (kink) and sausage instabilities. These arise due to finite plasma conductivity,triggered by transverse perturbations. The kink instability may be stabilised by the external coaxial conducting cylinder, which compresses the B_θ field of the approaching column and thereby keeps the kink away from the wall. Externally applied axial magnetic field can suppress sausage instability due to the outward pressure of trapped axial magnetic field. In addition, the beam can be subject to microscopic instabilities like Buneman,two stream,cyclotron [Mikhailovskii, 1974], filamentation [Wiebel, 1973] etc. Buneman, two stream and cyclotron instabilities are seen for charge neutralised, but current unneutralised beams. The former may occur when plasma density is of the order of the beam density and the latter ones, when plasma density greatly exceeds the beam density.Filamentation instability may occur for current neutralised beams.

1.2. Rotating Relativistic Electron Beams

Rotating relativistic electron beams have been used in the formation of field reversed configuration [Andrews et al, [1971(a)], Roberson et al,(1978),Sethian et al,(1978), Jain & John, (1984)], collective ion acceleration [Christofilos, (1969), Laslett & Sessler, (1969), Reiser, (1971)] etc. The use of a field reversed magnetic field configuration created by axis encircling high energy relativistic electrons/ions for confining and heating a thermonuclear plasma was first proposed by Christofilos (1958). The basic mechanism of generation of the relativistic electron/ion rings involves injection of elctron/ion beam into a slightly focusing magnetic field or through a cusp magnetic field.Experimentally,the simplest method of producing rotating electron/ion beam is by injecting the beam through a cusp magnetic field.First attempt in this regard using relativistic electron beam was done by Friedman (1970). In the case of an unneutralised intense relativistic electron ring formed with a background neutral gas present,electrons just in the potential well of the electron ring ionise the gas.The ions so formed provide additional focusing against electrostatic repulsion for the ring and are accelerated collectively along with the ring. These rings are characterised by their holding power, defined as the maximum electric field strength that holds the ions in the accelerated ring.If this quantity is too small and if the rings are accelerated too fast,the ions

fall out of the ring and get lost.

1.2.1. Relativistic electron beam dynamics in a cusp magnetic field:

Early studies on the dynamics of nonrelativistic charged particles have been done by Schmidt (1962).The study has been extended to relativistic electron beams by Rhee and Destler (1974). The study essentially relates to the dynamics of an electron in the external cusp magnetic field without the self fields included.The external cusp magnetic field can be modelled as $B_{ze} = B_o \tan h(z/\zeta)$, ζ = parameter deciding the cusp width.For $z >> \zeta$, $B_{ze} \simeq B_o$, the uniform field value. For an axisymmetric system,the canonical angular momentum is a constant of motion.i.e. $P_\theta = m_o \gamma r^2 \dot{\theta} - erA_\theta$ = constant. γ is the relativistic mass factor and A_θ is the azimuthal component of the vector potential. For a beam with initial velocity in the axial direction, conservation of canonical angular momentum gives the azimuthal component of the velocity as $v_\theta = - \omega_c (r_o^2 + r^2)/2r$ in the postcusp region. ω_c = beam cyclotron frequency = $e B_o/(m_o \gamma)$, r_o = beam radius at the time of injection.So the cusp magnetic field converts part of the axial velocity into azimuthal and the beam will consist of electrons executing helical orbits after crossing the cusp.If the magnetic field is large requiring a value of v_θ large compared to the initial beam velocity, then the beam will be reflected from the cusp.The critical velocity for beam transmission is given by $v_{crit} = r_o \omega_c$,for $r \simeq r_o$ (central ray). Due to finite Larmor motion of the

electrons in the precusp region, an incoherent off-centering of electron orbits occurs in the postcusp region. The off-centering of electron orbits in the postcusp region is equal to the Larmor radius of the electron in the precusp region. The direction of off-centering is determined by the instantaneous electron position at the cusp transition, and may be quite random in any actual experiment. This gives a maximum width to a beam of electrons, initially annular, of magnitude equal to twice the precusp Larmor radius. A cusp with finite width gives rise to another off-centering of the electron orbits. Here all the electrons passing through the cusp will be off-centered by an amount $\Delta R = \ell/2 \ \mathrm{Sin}^{-1}(r_o \omega_c / v_o)$ in the direction 90^o from the point where they pass through the cusp, giving rise to a coherent off-centering. As a result, a hollow beam of electrons of small energy spread would be expected to have a beam envelope in the postcusp of wavelength

$$\lambda = 2\pi r_o (v_o^2 / r_o^2 \omega_c^2 - 1)^{1/2}$$

1.2.2 Effect of self fields on the propagation and dynamics of rotating relativistic electron beams:

In order to have an intense REB carrying current above the space charge limiting value, it is required to charge neutralise the beam. One of the ways of providing a charge neutralisation background to the beam is by injecting the beam through neutral gas. Here, the gas gets ionised by the beam producing a plasma. The plasma electrons get repelled from the system by the beam self electric fields, making the beam charge neutralised. Here, the charge neutralisation

factor, f_e, is decided by the charge neutralisation processes, which is a function of the beam self fields and the external parameter such as the neutral gas pressure and external magnetic field. The beam inductive fields will cause currents to flow in the plasma channel formed producing beam current neutralisation. The magnetic neutralisation factor (f_m) can be defined as the ratio of the plasma current to the beam current. The values of f_e and f_m decide the basic equilibrium properties for a linear REB propagating through neutral gas. For $f_e = 0, f_m = 0$, the beam channel will blow up radially. For $f_e = \gamma^{-2}, f_m = 0$, the beam is said to be force neutral and straight trajectories should occur. For $f_e = 1, f_m = 0$, the electrons will oscillate radially due to the Lorentz force. For $f_e = 1, f_m = 1$ (charge and current neutralised beam), there are no forces and the beam will again have straight trajectories. The beam self fields thus play a major role in deciding the equilibrium properties.

In the case of a rotating beam, the radial forces due to the Lorentz force, $qv_\theta xB_z$ (radially inward) and the centrifugal force, mv_θ^2/r (radially outward) also influence the equilibrium properties. For an unneutralised rotating relativistic electron beam, with increase in the beam current, the equilibrium beam radius shifts towards the radial wall. It has been shown by Striffler and Kim (1978) that in this case the beam azimuthal velocity increases and the beam axial velocity decreases. They have shown the existence of a critical magnetic field, below the single

particle cusp cutoff, above which the electrons get reflected back.This happens when the energy in the electron layer in the form of axial velocity is insufficient to overcome the increase in the electrical potential energy as the beam current increases. A proper understanding of the role of self electric fields on the beam equilibrium properties require a thorough investigation of the charge neutralisation phase of the beam.

The self axial and azimuthal magnetic fields produced by the intense rotating relativistic electron beam will have strong influence on the beam dynamics.The electrons that are injected into the system after the self fields have peaked, will see a cusp magnetic field modified by the strong self fields.The single particle description will now be quite inadequate to explain the cusp transmission, conversion of axial velocity to azimuthal etc.

1.3. Summary of Theoretical,Numerical and Experimental Work

The effect of self fields on the propagation of REB trough neutral gas in the presence of an external cusp magnetic field can be classified into two phases -

1. The charge neutralisation phase,involving the effect of self electric fields and

2. Phase involving the effect of self magnetic fields on REB dynamics in a cusp magnetic field.

In the next two subsections, the existing studies related to these two aspects are summarised.

1.3.1. Charge neutralisation phase:

In the earlier investigations on the propagation of a REB through neutral gas by Poukey and Rostoker [1971], Swain [1972], and McArthur and Poukey [1973], the major ionisation mechanism for the neutral gas was considered to be by collisions with electrons and the secondary electrons. In the numerical simulation of Poukey and Rostoker, slowing down of the beam front was observed. The beam was found to propagate faster approaching the injection velocity, with increase in the ionisation cross section corresponding to better space charge neutralisation. The fields generated by the beam and the axially dependent background plasma conductivity were calculated by Swain in a self consistent manner. In the work of McArthur and Poukey, the primary electron cross section was taken to be enhanced by a factor $\simeq 3$ (measured enhancement factor for Nitrogen gas) due to further gas ionisation by the secondary electrons. The radial electric field becomes smaller than the inductive E_z field only after the charge neutralisation time. So the return current caused by the inductive E_z field was considered to be initiated after the charge neutralisation time. For higher pressures (> 20 Torr of Nitrogen), the cross section for recombination reaction was found to be significant.

The charge neutralisation processes, for an intense REB propagating in a low pressure (~ 0.1 Torr) neutral gas, was

examined in detail by Olson (1975).The processes examined include electron impact ionisation,electron avalanching,ion impact ionisation,ion avalanching,charge exchange,precursor ionisation, secondary electron esape,recombination,diffusion and attachment. Electron impact ionisation is given by

$$\frac{\partial n_i^s(t)}{\partial t} = \frac{n_b(t)}{\tau_e} \quad ; \quad \frac{\partial n_e^s(t)}{\partial t} = \frac{n_b(t)}{\tau_e} - \frac{n_e^s(t)}{t_s},$$

$n_{i\,e}^{s}$ = secondary plasma ion (electron) density, n_b = beam density, τ_e = collisional ionisation time ($\simeq 5/p$(Torr) nsec for Hydrogen, p is the neutral gas pressure.) The plasma electrons so formed get repelled to the walls guided by the self fields, t_s is the secondary electron escape time.For $E/p \sim 10^2$-10^3 V cm^{-1}Torr^{-1} for Hydrogen (E = electric field), the mean free path for collisional ionisation becomes less compared to the system length.Here the secondary electrons will undergo further collisional ionisation resulting in avalanche. The additional source for ions and electrons is given by $n_e^s(t)/t_e$,where t_e = electron avalanche time.

The net electron charge density associated with an unneutralised intense beam will effectively create an electrostatic potential well.The well depth may be > T/e,T is the injected electron energy and e = magnitude of electron charge. Any ions created by electron impact ionisation will be accelerated towards the centre of the well and proceed to oscillate about the well centre.When an ion has energy > 50 KeV,it will ionise the background gas. New secondary ions formed will likewise be accelerated and produce further ionisation resulting in the avalanche.The

rate of production of ions and electrons by ion avalanche is given by $n_i^s(t)/t_i$, t_i is an effective avalanche time. If the well electric field is sufficiently high, so that t_a, the time it takes an ion to be accelerated to 50 KeV is small compared to t_i, then $t_i \simeq 0.33/p$ (Torr) nsec for Hydrogen gas.

For accelerated ion energy < 50 KeV, charge exchange reaction takes place. An important consequence of charge exchange is that it can present a cut off barrier for ion acceleration, and hence effectively stop ion-avalanche process. Roughly, cut off will occur if $t_a > \tau_x$, the charge exchange time.

Additional ionisation can come from precursor effects, prominent being from beam tip precursor bunch. This happens for high current REB with current rise time comparable to the charge neutralisation time. The precursor bunch is the initial electrons that propagate before the beam current exceeds the space charge limiting current. This bunch of electrons produces electron impact ionisation, producing an initial plasma of typical density ~ 1% of n_b. The ions so formed may be sufficient to initiate ion-avalanche when the beam front arrives with its attendant, large E field.

Other factors that can effect charge neutralisation processes are recombination and attachment. But for the secondary electrons of relatively high energy, these may be neglected.

The radial expansion of REB propataging through neutral gas has been investigated by Briggs et al (1976). In the

limit that expansion is slow compared with the time scale of electron betatron motions, the beam is predicted to evolve via scattering to the Bennet profile given by, $J_b(r) = I_b/(\pi a^2).(1 + r^2/a^2)^{-2}$. I_b and J_b are beam current and beam current density respectively, a is the beam radius. The scattering continually adds energy to the transverse motion, but it is balanced by the work done in expanding against the self fields. Hence scattering only randomises transverse velocities without increasing the temperature. The beam radius, a, increase in time, while the current profile maintains the Bennet profile.

Numerical simulation of the plasma channel formed and the REB dynamics was done by Girgorev et al (1979,1984).The radius of the plasma channel was found to be much larger than the beam radius and the difference increases with decreasing pressure and increasing tube radius.The current induced by the beam in the plasma is carried primarily by plasma electron in the beam region.The beam was seen to be cut off at the trailing edge at pressures above 5 Torr, resulting in a shortening of the beam pulse and a reduction in the peak value of the beam density at the exit of the drift tube. The beam cut off was considered to be arising due to beam loss because of the gradient in B_θ during the beam transit to the exit of the drift tube.The plasma conductivity was seen to decrease with pressure.So for pressure less than 5 Torr, higher current neutralisation near the entrance of the drift tube was considered to weaken the axial B_θ gradient,and so does not result in beam

loss at the trailing edge.

Investigation regarding the stability of a partially neutralised hollow REB has been done by Kapetanakos et al (1973), Chen (1984) etc.Thin hollow REB propagating through neutral gas has been shown to be subject to diocotron instability before the charge neutralisation factor becomes greater than γ^{-2}. Kapetanakos et al have shown the stabilising effect of bringing the conducting boundary closer to the beam boundary.An ion background within the beam has been shown to aid diocotron instability by Chen.In the presence of an ion background,the $\ell = 1$ mode becomes unstable causing a sideways displacement of the whole beam in the cylindrical geometry thereby breaking the axial symmetry. The collective acceleration of heavy ions in the centre of the annular beam have been mentioned to enhance the diocotron instability.

Most of the experiments reported so far relate to the study of plasma production and the propagation characteristics of REB.These are summarised below.

Graybill (1971) has investigated the propagation characteristics of an REB through neutral gas.The net beam current decreases with the neutral gas breakdown time as the pressure increases and then increases with decreasing decay time above 1 Torr.The decrease of the net current is due the reverse plasma current driven by the inductive electric field. As the pressure is increased above a few Torr, the plasma conductivity decreases due to the short mean free path available to the secondary electrons.

In the experiments of Andrews et al [1971(b)], axial periodicities in the light intensity were observed for beams propagating in gases. These periodicities were found to be correlated with periodicities in the propagation of beam front, in the microwave activity, and in the net beam current. The wavelength of the periodicity was found to be inversely proportional to the gas pressure p. At low pressures (~ 150m Torr of air), the beam head after travelling almost with the velocity of a single electron slows down considerably and proceeds again only after a delay time which appears to be roughly proportional to $(1/p)^2$. Proper explanation of these instabilities is not given and are considered to be caused by some instability in the ionisation neutralisation of the beam in the gas.

In the experiments of Miller et al (1972), the study has been made for REB injected into thirteen different gases. The REB transmission was found to scale in pressure from gas to gas inversely with the ionisation cross sections of the gases. At low pressures, pronounced beam front erosion was seen leading to steeper beam rise time, owing to the slow build up of radial force neutralisation of the electrons. For experiments done in high pressure gases (few Torr of air) by Miller and Gerado (1972), some instability was seen to develop attenuating the beam greatly at pressures which vary inversely with the gas ionisation cross section. A mechanism has been proposed for this. Radial gas breakdown occurs prior to the time at which the beam front reaches the end of the tube. This breakdown process

occurs in a nonsymmetric pattern, forming filamentary discharges, and drives the trailing primary beams into the walls by the nonsymmetric forces.

REB propagation through gases at pressures in the range of 10 Torr to 1.5 atm was studied by Rudakov et al (1972) and Kingsep et al (1973). The contribution to the plasma production has been considered to be from collisional ionisation due to the electron and the secondary plasma electrons. The rate of ionisation by the secondary plasma electrons, accelerated by the beam self electric field, was found to decrease with increase in pressure. Increase in pressure above 300 Torr was seen to cause the beam to stop over a distance of 10 to 20 cm.

Genuario et al (1974) investigated the charge and current neutralisation phenomena for a very short pulse (5 nsec) beam. The ionisation mechanism has been considered to be by primary beam impact ionisation. An enhanced electron neutral collision cross section was used to account for the further ionisation by the energetic secondary electrons. The transmitted beam current was found to increase with pressure. With increase in pressure, charge neutralisation is approached. Maximum beam transmission (0. 7) was seen at a pressure of about 250 mTorr of air. For pressures 150 mTorr to 300 mTorr, oscillations of period $\simeq$ 2 nsec, believed to be Langmuir oscillations, were seen. Above 400 mTorr, current neutralisation was seen to reduce the net transmitted current.

An interesting phenomenon of beam current amplification

was seen in the experiments of Wachtel and Safran (1974).At low pressures (0.1 Torr of nitrogen),the peak net current was seen to exceed the beam current by as much as a factor of 2. A smooth transition to condition of magnetic neuralisation takes place as the pressure is increased.The width of the amplified current spike increased with decrease in pressure and was roughly consistent with the time required to establish space charge neutralisation.The current amplification was attributed to the motion of secondary electrons, trapped by the beam B_θ field,parallel to the direction of propagation of the beam.

An investigation of the production mechanism and nature of plasmas produced by a short pulsed (3nsec) REB injected into neutral gases without an external field was made by Kouichi Ono (1979).For beam rise time less than the space charge neutralisation time, the plasma current was seen to flow parallel to the beam current,similar to the observation of Wachtel and Safran (1974).The pressure at which the transmitted beam current and current density reach a maximum was found to shift to lower values for increasing ionisation cross section of the gas by the beam. The current due to the expelled plasma electrons was seen to decrease with increase in pressure,and the pressure at which the plasma electron current peaks was also found to decrease with increase in the ionisation cross section.

The experimental study of Arutyunyan et al (1983) was concerned with the injection of REB through gases in the pressure range of 0.01 to 750 Torr.The quantities measured

were the beam potential, electron current and REB energy loss. The peak beam potential was found to decrease with increase in pressure upto about 1 Torr.Above 1 Torr,it was found to increase with pressure.Also the beam potential was seen to oscillate during the space charge neutralisation time. The measured energy loss of REB at low pressures was found to be more than that predicted without the collective effects included. At higher pressures,the measured loss was less than that predicted.Proper explanation to these is not given. The discrepancy at higher pressures has been considered to be due to electron scattering and decrease in effective path length of REB through gas.The discrepancy at lower pressures has been thought of being due to collective mechanism stimulated by the plasma return current.For low pressures (< 0.1 Torr), possibility of some additional ionisation mechanism such as ionisation by the return current, beam space charge field, high frequency field excited in a plasma or by ions has been mentioned.But direct evidence for these have not been observed.

In the experimental study by Smith et al (1986),the REB propagation through Helium,Nitrogen and Argon gases in the pressure regime 10 mTorr to 320 mTorr was investigated.The transport efficiency was seen to increase with pressure. Optimum beam current transport was seen at about 80 mTorr for Nitrogen and Argon. For pressures below 40 mTorr for Nitrogen and Argon, beam propagation was not seen to exist during the beam rise time and has been attributed to low initial charge neutralisation of the beam. The charge

neutralisation factor, calculated using a simple model, was seen to be greater at higher pressure and for gases with higher ionisation cross section.

The experiments reported so far relate to the laminar beam propagation. The effect of the extent of charge neutralisation on beam propagation was also seen for rotating beams produced by injecting laminar beam through a cusp magnetic field [Kapetanakos (1974), Roberson et al (1978)]. In the experiments of Kapetanakos, at a pressure of 0.035 Torr, the current pulse was seen to get distorted and the distortion decreases with increase in pressure. Space charge accumulation in the cusp region, at low pressures, has been considered to influence the beam propagation. The peak beam current and energy were seen to increase with pressure reaching a maximum at about 0.2 Torr, and decrease thereafter with increase in pressure. The maximum transmitted energy was about 88%. In the experiments of Roberson et al, the diamagnetic field produced by the rotating beam was seen to decrease with pressure and was related to low cusp transmission efficiency at low pressures.

1.3.2. Effect of self magnetic fields on REB dynamics in a cusp magnetic field:

The nonadiabatic trajectories of charged particles in cusp field allow an efficient conversion of longitudinal particle velocity to rotational velocity, and make possible the use of such field configurations for the generation of strong E layers and electron rings with properties attractive for ion heating and acceleration. Proper knowledge of the beam dynamics in a cusp field is thus essential.

Calculation regarding equilibrium radius for a non-neutral E layer has been done by Davidson and Mahajan (1974). Self axial magnetic field acts as a focusing field which tends to decrease the radial width of the E layer. The radial self electric field acts as a defocusing field which tends to increase the radial thickness of the E layer.

For rotating hollow beams, the force $ev_\theta xB_r$ was seen to enhance the space charge limiting current [Poukey and Freeman (1974)].

Macroscopic equilibrium properties of hollow REB have been investigated by Davidson and Lebedev (1975). Two classes of rotational equilibria have been shown to satisfy the equilibrium force equation. Slow rotational equilibrium corresponds to zero rotation at the inner edge of the beam and the faster one corresponds to an angular rotational frequency at the inner edge greater than zero. For $(1-f_m)^2 > (1-f_e)$ and $\frac{d\omega}{dr} < 0$, the slow one gives

pramagnetism within the beam, where ω = beam angular frequency.

Numerical single particle trajectory calculations using realistic cusp width to Larmor radius ratios has been done by Bora and John (1981). Phase spreading resulting from either an angular divergence or from anode foil scattering has been included in the calculations.The final azimuthal velocity attained by the beam after passing through the cusp region was found to be strongly dependent on the initial phase of the electrons.The final azimuthal velocity was also seen to increase as the cusp width decreases.The coherent off-centering of the electrons was seen to decrease in sharp cusps.

The first experimental study of the dynamics of charged particles in a cusp field has been made by Sinnis and Schmidt (1963). The study was done using a low current beam of 2 KeV electrons. Their experiments basically confirmed the single electron theory regarding the conversion of axial velocity to azimuthal by the cusp,the critical field for cusp cutoff,etc.

The transmission efficiency for a relativistic electron beam through the cusp with a background pressure of about 2×10^{-4} Torr, has been investigated by Friedman (1970).The energy of the beam transmitted through the cusp begins to drop somewhat exponentially at about 5 Kgauss,corresponding to the critical field for cusp cutoff.The efficiency of the number of electrons transmitted through the cusp was found to be low. The reason for this was given as due to (1) the

ripples in the beam created in the transition region, and (2) a possible presence of space charge potentials in the vicinity of the cusp.

Kapetanakos (1974) investigated the propagation of REB through a cusp magnetic field with a background pressure of 50 mTorr to 1000 mTorr. The peak beam current and energy increase with pressure reaching a maximum value of about 88% at a pressure of 0.2 Torr and decrease thereafter with increase in pressure. The observed critical field for cusp cut off was less than the theoretical value. The reason has been given to be due to the non zero azimuthal velocity component of the injected beam electrons. But it should be noted here that reduction in the value of critical field will occur only if the initial azimuthal velocity has the same direction as that expected for the postcusp region. For initial azimuthal velocity in the opposite direction, the critical field will increase. A reduction in the beam current pulse rise time and width was observed in the postcusp region. This was attributed to low energy velocity electrons getting reflected from the cusp.

In the experiments of Destler et al [1975(a)], plots of maximum beam width in the postcusp and the self $B_z(\Delta B_z)$, as a function of the applied magnetic field(B_o) were found to agree with the theoretical plot only for the case where $\Delta B_z/B_o$ was small. Experiments of Destler et al [1975(b)] done for the electron beam of the Maryland ERA experiment showed the dependence of $\Delta B_z/B_o$ vs. beam current to be different from the linear behaviour predicted

by theory. At higher currents, $\Delta B_z/B_o$ was seen to increase with beam current at a rate less than the linear rate.The radial and axial compression of a hollow electron beam using an asymmetric magnetic cusp was examined in the experiments of Destler and Rhee (1977).The electron orbits will be tangential to the circles of radii $r_f = r_o/k$ and r_o and enclosed within the circles. Here r_o is the cathode radius and k is the ratio of magnetic field in the postcusp to that in the precusp, with $k > 1$.Measurement of r_f,the radial point where the beam density is peaked,as a function of k showed good agreement with experiment and theory.

In the experiments done by Fleischmann and collaborators [Andrews et al (1971),Tuszewski et al (1979)], an electron beam was injected almost normal to a slightly focusing magnetic field (magnetic mirror) and the electron ring so formed was trapped between the magnetic mirrors.The self axial magnetic field produced by the electron ring was seen to produce field reversed configuration. A field reversal factor (beam self field/external field) less than 4 lasting for about 1 msec has been achieved.

The experiments of Sethian et al (1978) were on the generation of field reversed configuration using a half cusp field, with zero external magnetic field in the postcusp region. The net beam current was only 68% of the diode current. The cause of reduction has been given to be due to either current neutralisation and/or cusp loss.The beam self field was seen to increase by a factor of 2 as the end wall was approached.This being attributed to the

rotating current piling up against the end screen.

Roberson et al (1978) studied the variation of the beam axial self magnetic field as a function of the external field. The observed self field was more than a factor of 2 greater than the calculated value. This was explained as resulting from a breaking of the beam and an increase in the azimuthal current due to a pile up of the beam after the cusp.

In the numerical simulation done by Golden et al (1981) for the NRL ion ring experiment, showed drastic distortion of the cusp by the self fields. The self fields were seen to produce a somersaulting, i.e. ions at the head of the beam were decelerated and ions at the tail accelerated, resulting in a spreading of the distribution of the ion energy. The experimental measurements of the diamagnetic field produced by the ion ring were seen to increase with decrease in the radial electric field. This has been attributed to the reduction in the radius of the azimuthal current distribution as the ions move inward with the azimuthal current remaining the same.

1.4. Scope of the Thesis

From the experiments reported so far, it can be seen that the charge neutralisation processes and the dynamics for a REB, under the influence of its own self fields, with the REB injected through a cusp magnetic field have not been studied in detail.

All the earlier experiments were done using short pulse beams, where the charge neutralisation time is comparable to the beam rise time.Here the beam is under the influence of strong self electric and magnetic fields, both occuring together. Use of a long pulse REB with the beam rise time much longer than the charge neutralisation time,provides temporal seperation of the phases when the propagation is influenced by the self electric and magnetic fields.The present study involves a long pulse rotating relativistic electron beam. The study can be classified into two phases. The first one involves the effect of self electric fields - charge neutralisation phase,and the second one involves the effect of self magnetic fields on beam dynamics.

Even though detailed theoretical studies for the charge neutralisation processes exist, detailed experimental investigation has not been carried out.The importance of sufficient charge neutralisation (a neutral gas pressure of about a few hundred mTorr) in order to have better propagating characteristics for a beam injected through neutral gas, has been seen in the previous studies.The present study aims to estimate the charge neutralisation factor as a function of the various beam and external parameters from a direct measurement of the beam potential. Specifically the study is related to rotating beams. Estimation of the charge neutralisation factor would thus enable to identify the charge neutralisation processes taking place for a rotating relativistic electron beam.

Theoretical and numerical single particle calculations

exist for REB dynamics in a cusp magnetic field.But for an intense rotating REB,self magnetic fields are comparable to the external field as in the context of field reversed configuration and compact torus.In the experiments reported so far, it can be seen that proper attention has not been paid to the REB dynamics when the self magnetic fields are comparable to the external field.The present study aims at measuring the extent of modification of the external cusp by the strong self magnetic fields and its influence on beam transmission.

The experimental device, its operating characteristics and the various diagnostics elements used in the course of the investigation are described in Chapter II.

Results on the study of charge neutralisation processes for a rotating relativistic electron beam and the discussion are presented in Chapter III. The effect of external magnetic field and background gas pressure on the charge neutralisation processes are also a part of the study.

In Chapter IV,the effect of self magnetic fields on the dynamics of a rotating REB is studied and discussed. Observation regarding the modification of the external cusp is presented. This chapter also includes the results of numerical single particle trajectory calculations done using a model for the self fields based on measurements.

The main results of the thesis work are briefly summarised in the last chapter.

CHAPTER II

EXPERIMENTAL DEVICE AND DIAGNOSTICS

An experimental system used for short pulse relativistic electron beam experiments has been suitably modified for studying the effect of self fields on the propagation of long pulse rotating relativistic electron beam. A schematic of the experimental device is given in figure 2.1. It consists of a vacuum chamber, system of magnetic field coils, and a relativistic electron beam generator. A number of diagnostics have been used at various places for measuring the desired experimental parameters. The details of the experimental device and diagnostics are described in the following sections.

2.1. Vacuum Chamber

The cylindrical chamber is 2.3 meter long and of 30 cm diameter, made of stainless steel of 3 mm wall thickness. The magnetic diffusion time through the walls corresponds to about 50 μsec. This is fast enough for the penetration of external magnetic field, but long enough compared to the beam and plasma duration, so that it acts as a flux conserving conducting shell. The chamber is pumped by rotary pumps and neutral Hydrogen gas is fed in through a needle valve to have a steady pressure of ~ 100 mTorr. Nineteen ports are available along the length of the chamber for diagnostics purposes.

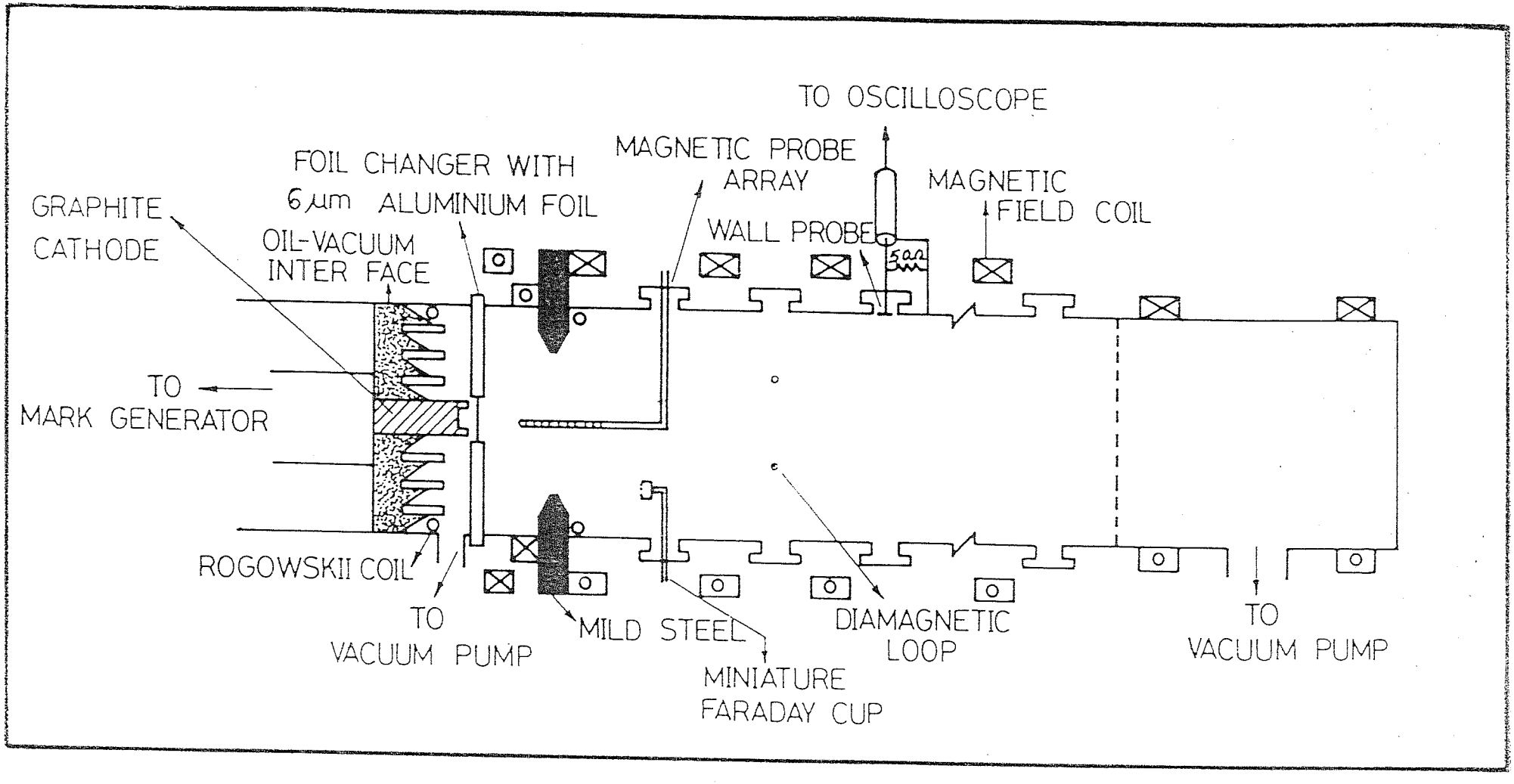

2.1 Experimental system.

2.2 Magnetic Field Configuration

The existing system of magnetic field coils has been suitably arranged to give a cusp magnetic field with the field uniform on either side of the cusp (figure 2.2).The field coils are of 40 cm inner diameter placed around the s.s. chamber and are energised by a 8.0 K Joule capacitor bank. The current pulse passed through the coils has a quarter period of 2 msec producing a uniform field of value about 1.35 gauss/Amp. The nonadiabatic cusp field is produced by reversing the direction of the current in the first 3 coils of the magnetic field assembly.A 25 mm thick mild steel annular plate of 14 cm inner diameter is introduced between the two sets of coils,carrying currents in the opposite directions in order to make the cusp strongly non-adiabatic.

2.3 Relativistic Electron Beam Generator

The basic principle for a long pulse relativistic electron beam generator is illustrated in figure 2.3.It consists of a Marx generator for producing a high voltage pulse of about 1 μsec duration and a field emission diode for producing the long pulse beam.The details of the major constituents of the beam generator are described below.

2.3.1. Marx generator

The basic principle involved is the transient series

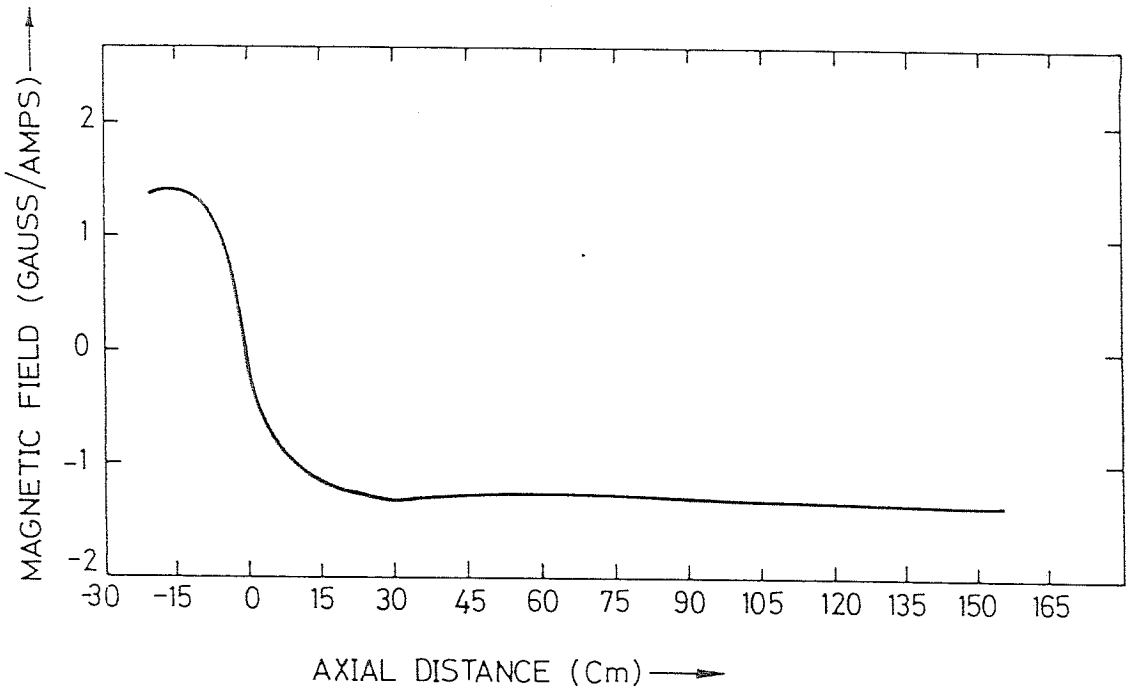

2.2 Magnetic field configuration

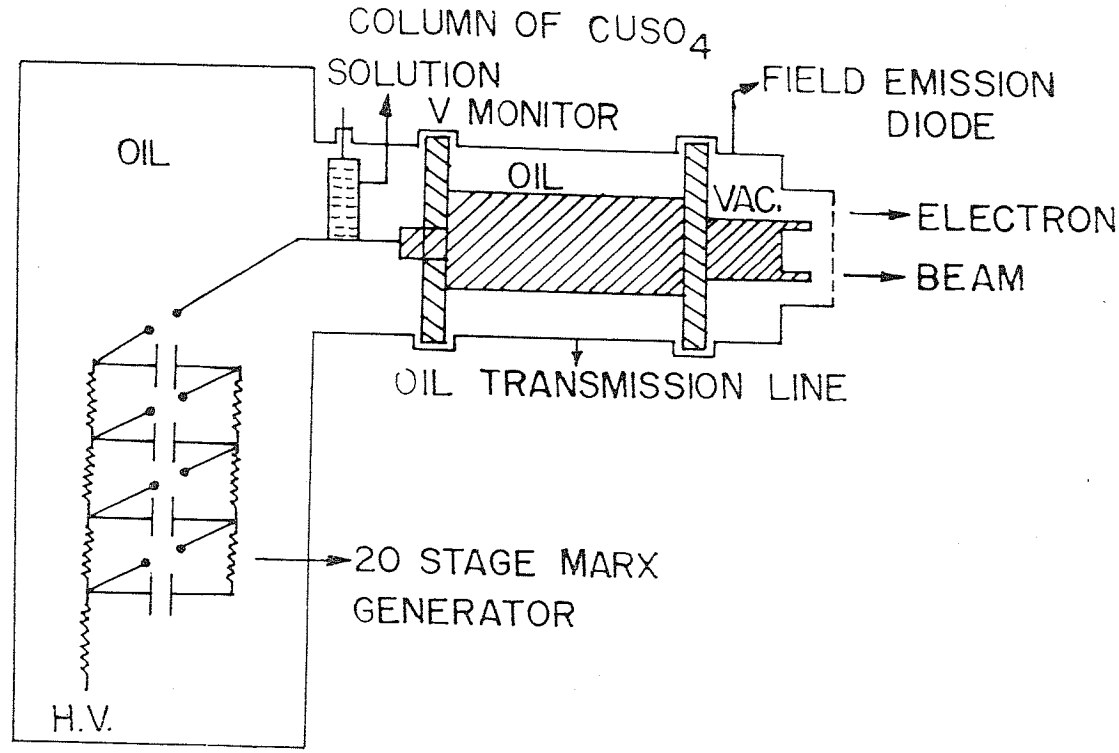

2.3 Functional diagram of the Marx generator.

connection of a number of electrostatic energy storage modules. The capacitors are charged in parallel via the charging resistor in the high voltage leg of the circuit, while the other side is connected to the ground via the ground leg resistor chain.The Marx generator is erected by triggering a series of air spark gaps.When this happens,the low impedence spark gaps effectively connect the capacitors in series.The net voltage achieved with the Marx circuit is equal to the charging voltage per stage times the number of stages.

The Marx generator modified for the long pulse operational mode consists of twenty 0.4 μF, 50 KV capacitors and two columns of copper sulphate solution with 40 Kilo Ohm resistance each used as charging resistors.A variable 0-50 KV high voltage power supply is used for charging the capacitors in the Marx generator.Twenty spark gap switches are housed inside a common pressure sealed 1.5 meter long chamber. Each spark gap is made of brass electrodes having a diameter equal to 20 mm,while the electrode gap is about 8 mm.A trigger generator in the form of a sliding spark source is used to erect the Marx Generator.

The Marx generator is connected directly on to a field emission diode via an oil transmission line.It consists of a central cylindrical conductor of radius 2.5 cm and an outer conductor of 15 cm radius. Oil was used as the dielectric because of its higher voltage holding characteristics.

Marx circuit analysis for the long pulse mode:

Figure 2.4 (a) gives the equivalent circuit for the long pulse generator.The capacitance and inductance of the Marx are represented by C_M and L_M respectively and those of the transmission line are represented by C_T and L_T.Z_L = load impedance and C_L = load capacitance.

The Marx voltage rises in a few nsec,decided by the switching time. Also a stable diode operation commences a few nsec after the application of the high voltage [Parker et al, 1974]. Hence for $0 < t < t_1$,t_1 = rise time,the load can be taken as open. Effective stray capacitance, $C_S = C_T + C_L \simeq C_T << C_M$. So here the Marx acts as a constant voltage source of voltage V_M (final Marx output voltage). Figure 2.4 (b) gives the reduced equivalent circuit.

The output voltage V_S is given by

$$V_S = V_M \, \mathrm{Sin}(\omega t), \quad \omega = 1/(L_T \, C_S)^{1/2}.$$

The effective rise time of the Marx output voltage will be decided by the above value or the Marx erection time, whichever is longer.

After $t = t_1$,the diode impedance becomes finite and the capacitors start getting discharged. Here the current flowing through the capacitors and inductances of the Marx bank has to be considered.The reduced equivalent circuit is shown in figure 2.4 (c).

Here two general situations arise -

(1) $R_L > 2 Z_M$,$Z_M = (L_M/C_M)^{1/2}$,The Marx transient impedance

The load voltage is given by

$$V_L = V_M R_L \exp[-R_L t/(2L_M)] \, \mathrm{Sin\ h}(\omega_1 t)/Z_1$$

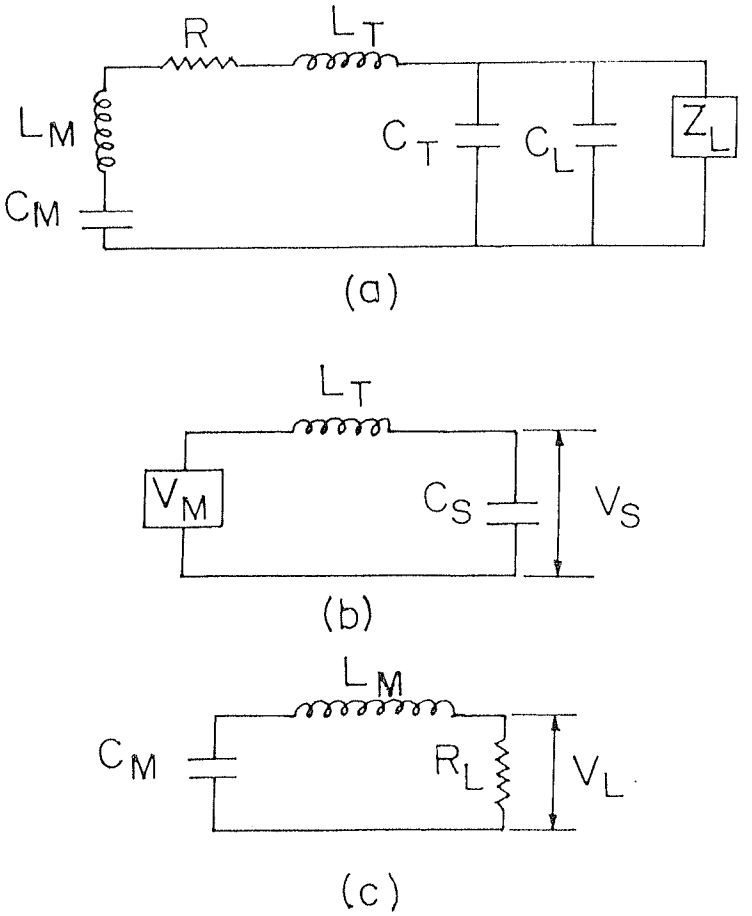

2.4 Equivalent circuit of the Marx generator.

where $\omega_1^2 = (R_L^2/4L_M^2 - 1/L_M C_M)$ & $Z_1 = L_M \omega_1$

(2) $R_L < 2Z_M$

Here, $V_L = V_M R_L \exp[-R_L t/(2L_M)] \sin(\omega_2 t)/Z_2$

where $\omega_2^2 = 1/L_M C_M - R_L^2/4L_M^2$,& $Z_2 = L_M \omega_2$

For impedance matching, one goes for $R_L \simeq Z_M$ and so the output will be given by (2).

The Marx inductance was determined by discharging it into a resistive load consisting of a column of Copper Sulphate solution. The current through the load was measured using a fast Pearson current transformer. As the resistance of the Copper Sulphate solution is difficult to be measured exactly, it was taken as a parameter to be fitted besides the inductance parameter. A best fit for the current profile was obtained with $R \simeq 36.3\ \Omega$ and $L \simeq 7.55\ \mu$Henry. The measurements and the fitted curves are shown in figure 2.5.

The effective capacitance of the erected Marx $= 0.02\ \mu$Farad. So the Marx transient impedance, $Z_M \simeq 19.4\ \Omega$. The inductance of the transmission line $\simeq 0.013\ \mu$Henry and the capacitance $\simeq 0.56$ n Farad. Inclusion of the inductnace of the strips connecting the Marx output to the transmission line, gives an effective value of $\simeq 0.62\ \mu$Henry to L_T in the equivalent circuit. This corresponds to a diode voltage rise time $\simeq 18$ nsec. The period of the diode current will be given by

$$\tau = 2\pi/(1/L_M C_M - R_L^2/4L_M^2)^{1/2}$$

For the matched condition of $R_L = \sqrt{L_M/C_M}$, the half period $\simeq 1.4\ \mu$sec.

2.3.2. Oil vacuum interface:

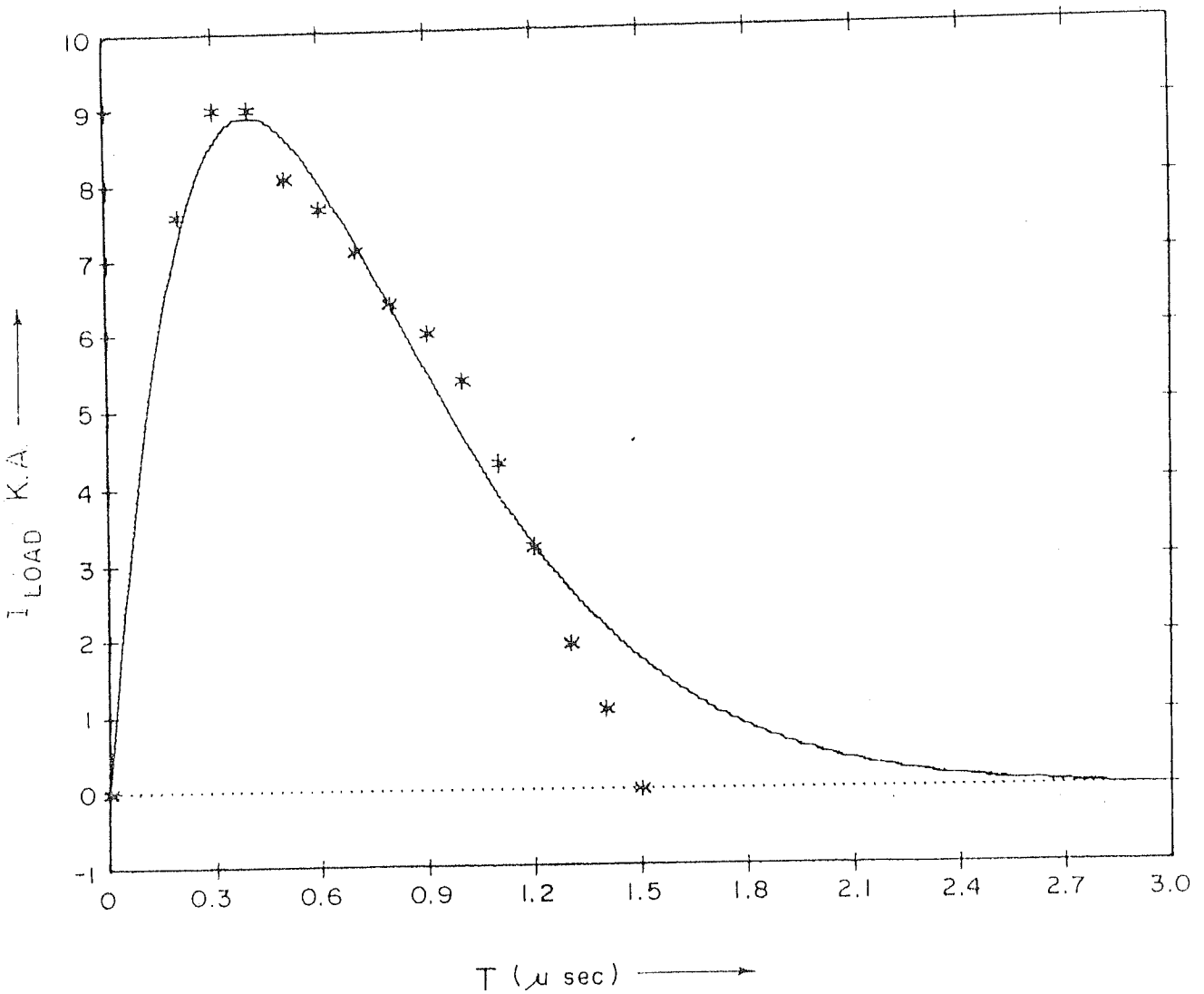

2.5 Marx discharged into a resistive load.

This is the insulation separating the oil side of the Marx and transmission line from the vacuum side of the diode. It has to be suitably designed to avoid surface voltage breakdown. The physics of the breakdown is illustrated using figure 2.6.For the configuration shown in figure 2.6(a), any free electron present between the high voltage electrodes gets accelerated to the electrode of positive polarity undergoing minimum collision with the insulator surface.But in the case of configuration shown in figure 2.6(b), the initial free electron has to slide along the insulator surface to reach the electrode of positive polarity. This results in more electrons liberated from the insulator surface,each of them colliding with the insulator surface atoms and thereby enhancing the number of free electrons. This eventually leads to an avalanche leading to surface voltage breakdown.In order to have better breakdown characteristics, the optimum angle between the normal to the dielectric surface and the electric field on the vacuum side has to be 45°.In addition to the angle,the breakdown electric field E_F,depends on the insulator length,ℓ and the pulse duration τ as, $E_F \propto \ell^{-0.5} \tau^{-1/6}$ [Suzuki and Kato, 1984]. The above factors have to be considered while going for the design of an oil vacuum interface.In the commonly used diode assemblies,one makes use of either an interface with axial gradings or a single radial insulator [Nation, 1979]. The first type would give higher diode inductance and also is not suitable for the existing diode dimensions used for produing a short pulse REB [Jain and John,1981].A

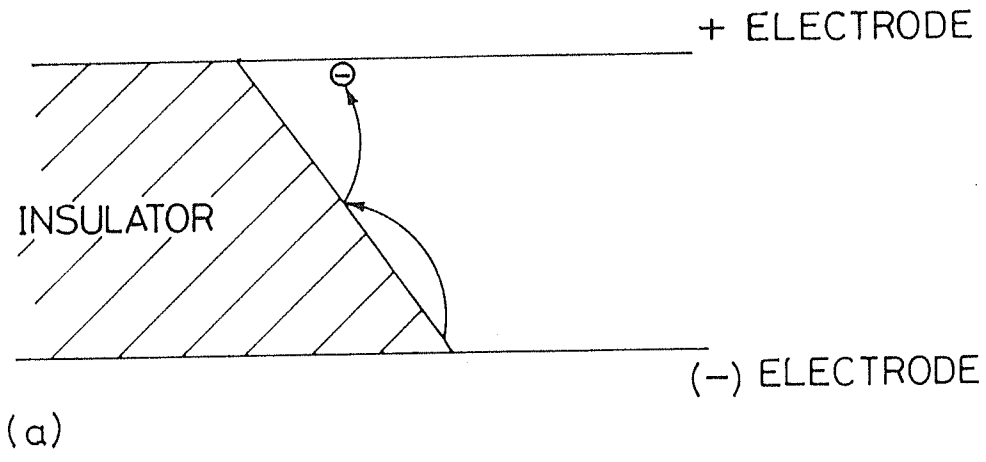
+ ELECTRODE
INSULATOR
(−) ELECTRODE

(a)

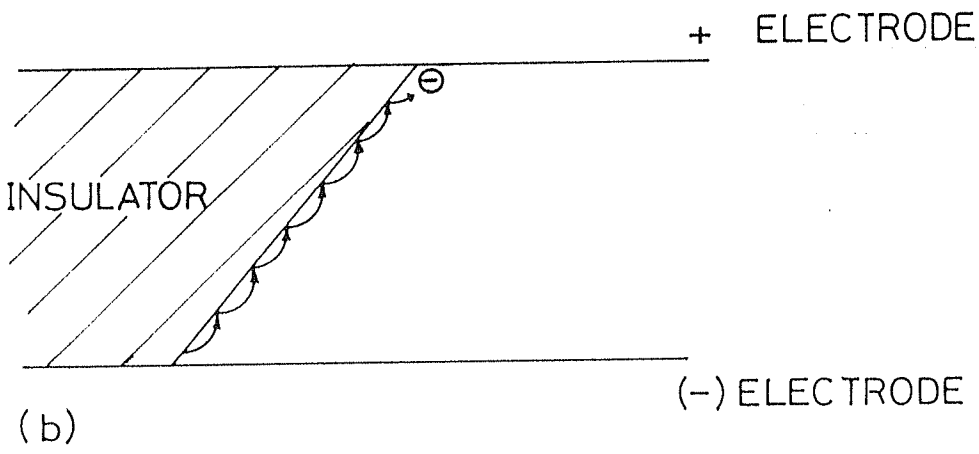
+ ELECTRODE
INSULATOR
(−) ELECTRODE

(b)

single radial insulator was found quite inadequate for the long pulse mode. So we have gone for one with radial gradings [Suzuki and Kato, 1984]. From the reported data, $E_F \simeq 17 \times 10^4 \, \ell^{-0.5} \, \tau^{-1/6}$ volt m^{-1}. For our diode geometry (inner radius = 3.5 cm, outer radius = 8.7 cm), the maximum electric field for the peak Marx operating voltage of 500 KV gives $\simeq$ 160 KV cm^{-1}. A choice of ℓ = 1 cm for the spacing between the gradings would roughly give a safety factor of about 2 (ratio of breakdown field to the peak operating field). The design is shown in figure 2.7.

During the operation of the field emission diode, the Aluminium foil (anode) fragments were found to be getting deposited at the interface. This was resulting in a surface flashover after 2 or 3 shots. This problem was solved by using a perspex plate between the interface and the anode to stop the flow of the anode fragments. The position of the plate is shown in figure 2.7.

2.3.3 Field emission diode:

This is the region where the electrical energy is finally converted to particle energy. The diode consists of an annular graphite cathode of average radius = 2 cm and a radial width of about 3 mm, and a 6 μm Aluminium foil anode. The foil gets punctured after each shot of REB. A gear operated foil changer was used for changing the foil after each shot without having to break the vacuum [Jain and John, 1981]. The existing foil changer was modified so as to provide isolation between the experimental region ($\sim$ 100 mTorr) and the vacuum side ($\sim 10^{-4}$ Torr) of the diode

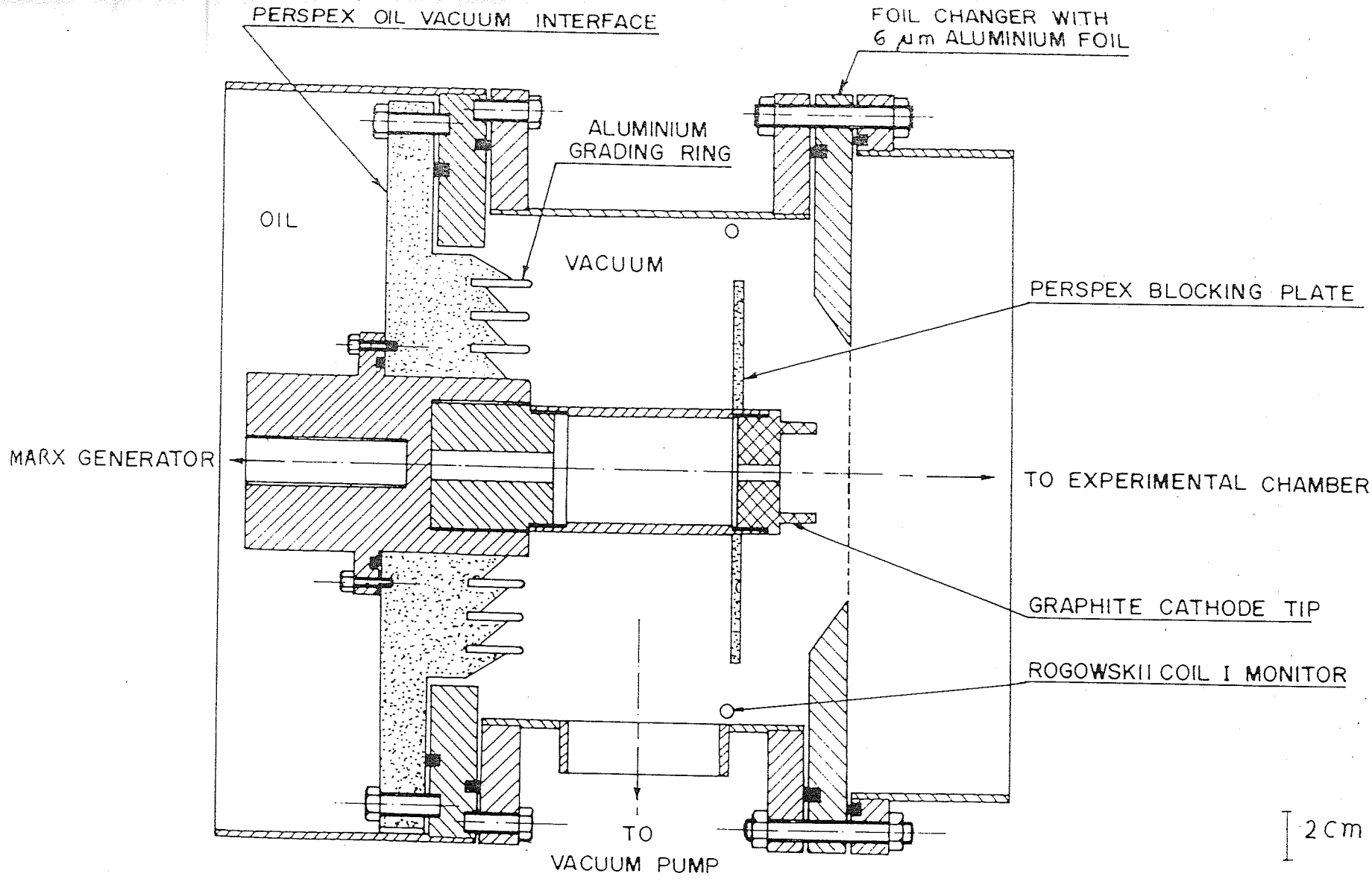

2.7 Oil-vacuum interface.

region, with the foil in its strethed position.The diode region was pumped using a separate diffusion pump.

The mechanism associated with electron beam generation in field emission diodes is fairly well understood [Yonas, 1974]. Upon application of the electric field,microscopic projections on the cathode are heated by ohmic currents and after a few nanoseconds,the projections vaporise forming a plasma sheath which emits electrons copiously.The diode current satisfies the Child-Langmuir relation for the geometry as long as the current is less than the critical value for self-pinching given by $I_c = 8500\,\beta\gamma R_c/d$ Amps (Clark & Linke, 1971), where,R_c is the cathode radius,d is the anode-cathode separation, β is the ratio of electron velocity to c and γ is the relativistic mass factor.

For our case,$I_c \simeq 12$ KA,and the maximum diode current $\simeq$ 6 KA. So the diode impedance is given by the Child-Langmuir relation, $Z_D = 136[d_o - S(t)]^2/[V^{1/2}(R_o^2 - R_i^2]$ in ohm,(Kirstein et al, 1967; Parker et al, 1974),d_o = initial anode-cathode spacing; S(t) = relative distance moved by the cathode/anode plasma leading to effective reduction of the anode-cathode spacing; V is diode voltage in MV;R_o and R_i are the outer and inner cathode radii respectively.

A measurement of the diode voltage and current enables one to calculate the diode impedance which gives information regarding the diode closure.The measurement of diode voltage was done using a resistive divider and of diode current using Rogowski coil encircling the cathode shaft. The measured voltage after correcting for the

inductance at the diode side, was used for computing the diode impedance. The traces of diode voltage and current are shown in figure 2.8. In the first 200 nsec, diode voltage signal shows large oscillations. This is partly due to measurement problem and partly because the diode formation time is a few nsec after the appearance of the high voltage [Yonas, 1974]. The plots of diode impedance and $(Z_D V^{1/2})^{1/2}$ vs. time are shown in figure 2.9. A best fit was obtained for $S(t) = d_o(1-e^{-\alpha t})$, with $\alpha \simeq 0.0031$/nsec. The plasma velocity $u(t) = \alpha d_o e^{-\alpha t}$. At $t=0$, $u(0) \simeq 4$ cm/μsec.

Friedman and Ury (1972) reports a constant plasma velocity of $\simeq 5$ cm/μsec for their long pulse electron beam. The exponential decrease of the plasma velocity in our case can be explained to be because of the effect of the self B_θ field, which becomes prominent as the critical current for self-pinching is approached (Creedon et al, 1973). There is experimental evidence that the relative plasma velocity goes to zero for currents exceeding this critical current (Cooperstein and Condon, 1975).

2.4 Diagnostics

Being a pulsed experiment, fast response diagnostics were used to monitor the different experimental parameters. Two current sources were used for calibrating most of the diagnostic elements. One of them was a 100 nsec, 40 Amps current pulse (for fast response) generated by a co-axial cable pulse-forming line terminated with a matched load. The

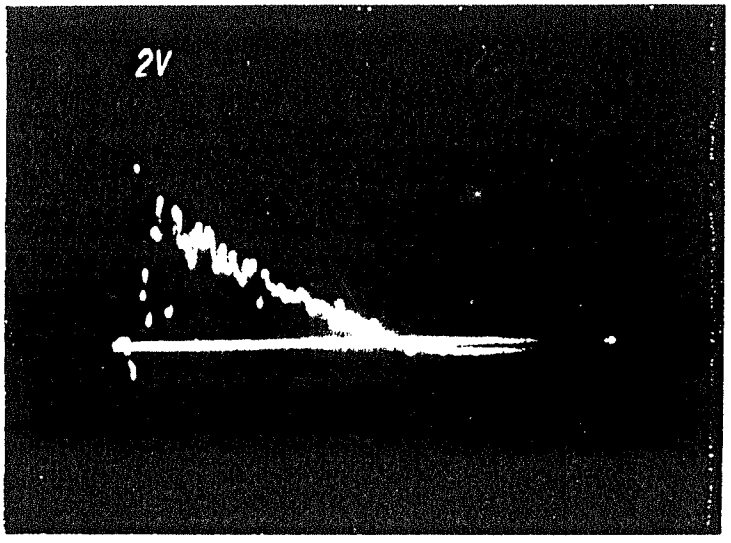

DIODE VOLTAGE

70 KV

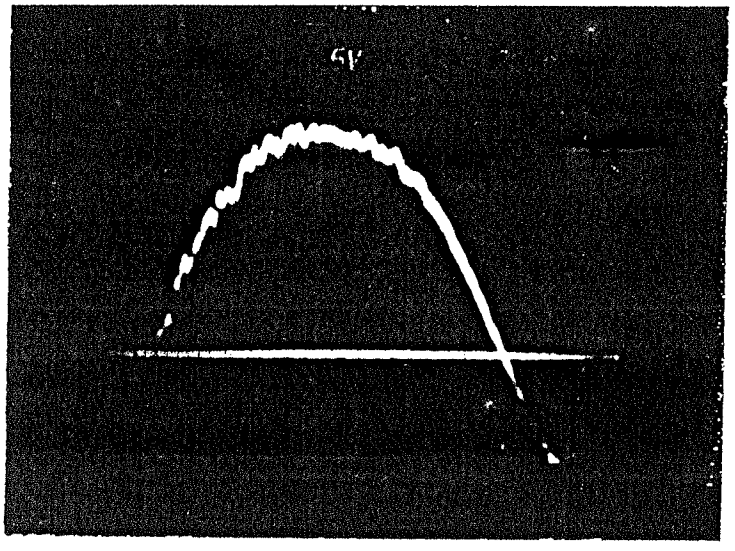

DIODE CURRENT

1.4 KA

200 nsec

2.8 Diode voltage and current traces.

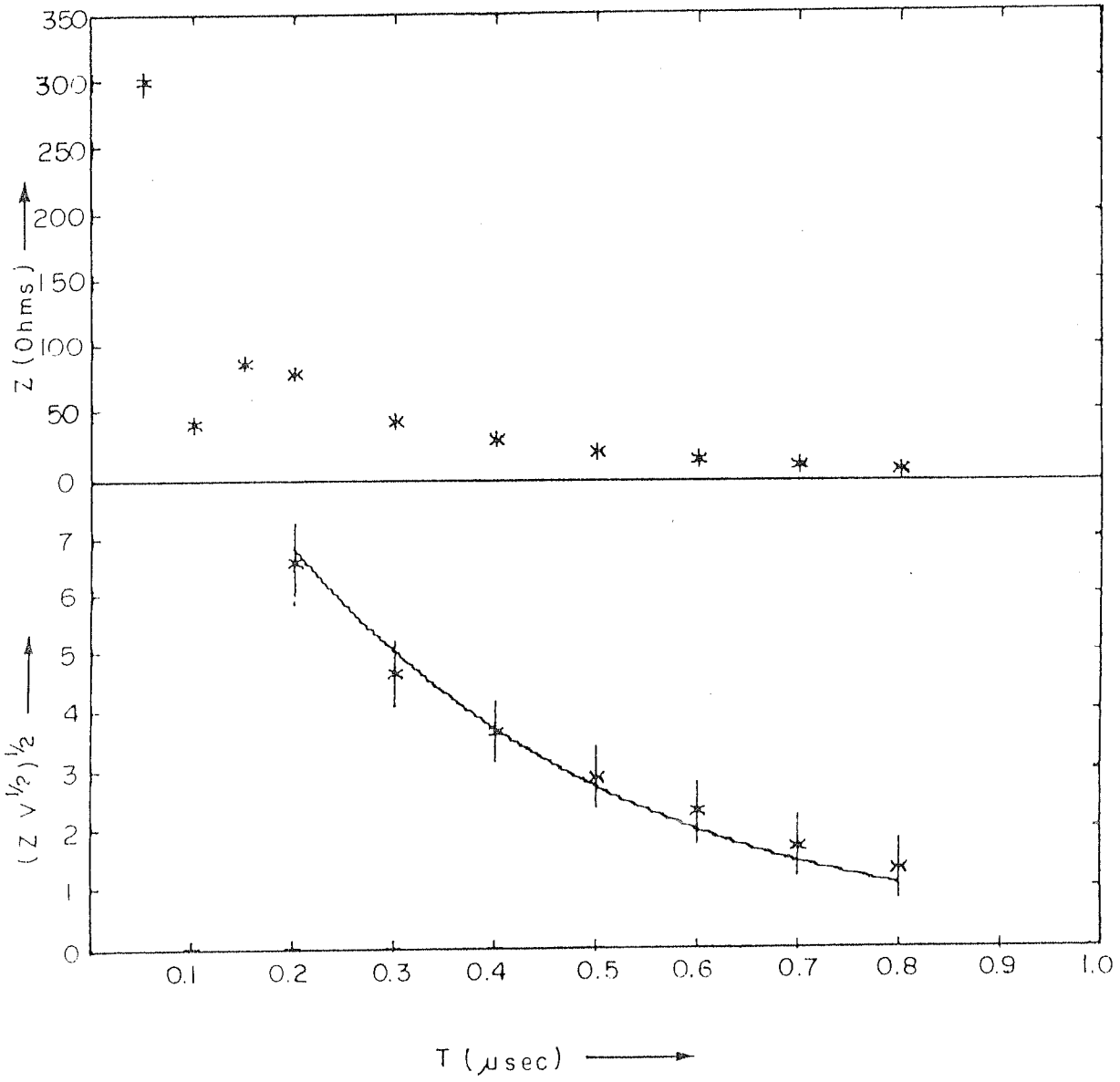

2.9 Diode impedance and $(Z_D V^{1/2})^{1/2}$ vs. time.

other was a LC pulse forming network giving 1 μsec,50 Amps current pulse (for slow response).Details of the various diagnostics used in the present experiment are described below.

2.4.1. Voltage divider:

The diode voltage, which gives the beam energy,was measured using a linear resistive voltage divider given in figure 2.10. The voltage monitor consists of three copper electrodes, placed in a perspex container filled with Copper Sulphate solution. The total resistance of the column is about 1 K Ohm. The voltage divider was calibrated using a 1 μsec high voltage pulse.

2.4.2. Rogowski coil:

The diode current and the net beam current were measured using self-integrated Rogowskii coils.A Rogowski coil mounted over the cathode shank was used to measure the diode current. The Rogowski coil was made from copper windings, mounted inside perspex enclosures.The two ends of the coil were connected by a short wire of negligible resistance and inductance.The current through the wire was measured using a current transformer (figure 2.11).

2.4.3. Faraday cup:

A Faraday cup of 3 cm diameter was used to determine the relativistic electron beam loss at the cusp.The cup was made of Aluminium having an opening of 3 cm diameter and has a graphite disc as the collector.The collector was connected to ground using a low inductance path and the current flowing through it was measured using a current

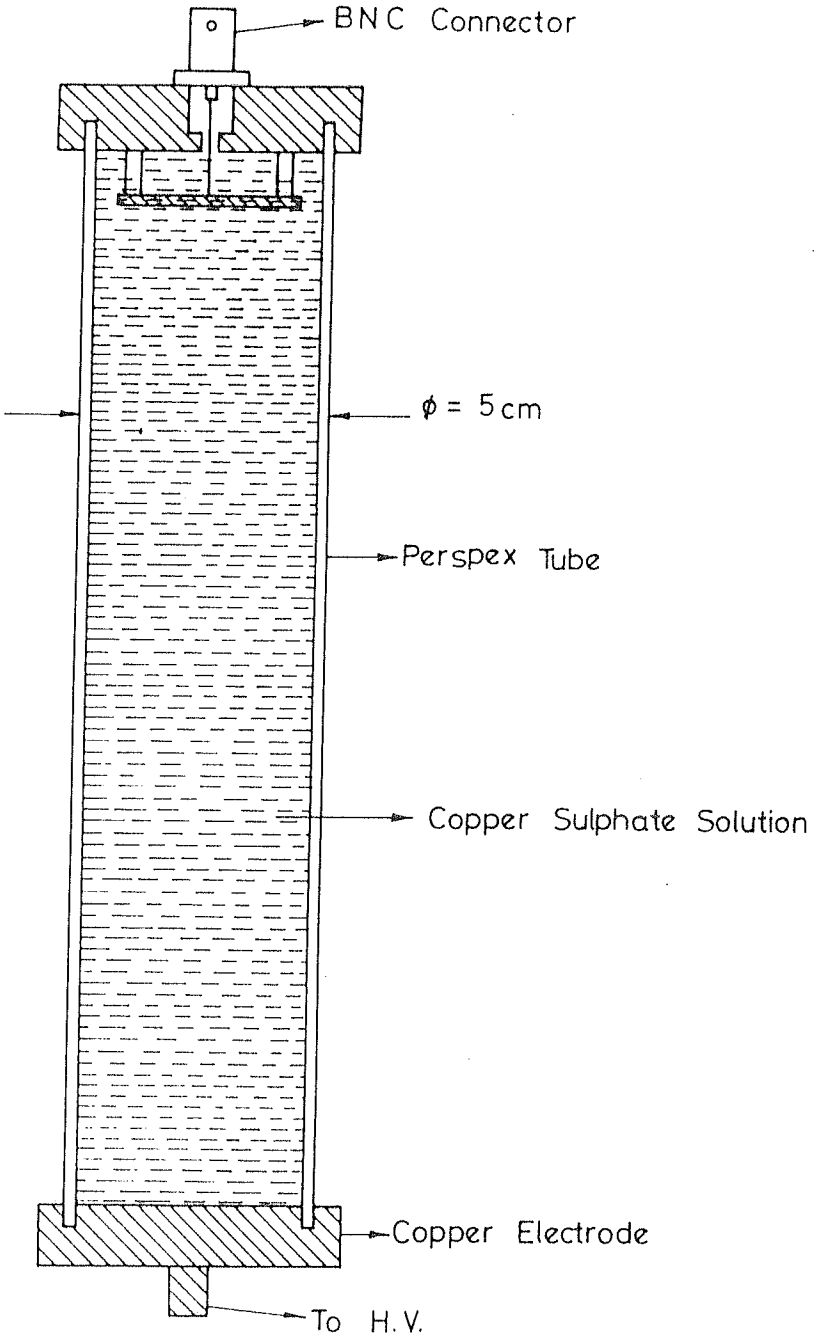

2.10 Voltage divider.

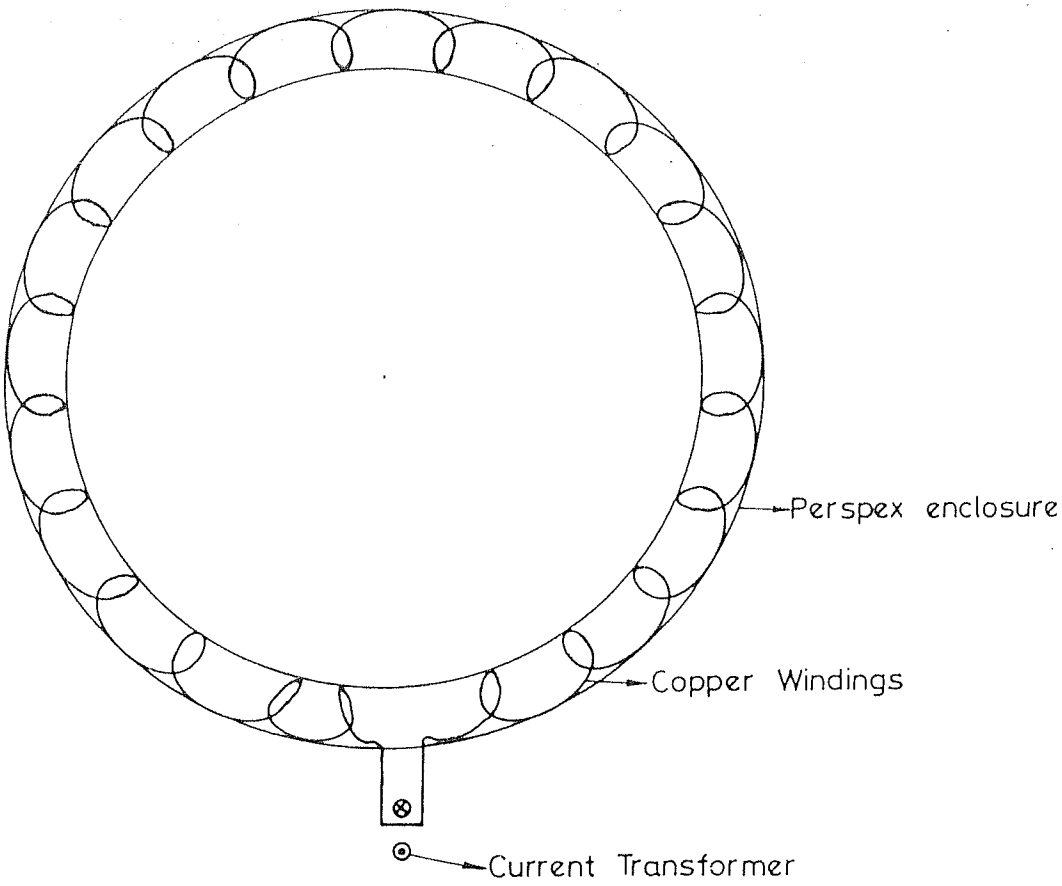

2.11 Rogowski coil.

transformer (figure 2.12). The cup was covered by 6 μm Aluminium foil to prevent the plasma particles from getting collected. The inaccuracy in absolute current measurements by the Faraday cup can occur due to secondary emission from the cup and reflection of the relativistic electron beam from the collector.The secondary emission co-efficient for graphite is less than 3% (Bruning,1954) and any current generated by the secondary emission will be opposed by the relativistic electron beam and hence this effect is insignificant.

2.4.4. Miniature Faraday cup:

This was used for measuring the radial profile of the beam current density at various axial locations.The cup is shown in figure 2.13.The cup is made of Aluminium with 8 mm opening and has a graphite disc as collector.The cup was covered by 6 μm Aluminium foil to cut off the plasma particles. The output from the cup was taken through a stainless steel tube and connected to a BNC connector. Measurement of the collected current was done as for the bigger cup.The stainless steel tube passes through a vacuum feedthrough and can be moved radially in and out.At each axial location,the cup was moved radially from shot to shot to get the beam current density profile.The shots for each r and z were repeated 2 to 3 times for statistics.

2.4.5. Miniature Faraday cup array:

This was used for getting the axial profile of the cusp loss and is shown in figure 2.14.It consists of ten 8 mm. diameter graphite discs placed in the cavities made in a

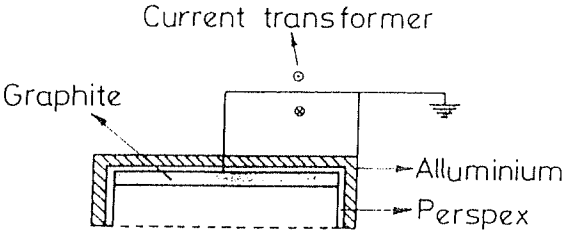

2.12 Faraday cup.

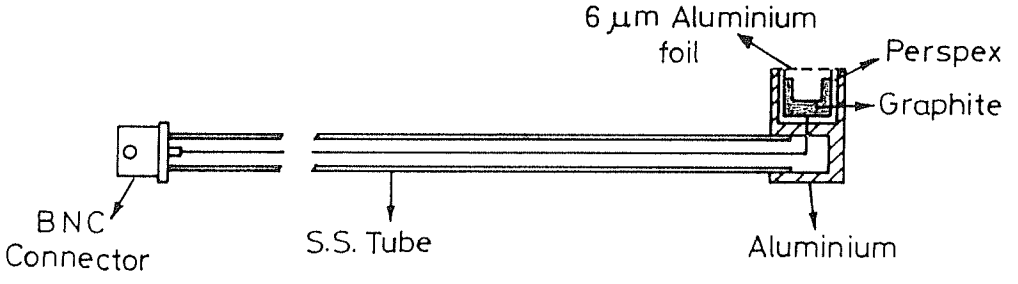

2.13 Miniature faraday cup.

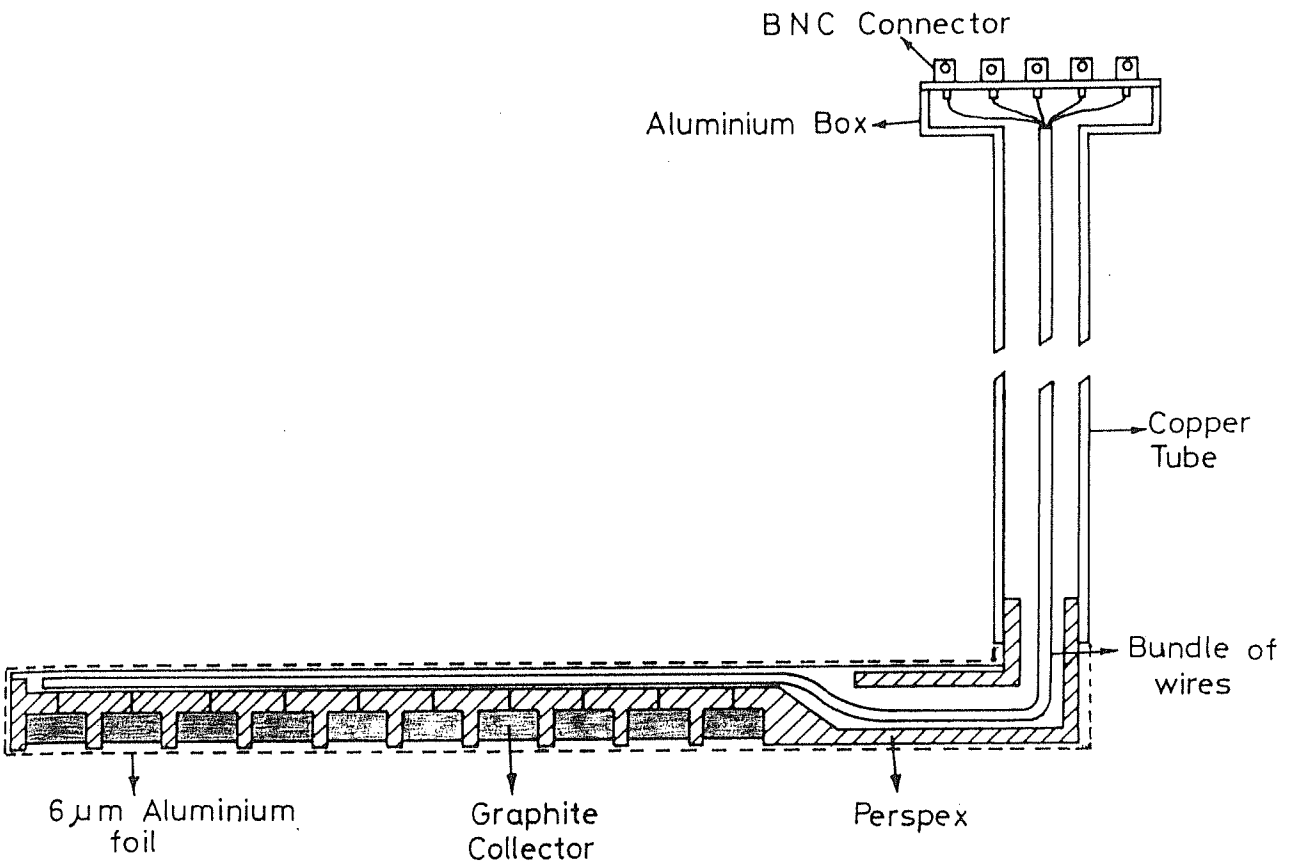

2.14 Miniature Faraday cup array.

perspex rod. The whole structure is covered by 6 μm Aluminium foil. The outputs from the collectors were taken through a 8 mm. diameter copper tube,which passes through a vacuum feedthrough. The outputs from the individual collectors were connected to BNC connectors assembled on an Aluminium box.For measuring the cusp loss profile,the array was mounted at a radial distance of about 7 cm (just touching the inner surface of the mild steel annular plate of the cusp), with the cup openings facing the axis.The output currents from the cups were measured as for the miniature Faraday cup and the bigger Faraday cup.

2.4.6. Magnetic probe array:

Mapping of the beam self magnetic field as a function of radius for different axial locations was done using an array of magnetic probes shown in figure 2.15.In such a probe, the change in the magnetic flux threading the probe produces an induced voltage given by V_{in} = NA dB/dt,where N is the number of turns of the magnetic probe,A its cross sectional area and B the magnetic field.When the voltage is integrated with a passive RC integrator,the output voltage is given by, V_{out} = NAB/RC,giving a direct measure of the magnetic field.

Each probe consisted of a pair of coaxial coils of length about 6 mm. and diameter about 8 mm. having 10 turns of thin copper wire. One end of each coil was grounded in such a manner that when one of the coils gives a positive output, the other gives a negative output.Both the coils were terminated by a 50 Ω resistor and the signals were

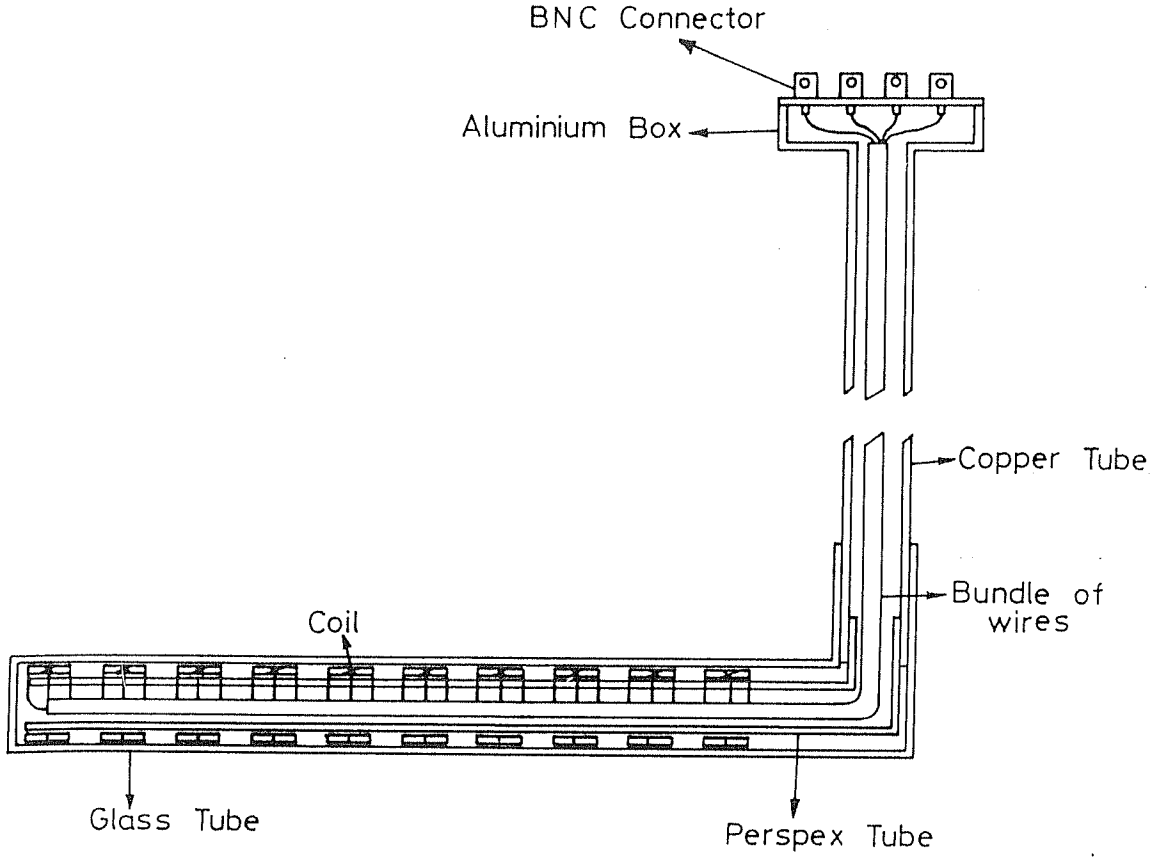

2.15 Magnetic probe array.

integrated using a passive RC integrator.The integrated outputs from a pair were substracted from each other at the oscilloscope so that the electromagnetic noise gets nullified while the signals gets doubled.All the probes were wound on a single perspex tube and the outputs taken through a copper tube to the BNC connectors.The probe array could be moved radially to get the radial dependence of the self-magnetic field.

2.4.7. Diamagnetic loop:

A diamagnetic loop encircling the beam plasma region measures the change in the magnetic flux created by the beam passage, without perturbing the beam.Figure 2.16 shows the construction of a typical diamagnetic loop. The diamagnetic loops were fabricated using 5 turns of thin teflon coated wire wound inside a copper tube of 8 cm inner diameter. The copper tube served as an electrostatic shield with a poloidal cut so as to preclude the formation of eddy currents, which would otherwise oppose the peneteration of the change in flux into the loop windings.The output of the loops were terminated with a 50 Ω resistor and the signals integrated by a passive RC integrator at the oscilloscope.

2.4.8. Wall probe:

This was used to measure the potential due to the net charge in the system (beam and plasma).It consisted of 1.5 cm diameter copper disc mounted flush with the wall as shown in figure 2.17. The potential due to the net beam charge, charges up the beam wall capacitor.The current in the wall probe circuit,corresponding to the charge acquired

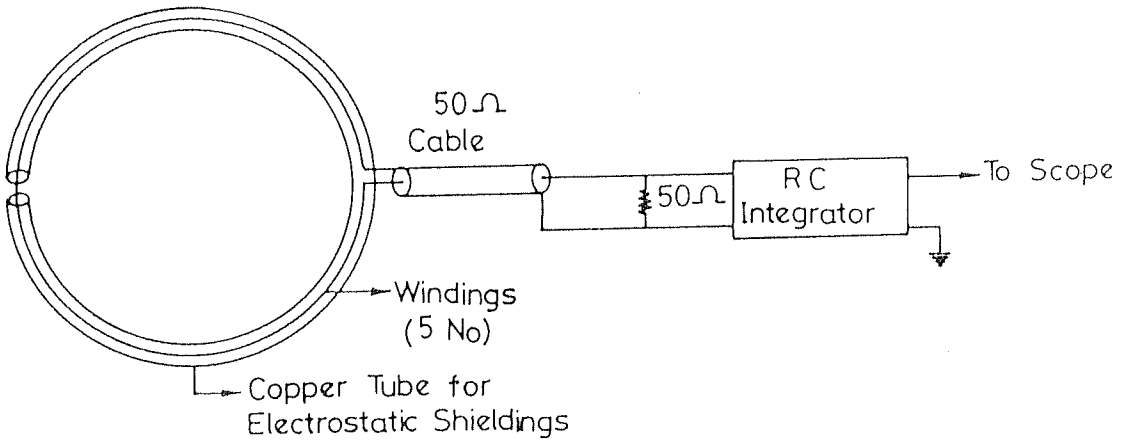

2.16 Diamagnetic loop.

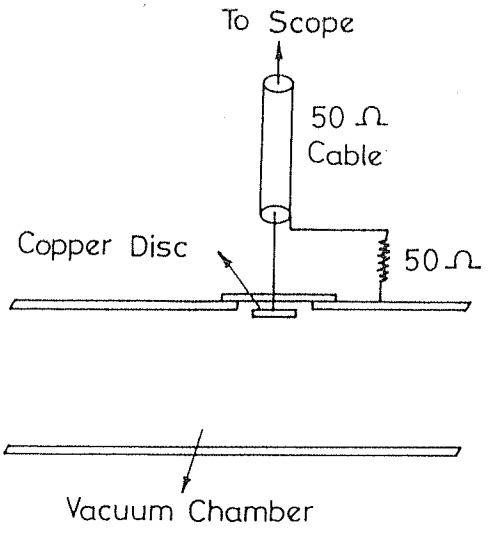

2.17 Wall probe.

by the beam-wall probe capacitor, gives a measurement of the net beam potential.

The calibration of the wall probe was done by applying a voltage pulse of about 25 nsec rise time, 50 nsec duration and 2 KV peak value between a centrally placed cylinder and the wall. Cylinders of different outer diameter from 4.5 cm to 11 cm were used. The 1.5 cm diameter copper disc of the wall probe was connected to the ground through a 50 Ω resistor. The output across the 50 Ω resistor was recorded on a storage oscilloscope. From the oscilloscope trace, the current through the wall probe circuit was integrated to get the charge stored in the beam-wall probe capacitor (Here the beam is simulated by the central cylinder). Knowing the applied potential difference, the beam-wall probe capacitance could be evaluated. The capacitance was seen to have the same radial dependence as for the co-axial geometry and is given by, $C = \pi \varepsilon_0 d^2/(4r_w \ln(r_w/r_o))$, d = diameter of the probe, r_w = wall radius and r_o is the beam outer radius.

CHAPTER III

CHARGE NEUTRALISATION PHASE

3.1 Introduction

In order to have a propagating relativistic electron beam carrying a current more than the space charge limiting current, it is required to charge neutralise it by injecting it into a plasma or neutral gas.For a beam injected into neutral gas, the gas is ionised by the beam.The plasma electrons so formed get removed from the system guided by the beam self fields, providing charge neutralisation for the beam and this constitutes the charge neutralisation phase. Here the beam propagation characteristics will be under the influence of self electric fields.This chapter deals with a study of charge neutralisation processes for a rotating relativistic electron beam [Vijaya Sankar & John, in press], relevant in the context of formation of field reversed configuration, collective ion acceleration etc.The charge neutralisation factor, which gives the net beam charge, has been estimated from beam potential measurements. The charge neutralisation factor as a function of the beam and external parameters is of importance in understanding the self electric field effects on the beam propagation.

3.2. Experimental Set Up

The experimental system has been described in Chapter II. The experimental region contained Hydrogen gas in the pressure regime 50 mTorr to 250 mTorr in the steady state. The peak beam energy $\simeq$ 200 KeV with a duration of $\simeq$ 800 nsec and carrying a peak current $\simeq$ 3 KA.The diagnostics consisted of wall probes and Rogowskii coils.

3.3 Experimental Results

The voltage waveforms from the wall probes corresponding to the current collected by the beam-wall probe capacitor were displayed on storage oscilloscopes.The oscilloscope traces were manually digitised and integrated to get the time profile of the charge stored in the capacitor. Figures 3.1 and 3.2 correspond to typical oscilloscope traces and their time integrated profiles. Figure 3.1(a) and 3.2(a) correspond to pressures above 150 mTorr and a magnetic field ($B_o \simeq$ 500 gauss).Here it was seen that in the first 30 nsec, the beam wall probe capacitor gets charged up driving a current in the negative direction, corresponding to a negative potential difference appearing across the capacitor.The RC time constant of the circuit is in the psec range and is much less than the charging time. So the wall probe sees the instantaneous potential. When the beam potential starts decreasing,the charge stored in the capacitor decays driving the current in the positive direction.The current finally goes to zero

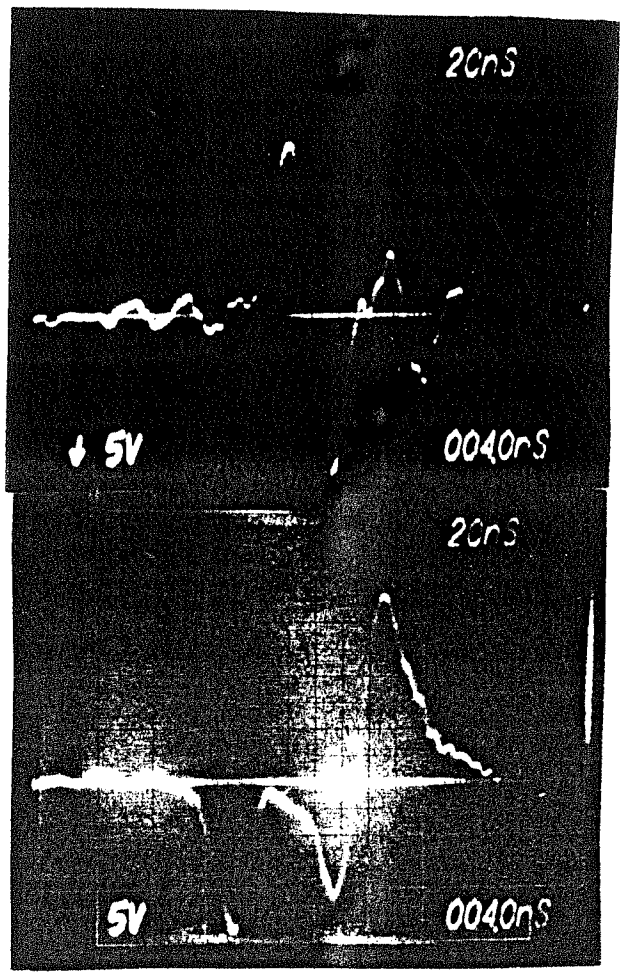

(a)

(b)

3.1 Typical oscilloscope traces from the wall probe.
(a) Pressures above 150 mTorr and B_0 around 500 gauss.
(b) Pressures below 150 mTorr and B_0 around 300 gauss.

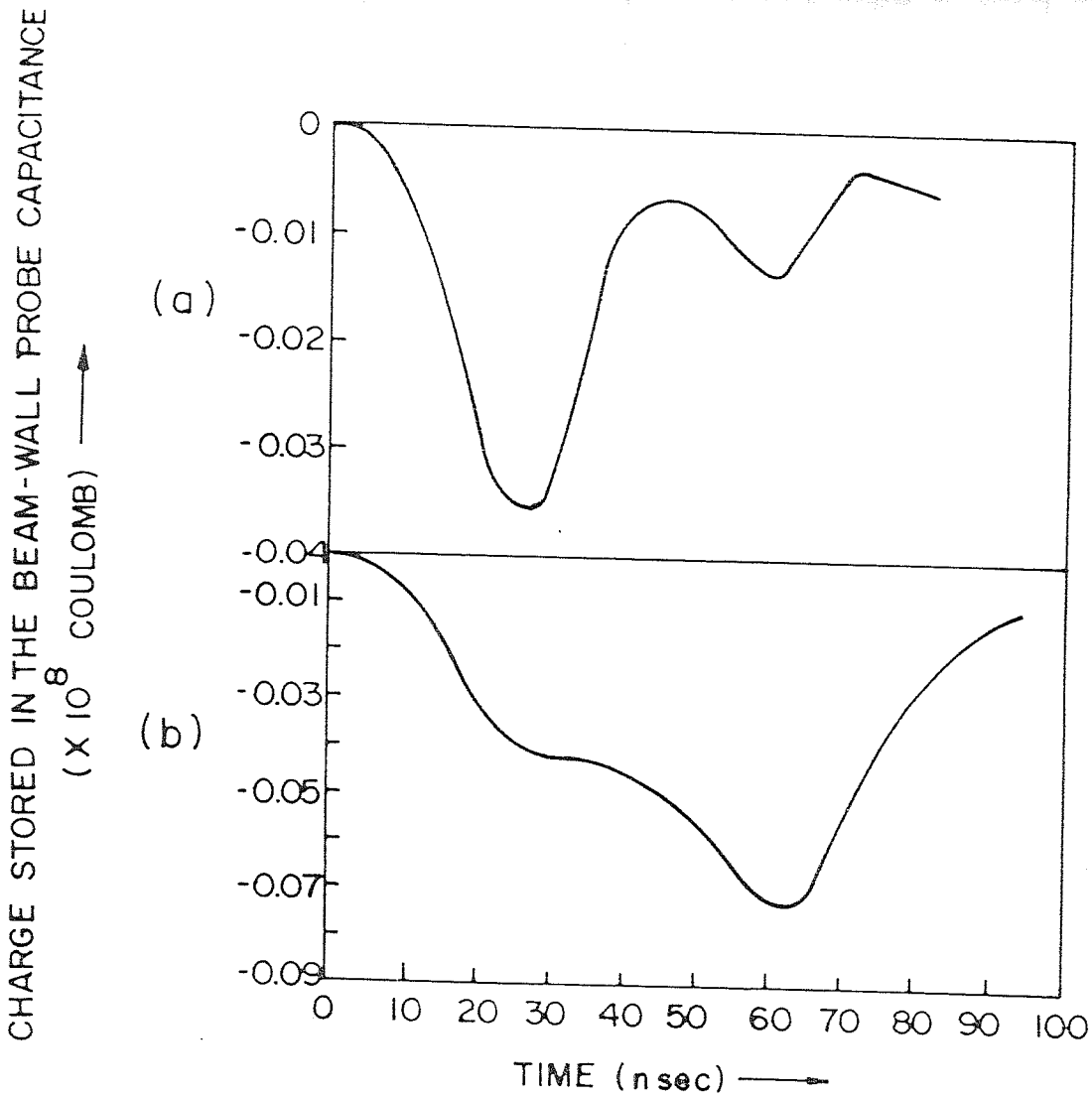

3.2 Charge stored in the beam wall probe capacitor vs. time.

when the potential goes to zero.It was seen from the trace that the current pulse oscillates in time before going to zero, corresponding to an oscillatory part in the decaying phase of the beam potential.The amplitude of oscillation decreases in time,roughly inversely proportional to time as has also been reported in the numerical simulation work of Godfrey (1977 and 1979).Similar oscillations are also seen in another experiment with laminar beam [Arutyunyan et al, 1983]. Attempts to measure the axial phase velocity of the oscillation by the time of flight was not successful, indicating a very high phase velocity (comparable to beam velocity) making the time of flight measurement difficult within experimental error. These oscillations may be of importance in the context of collective ion acceleration [Sloan and Dummond, 1973], whereby ions trapped in the potential well of the waves get accelerated as the wave propagates.

Figures 3.1(b) and 3.2(b) correspond to pressures below 150 mTorr and intermediate magnetic fields ($B_o \simeq 300$ gauss). It was seen that at lower pressures,a step like rise in the potential develops. The potential first rises steadily for about 30 nsec, the rate of rise then slows down,and then again increases at a faster rate till the peak is attained. Also it was seen that with increase in the magnetic field, the first step increases,corresponding to a faster rate of rise of potential. The second step decreases with increase in magnetic field and corresponds to a decrease in the rate of rise of potential in the later phase.The magnetic field

dependence can be attributed to the difference in the ionisation mechanism with external magnetic field and is discussed in section 3.6.

Figures 3.3 to 3.7 correspond to dependence of the beam potential with external parameters like external magnetic field (B_o),axial distance from the cusp (D),and neutral gas pressure (P).These results are discussed in section 3.6.The values of the beam potential plotted correspond to the absolute value. Figures 3.3 and 3.4 give the dependence on B_o. It was seen that the peak charge stored in the beam-wall probe capacitor increases with B_o for B_o = 50 to 200 gauss. Above 200 gauss,it starts to decrease indicating a critical magnetic field around 200 gauss for charge neutralisation process. It was seen that the observed charge stored in the capacitor was more at zero field than that at 50 gauss and 100 gauss.This together with the observation of increase of potential for B_o > 300 gauss can be related to the change in the beam outer radius with B_o,discussed in section 3.6. Figure 3.5 gives the time evolution of the charge stored in the probe capacitor as a function of distance.It was seen that at around 15 nsec,the peak negative potential appears at around D=80 cm. With increase in time, the peak in potential shifts to ≃ 60 cm.This indicates a faster rate of loss of secondary electrons from the region between D=60 cm and the far end wall (D=160 cm). The peak potential is attained in about 30 nsec. Thereafter the potential structure starts to collapse,not shown in the figure.Figure 3.6 gives the axial variation for different values of B_o

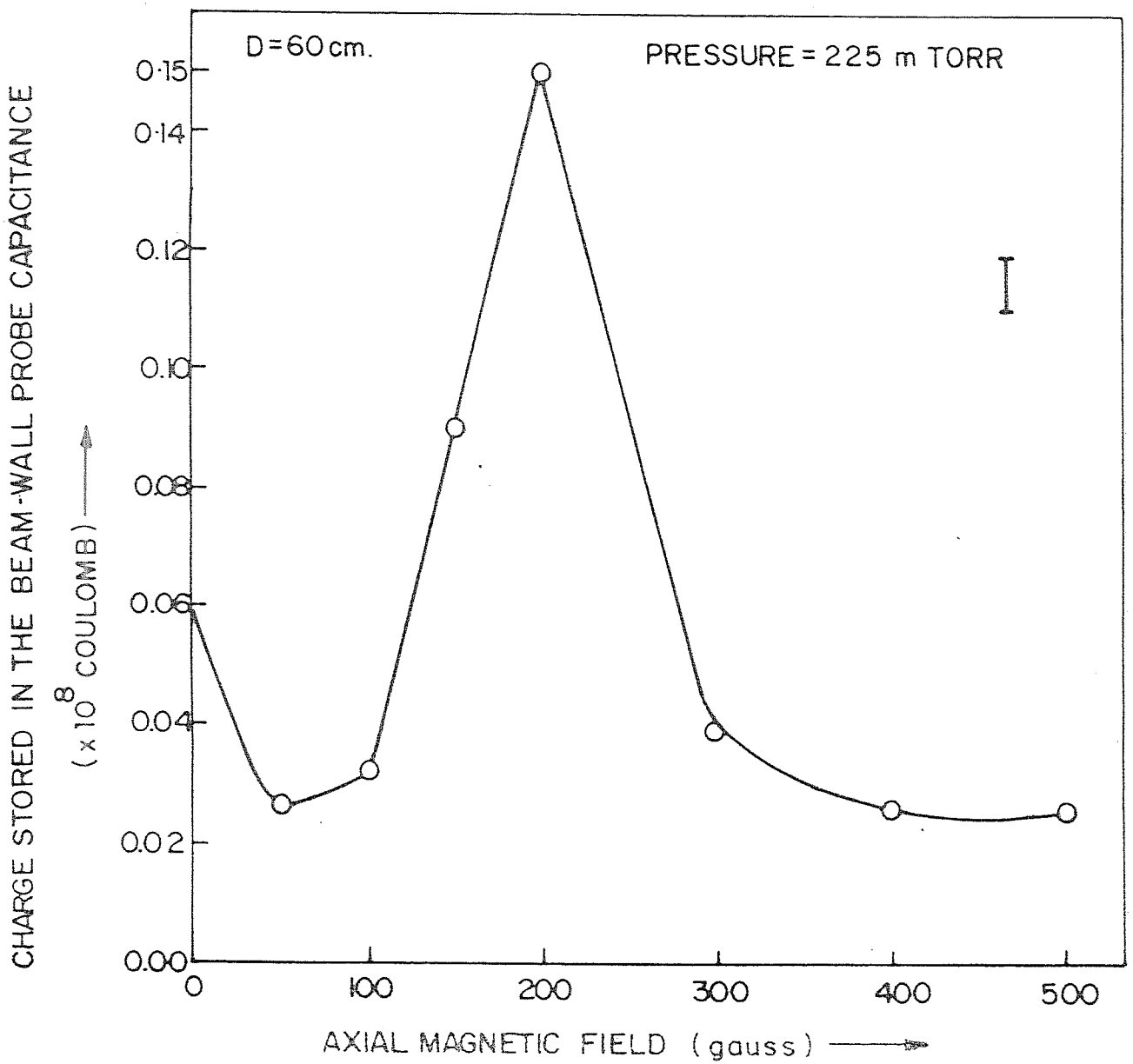

3.3 Peak charge stored in the beam wall probe capacitor vs. external magnetic field.

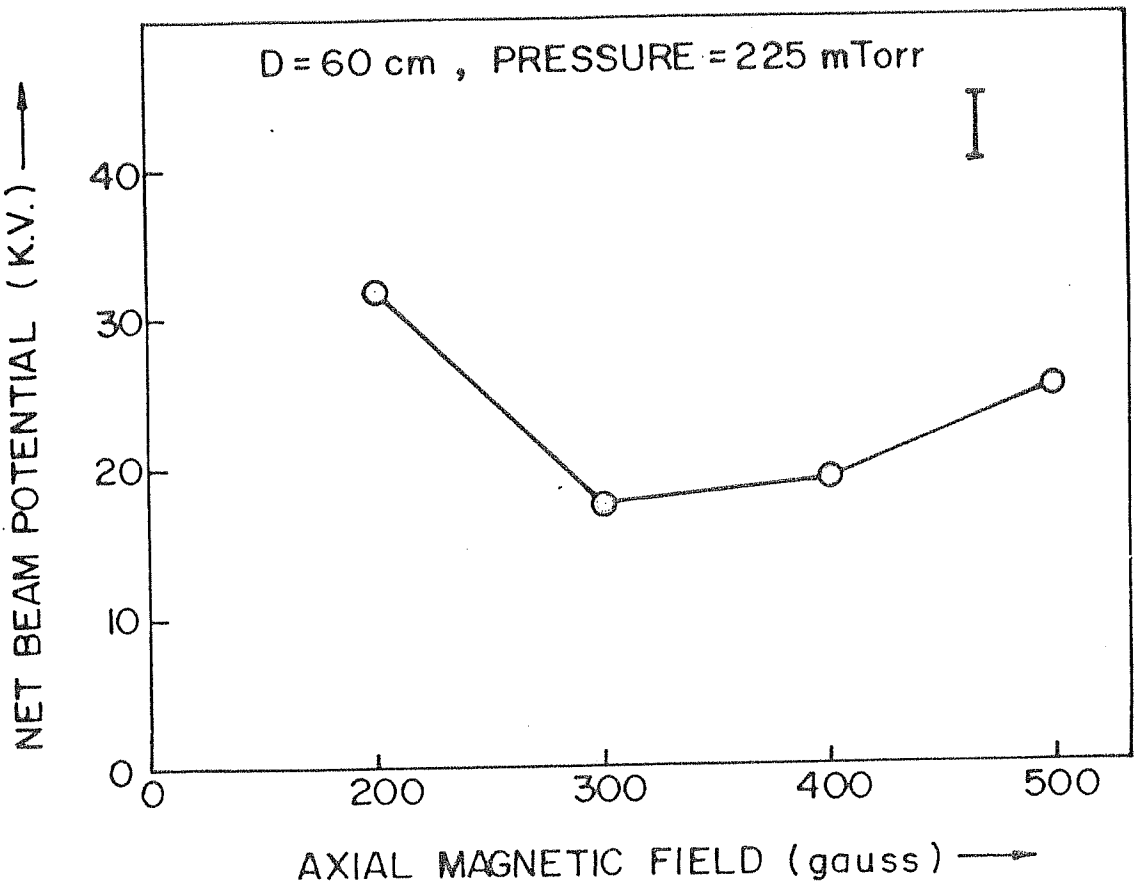

3.4 Peak beam potential vs. external magnetic field.

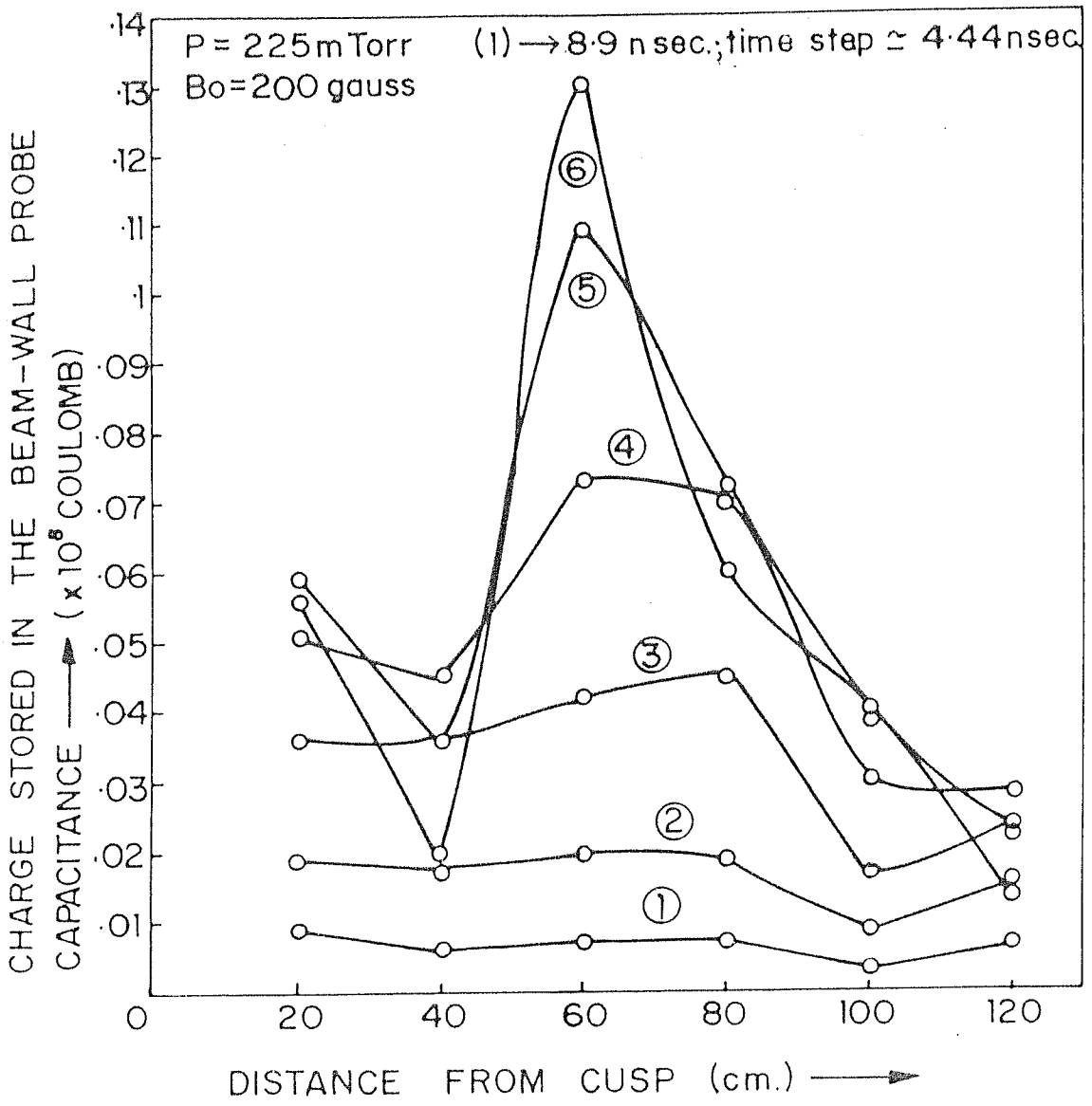

3.5 Time evolution of the charge stored in the beam wall probe capacitor vs. axial distance.

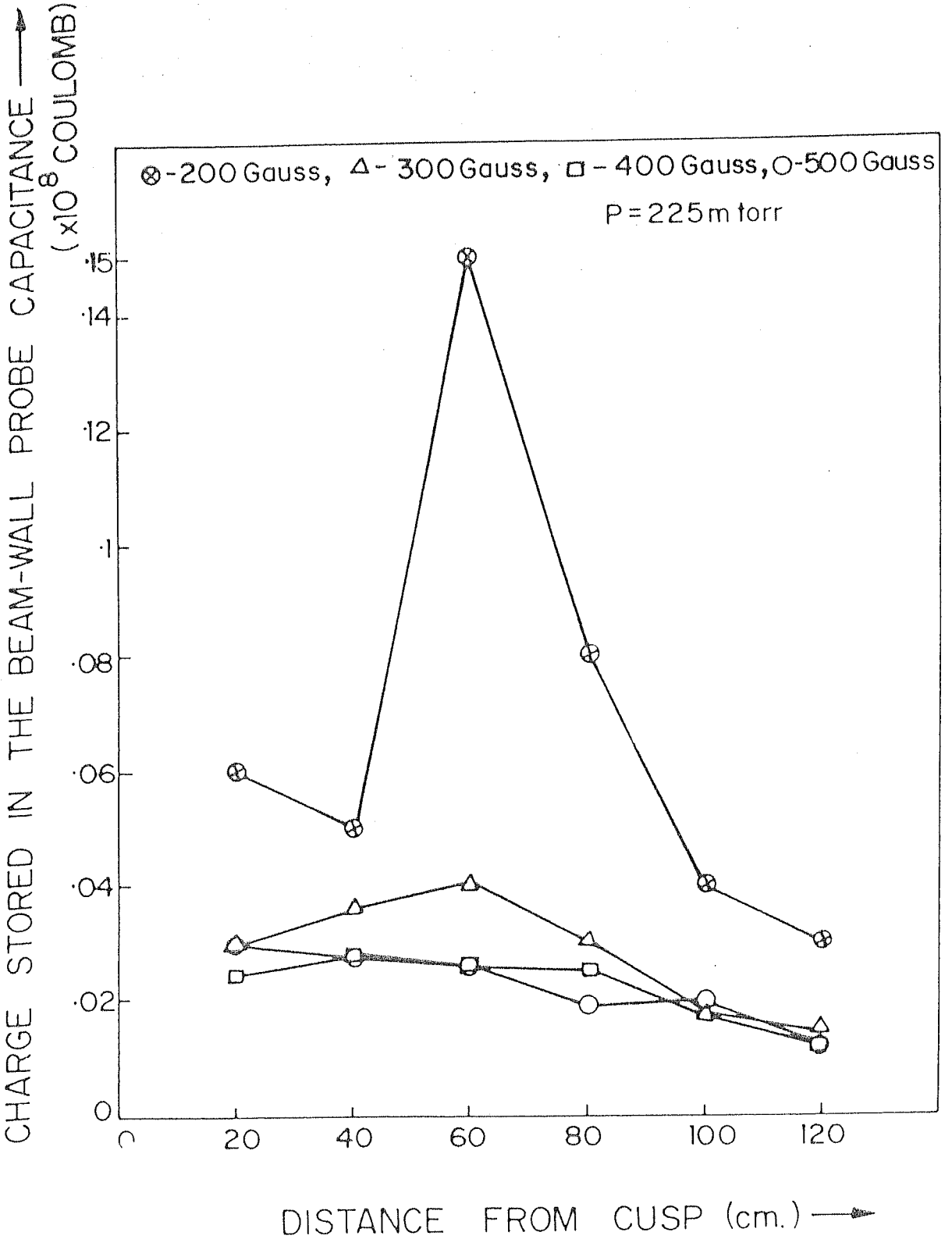

3.6 Axial variation of the peak charge stored in the beam wall probe capacitor for different values of external magnetic field.

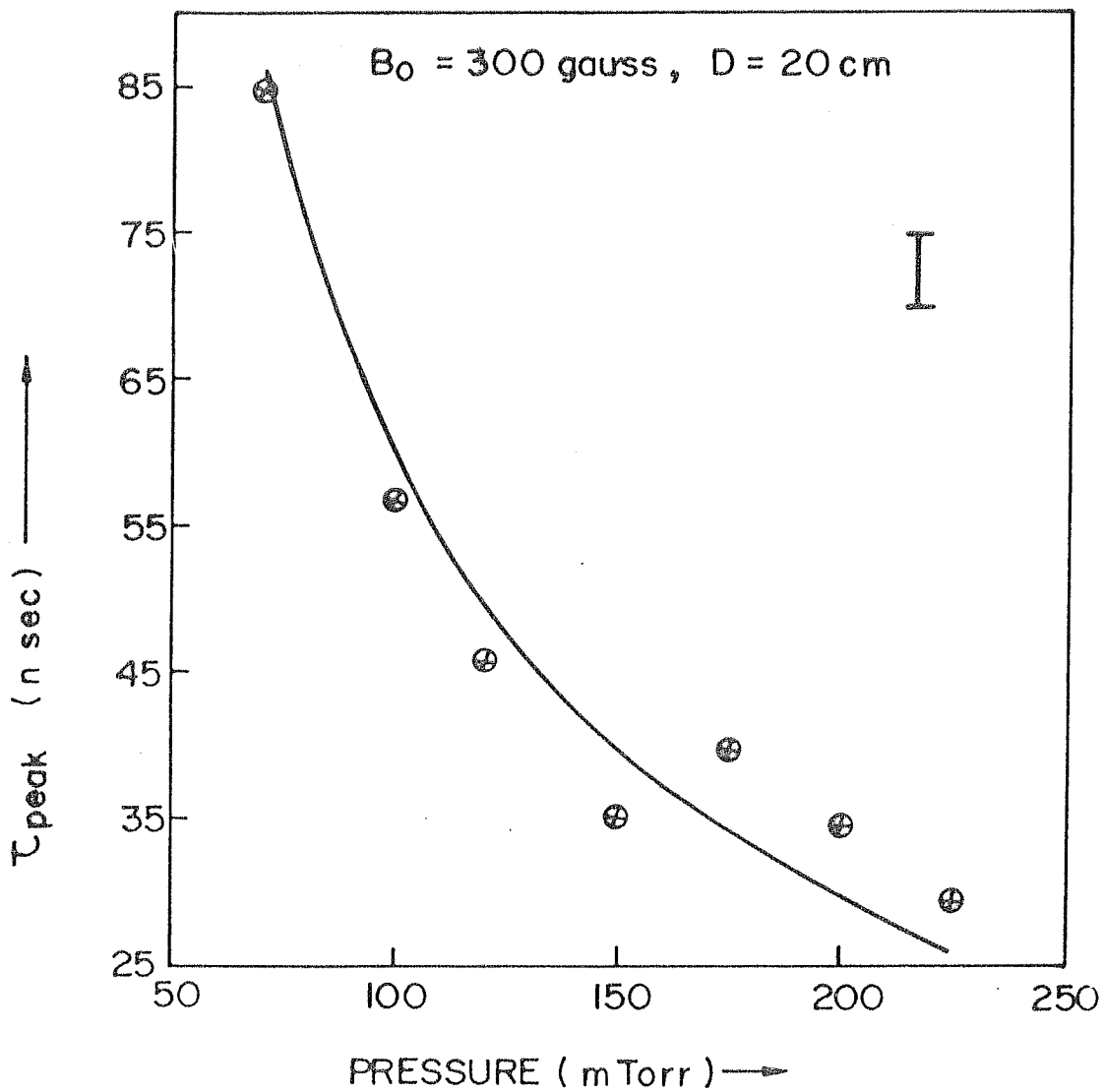

3.7 Rise time of peak beam potential vs. background gas pressure.

(B_o = 200 to 500 gauss). For all B_o values, the charge stored in the probe capacitor shows more or less the same type of axial decay for D > 60 cm. But for D < 60 cm, at B_o = 200 gauss, the rate of axial decay of the stored charge was seen to be faster. Figure 3.7 gives the time in which the peak charge is attained (τ_{peak}) as a function of pressure. τ_{peak} was seen to decrease with P as expected.

3.4 Model for Numerical Calculation

The plasma electron trajectory calculations were done using fourth order Runge-Kutta method with the external field and self fields (modelled based on measurements) present. This was done to estimate the escape time of the plasma electrons to the walls, an useful parameter for the charge neutralisation process. The beam of inner radius r_i, and outer radius r_o was assumed to have constant density. The beam and the outer conducting wall of radius r_w form an axisymmetric coaxial system. Here, it is necessary to make an estimate of the stability of the beam with regard to the usually observed instabilities like diocotron and filamentation. For magnetic fields above 200 gauss and background pressure above 150 mTorr, where the beam was seen to have radial equilibrium, the outer beam radius was 5.5 to 12 cm and the inner radius was 1.0 to 4.5 cm. For these cases, the beam is stable to the diocotron instability for a hollow beam (Kapetanakos et al, 1973), even for the case of zero charge neutralisation. The magnetic field required to stabilize filamentation instability for the case of zero

charge and current neutralisation is given by (Davidson et al,1975),as

$$B_o(\text{gauss}) > 3.21\times10^{-6} n_b^{1/2} [2-v_z^2/c^2]^{1/2}$$

n_b = beam density in m^{-3}.

The peak beam potential occurs at around 30 nsec and here our beam density $\sim 10^{15}$ m^{-3}.This gives the magnetic field required for stability to be greater than 153 gauss.So for our case of charge neutralisation factor greater than zero and $B_o > 200$ gauss,the beam is stable to the diocotron and filamentation instabilities.

The electrostatic potential can be written as,$\phi(r,z,t) = A\, f(r)\, f(z)\, f(t)$.

$A = -I(1-f_e)\ln(r_w/r_o)/(2\pi\varepsilon_o v_z)$ and corresponds to the measured peak beam potential. Here I_o = beam current,f_e = charge neutralisation factor and v_z = beam axial velocity. Form of f(r), appropriate to beam of length much greater than the radius,was taken,and is given by

$$f(r) = \begin{cases} \dfrac{r_o^2[1+2\ln(r_w/r_o)-r_i^2/r_o^2 x(1+2\ln(r_w/r_i))]}{2(r_o^2-r_i^2)}, & 0 \leq r \leq r_i \\ \dfrac{r_o^2[1+2\ln(r_w/r_o)-r^2/r_o^2-2r_i^2/r_o^2 x\ln(r_w/r)]}{2(r_o^2-r_i^2)}, & r_i \leq r \leq r_o \\ \ln(r_w/r), & r_o \leq r \leq r_w \end{cases}$$

(The above form is valid in the central region of the chamber, away from the end walls).Based on the dependence of ϕ vs. axial distance,

$$f(z) = \begin{cases} 1-[(0.6-z)/z_o]^n, & -0.2 < z < 0.6, z_o = 0.8 \\ 1-[(z-0.6)/z_o]^n, & 0.6 < z < 1.6, z_o = 1.0 \end{cases}$$

The distances are in meter, with the cusp centre as the

origin (z=0).(z = -0.2 m corresponds to the anode, z = 1.6 m corresponds to position of the far end wall and z = 0.6 m corresponds to the region where the measured potential was maximum). The measured dependence of ϕ vs. time can be approximated as,

$$f(t) \simeq \begin{cases} (t/\tau)^2, 0 \leqslant t \leqslant \tau \\ 1-[(t-\tau)/\tau_1]^2, \tau \leqslant t \leqslant (\tau + \tau_1) \\ 0, t \geqslant (\tau + \tau_1) \end{cases}$$

$\tau \simeq 30$ nsec and $\tau_1 \simeq 20$ nsec. The electrostatic components of the electric field are given by,

$$E_r = - \frac{\partial \phi}{\partial r} \quad ; \quad E_z = - \frac{\partial \phi}{\partial z} \quad ; \quad E_\theta = 0$$

The inductive components of the electric field are given by,

$$E_z^{ind.} = \int \left(\frac{\partial B_\theta}{\partial t} \right) dr$$

$$E_\theta^{ind.} = 1/r \int r \left(\frac{\partial B_z}{\partial t} \right) dr$$

as given for an infinitely long electron beam (axial dependence ignored). The self magnetic fields were modelled as,

$$B_\theta = - \frac{\mu_0 I(t)}{2\pi} \cdot \begin{cases} 0, & 0 \leqslant r \leqslant r_i \\ (r^2 - r_i^2)/(2(r_o^2 - r_i^2)), & r_i \leqslant r \leqslant r_o \\ 1/r, & r_o \leqslant r \leqslant r_w \end{cases}$$

$$B_z = \frac{\mu_0 I(t) v_\theta}{\pi(r_o + r_i) v_z} \cdot \begin{cases} 1, & 0 \leqslant r \leqslant r_i \\ 1-(r-r_i)/r_s, & r_i \leqslant r \leqslant r_o \\ 1-(r_o-r_i)/r_s, & r_o \leqslant r \leqslant r_w \end{cases}$$

$r_s = r_o(1 - r_o^2/3r_w^2)$, for flux conservation.

$I(t)$, the beam current $\simeq I_o t/\tau_R$, τ_R = beam current rise time $\simeq$ 500 nsec, I_o = peak beam current $\simeq$ 3 KA. v_θ and v_z are the beam azimuthal and axial velocities respectively. The above model for the self fields is quite approximate, but was

helpful in getting some useful information, given in the next section.

In the actual experimental situation, in the presence of the self fields, the beam electrons execute large radial oscillations. Correspondingly, the beam density will be larger at the inner radius than at the outer as has been seen in the experimental measurement of the radial profile of the beam density (Chapter IV). So the beam density can be assumed to be given by the simple model,

$$n_b = n_{bo}\begin{cases} 0, & 0 \leqslant r \leqslant r_i \\ 1-[(r-r_i)/(r_o-r_i)]^2, & r_i \leqslant r \leqslant r_o \\ 0, & r_o \leqslant r \leqslant r_w \end{cases}$$

n_{bo} = peak beam density at any given instant of time. The self fields based on this model were used for evaluating the radial oscillation of the beam electrons and the field energy at any given instant of time. Here since it involves solving the radial equation of motion over one radial oscillation period of the beam electron (much less than the field rise time), the fields were assumed to be static. Also the beam was assumed to be of infinite extent (axial dependence ignored). The net axial magnetic field during the charge neutralisation phase is nearly equal to the external field. The relevant self fields, E_r and B_θ are given by,

$$E_r = -I(1-f_e)f(r)/(2\,\varepsilon_0 v_z r_o)$$

$$B_\theta = -\mu_0 I\, f(r)/(2\,\pi r_o)$$

$$f(r) = \frac{6r_o^2(r^2-r_i^2)(r_o+2r_i)+r_o(8r_i r^3-3r^4-5r_i^4)}{r(r_o-r_i)^2\,(3r_o^2-5r_i^2+2r_i r_o)}$$

The external cusp field was modelled as,

$$B_z = -B_o \tanh(z/\zeta_1)$$

$$B_r = rB_o \operatorname{sech}^2(z/\zeta_1)/2\zeta_1$$

B_o = magnetic field value in the uniform field region, ζ_1 defines the cusp width and is $\simeq$ 3 cm.

3.5 Calculations

3.5.1. Estimation of the charge neutralisation factor from the measurement of beam potential

The potential difference between the beam of outer radius r_o and the wall probe is given by,

$$\phi = \frac{-I(1-f_e)\ln(r_w/r_o)}{2\pi\varepsilon_o v_z} \quad , \quad r_i << r_o \qquad -(1)$$

v_z = average axial velocity of the beam.

Capacitance of the beam wall probe system is given by,

$$C = \frac{d^2}{4r_w \ln(r_w/r_o)} \qquad -(2)$$

d = diameter of the probe.

Charge stored in the beam-wall probe capacitor,

$$Q = \phi \times C = -I(1-f_e)d^2/(8r_w v_z) \qquad -(3)$$

The conservation of canonical angular momentum gives,

$$v_\theta = eB_o(r_c^2+r^2)/(2m_o \gamma r) \qquad -(4)$$

assuming $v_\theta = 0$, at the injection plane (at the anode). (During the time in which the self electric fields peak, the beam energy $\simeq$ 200 KeV and the mean scattering angle by the Aluminium foil anode is less than 20^o [Birkhoff, 1958]

An estimation of the variation of v_z and γ over the radial extent of the beam was obtained in the following way.

The radial equation of motion was solved for the beam electrons with the self fields E_r and B_θ taken as $E_r = E_{ro} f(r)$ and $B_\theta = B_{\theta o} f(r)$, E_{ro} and $B_{\theta o}$ being given by $E_{ro} \simeq 1$ M.V. m^{-1} and $B_{\theta o} \simeq 10$ gauss, being the order of magnitude of the fields present in the system. The beam radii were determined iteratively. The percentage variation of v_z was < 5% and of γ < 2%. So,

$$[1-(v_z^2(\text{average})+v_\theta^2(r_o))/c^2]^{-1/2} \simeq \gamma(\text{average})$$

$$(\gamma_{in.} - \gamma_{av.})m_o c^2/e \simeq v_z/I \int_0^{r_w} (\varepsilon_o E_r^2 + B_\theta^2/2\mu_o) 2\pi r dr$$

While evaluating the field energy, it was assumed that $r_i << r_o$, as a simplification. Using equations 3,4,5 and 6, a fourth order algebraic equation was obtained for f_e. This was solved numerically. The estimated values of f_e are given in table 3.1. It was seen that f_e increases with external magnetic field (for B_o = 200 to 500 gauss). This is a consequence of the ionisation mechanism to be discussed in the subsection 3.5.3.

3.5.2. Radial extent of the beam column:

The radial forces acting on a beam electron are the following - (1) outward forces due to (a) the eE_r component of the electrostatic force; (b) the centrifugal force, mv_θ^2/r and (2) inward forces due to (a) $e(v_z \times B_\theta)$; (b) $e(v_\theta \times B_z(\simeq B_o))$. From the conservation of canonical angular momentum,

$$v_\theta = eB_o(r_c^2+r^2)/(2m_o \gamma r)$$

The net force from the terms containing v_θ is thus given by,

$$F(v_\theta) = -e^2 B_o^2 (r^4 - r_c^4)/(4m_o \gamma r^3)$$

To start with, $eE_r - e(v_z \times B_\theta)$ causes r to change from the

TABLE 3.1

B_o (gauss)	r_o (cm)	r_i (cm)	Field energy (KeV)	f_e	t_e (nsec)
200	12.0	4.4	71.5	0.24	-
300	9.5	0.9	17.6	0.55	9.0
400	7.0	0.85	11.0	0.71	6.6
500	5.5	0.96	10.0	0.78	6.0

initial value of r_c, the cathode radius.Now $F(v_\theta) \neq 0$ and acts as a restoring force.This will result in the radial oscillation of the beam electrons about an equilibrium radius, provided it exists.For an uniform beam,radial force balance gives the condition for existence of an equilibrium radius as,

$$f_e > 1-(v_z/c)^2 - \omega_c^2/2\,\omega_p^2$$

$\omega_c = eB_o/m_o\gamma$,is the cyclotron frequency,and

$\omega_p = [n_o e^2/2\,\varepsilon_o m_o]^{1/2}$,is the beam plasma frequency.

For a non-rotating beam ($v_\theta = 0$),the condition reduces to $f_e = 1-(v_z/c)^2$ [Miller,1982].For $v_\theta \neq 0$,equilibrium radial oscillations become possible for unneutralised beam, provided, $\omega_c^2/2\,\omega_p^2 \gtrsim 1-(v_z/c)^2$.So a rotating beam reduces the restriction on f_e. For our case, this condition is satisfied for $B_o > 100$ gauss.

Now for a given value of r and γ,the initial restoring force, $F(v_\theta) \propto B_o^2$.So higher B_o values will make the radial extent of the beam smaller.This was seen in the damage on the radiochromic film exposed to the beam.The radial extent of the beam was obtained by integrating the radial equation of motion.The values of r_o and r_i are given in table 3.1.It was seen that the beam electrons execute large radial oscillations of extent 5 to 8 cm.These are much larger than that due to finite cusp width (< 1 cm) [Rhee and Destler, 1974]. The oscillations result in an increase in the thickness of the beam.The radial width of the beam at the injection point is $\simeq$ 0.4 cm.

3.5.3. Model for ionisation process:

Based on the model given by Olson (1975), the rate of production of ions and electrons is given by,

$$\frac{\partial n_i^s(t)}{\partial t} = \frac{n_b(t)}{\tau_e} + \frac{n_e^s(t)}{t_e}$$

$$\frac{\partial n_e^s(t)}{\partial t} = \frac{n_b(t)}{\tau_e} + \frac{n_e^s(t)}{t_e} - \frac{n_e^s(t)}{t_s} .$$

$$f_e(t) = [n_i^s(t) - n_e^s(t)]/n_b(t)$$

$n_{i,e}^s$ = secondary ion (electron density), n_b = primary electron beam density, τ_e = ionisation time by the primary electrons, t_e = electron avalanche time and t_s = secondary electron escape time. Here ion avalanche is not included as the potential well formed is not of sufficient depth to accelerate ions to ionising energy. Roughly, electron avalanche can be said to occur when the mean free path for ionising collisions is less than the escape distance to the wall for the secondary electrons. Accordingly, one can define two modes of ionisation determined by the value of t_s.

1. Avalanche absent,

$f_e(t) = t/2\,\tau_e - t_s^2[\exp(-t/t_s) - 1 + t/t_s]\,\tau_e t$

for $t_s \ll \tau_e$, $f_e(t) \simeq t/2\,\tau_e$. $\tau_e \simeq 5/\text{Pressure (Torr)}$ nsec for Hydrogen.

2. Avalanche present (faster rate of charge neutralisation),

$f_e(t) = \tau^2[(\exp(-t/\tau)-1)t_e/(t_s-t_e) - t/t_s + t^2/2\tau t_s]/\tau_e t$

where, $1/\tau = 1/t_s - 1/t_e$.

External magnetic field plays a dominant role in altering the value of t_s and hence in determining the mode of ionisation. This can be seen by examining the Larmor radius of an escaping secondary electron. In the absence of an axial magnetic field, the plasma electrons will escape

primarily radially. The average energy of a secondary electron escaping radially correspond to the average potential within the system (averaged over the radius)

$\bar{\phi} = \phi(r_o)[1+22r_o/15r_w]/\ln(r_w/r_o)$, for $r_i << r_o$

Now when a magnetic field is applied, the Larmor radius ($r_L = v_\perp/\omega_{ce}$) decreases. A plasma electron at r_o can be considered to be lost to the radial wall if $r_L > (r_w - r_o)$. The peak observed potential correspond to 30 KV. For lower values of B_o, r_o > 10 cm. For these parameters, it is seen that for B_o < 150 gauss, r_L > 5 cm. So for B_o > 150 gauss, the plasma electrons start to get lost to the axial wall. Evaluation of the trajectory of a plasma electron, produced in the central region of the chamber at around 25 nsec, was done using the model described in the last section. It was found that as B_o was increased from 50 gauss to 110 gauss, the value of t_s increased from 1.6 nsec to 2.2 nsec. For B_o > 110 gauss, plasma electrons were seen to be moving more in the axial direction. The value of t_s becomes $\simeq$ 10 nsec at B_o = 200 gauss, and the radial extent of the motion was less than 2 cm. In this context, one can define a critical magnetic field, above which, magnetic insulation is provided to the plasma electrons against radial loss. Here, this critical field $\simeq$ 200 gauss. The increase in t_s with B_o upto B_o = 200 gauss, would correspond to a decrease in f_e with increase in B_o for B_o = 0 to 200 gauss.

Above 200 gauss, a different mechanism sets in changing the mode of ionisation from avalanche absent to avalanche present. As a consequence of the reduction in the beam outer

radius with increase in B_o, the axial inductive electric field increases. It increases by a factor of 2 from 0.8 KV m^{-1} to 1.6 KV m^{-1} as B_o is increased from 200 to 500 gauss. It causes a reduction in the net axial electric field in the region between the central region (region of peak potential) and the far end wall.Here the escape distance to the far end wall for a secondary electron $\simeq$ 1 m.It was seen in the trajectory evaluation of a plasma electron that t_s increases from 10 nsec to about 35 nsec as B_o is increased from 200 to 500 gauss. So here,the average energy of an escaping plasma electron decreases.The mean free path for electron impact ionisation is given by, $\lambda = (PS)^{-1}$ cm. [Olson, 1975;Riek and Prepejchal,1972],where P = pressure in Torr and S = electron ion pair created per cm per Torr. Accordingly, λ decreases from about 90 cm (B_o = 200 gauss) to about 15 cm.(B_o = 500 gauss).Reduction of λ below the secondary electron escape distance, for B_o > 200 gauss, causes avalanche breakdown to set in.This increases the rate of production of plasma.So for a given value of t_s,the rate of loss of secondary electrons increases, thereby increasing f_e. Based on Townsend avalanche breakdown mechanism [Alston,1969],electron avalanche time,$t_e = \lambda / v_e$, v_e = plasma electron velocity.For B_o = 500 gauss,it gives $t_e \simeq$ 5 nsec. The values of the effective avalanche time, corresponding to the estimated values of f_e at D = 60 cm, were calculated using the equation for f_e given earlier. These are given in table 3.1.It was seen that the value of t_e varies from 6 to 9 nsec.These are roughly equal to the

values based on Townsend breakdown mechanism.

3.6 Discussion and Comparison with Other Experiments

Charge neutralisation factor (f_e) has not been measured either directly or indirectly in any of the earlier experiments. In the experiments of Smith et al (1986), f_e was calculated using a simple model assuming only electron impact ionisation by the beam electrons to be present. They have correlated the beam propagation efficiency with the calculated value of f_e. In the present experiments, f_e was estimated from a measurement of the beam potential.

3.6.1. Dependence on external magnetic field:

The variation of the peak charge stored in the beam-wall probe capacitor as a function of external magnetic field (B_o) is shown in figure 3.3 for D = 60 cm from the cusp. The figure indicates an increase in the net beam potential as B_o is increased from 50 to 200 gauss. This is so because the value of f_e decreases as B_o is increased from 50 to 200 gauss, as discussed in the previous section. The observed higher values at $B_o = 0$ can be due to lack of beam equilibrium.

For $B_o > 200$ gauss, the peak charge shows a decrease with increase in B_o for B_o less than the critical field for cusp cut off ($\simeq$ 825 gauss). Also from the plot of the time evolution of the peak charge for $B_o = 200$ gauss (figure 3.5), it was seen that the region of the peak potential shifts away from the far end wall, with increase in time. There are indications of the role of the inductive axial

electric field in changing the mode of ionisation from avalanche absent to avalanche present, discussed earlier. Here f_e increases with B_o and hence the decrease in the peak charge. With increase in time, inductive electric field increases. This causes avalanche to set in between the central region and the far end wall, with increase in time. Avalanche causes an enhancement in the rate of production of secondaries and so for a given value of t_s, produces an increase in f_e. This results in the observed asymmetry in the axial potential structure around 30 nsec.

From figure 3.4, it is seen that the beam potential increases with B_o for $B_o > 300$ gauss. Here f_e increases from 0.24 to about 0.78 as B_o is increased from 200 to 500 gauss. f_e remains around 0.7 for B_o = 400 gauss and 500 gauss. But the value of r_o decreases with increase in B_o. This is the main cause for the increase in potential for $B_o > 300$ gauss. The contribution from the axial slowing down of the beam due to rotation will become significant only when B_o approaches the critical field for cusp cut off. The reduction in v_z due to rotation as B_o is increased from 200 to 500 gauss is only 15%.

In the context of collective ion acceleration using rotating REB [Roberson et al, 1976], it was seen that the relative yield of ions increases with B_o for $B_o > 800$ gauss, till the critical field for cusp cut off. As B_o approaches the critical field for magnetic insulation against radial loss of secondary electrons, it has been shown in the present study that f_e decreases with B_o. This can result in

the potential well getting well defined resulting in higher yield of ions with increase in B_o.

In the present study, it was observed that the values of $B_o > 200$ gauss provide magnetic insulation against radial loss for the plasma electrons. In the region between the central region of the chamber and the far end wall, these plasma electrons were essentially found to move in the direction of the beam. A related phenomenon was observed in the experiments of Wachtel and Safran (1974) and Kouichi Ono (1979), where they have observed an amplification in the beam current due to plasma electron flow parallel to the beam current.

3.6.2. Dependence on axial dependence from the cusp:

Plasma electrons near the end wall get lost faster than that in the central region. So for a given breakdown mechanism, the value of f_e increases as the end wall is approached. This accounts for the observed decrease in the peak charge stored in the probe capacitor for $D > 60$ cm, shown in figure 3.6. At the cusp plane, there is a mild steel annular disc of opening $\simeq$ 14 cm in diameter. So for lower magnetic fields, the outer beam radius being larger, there is an easier and faster loss mechanism for the plasma electrons and causes the peak charge in the capacitor to be lesser as the cusp wall is approached. But for higher fields, as the beam outer radius is smaller, the loss is mostly to the anode wall. So, this would not result in a drastic reduction in the beam potential as the cusp wall is approached.

3.6.3. Pressure dependence:

The time in which the peak potential is attained (τ_{peak}) as a function of pressure is shown in figure 3.7 for an external magnetic field of 200 gauss.It was seen that τ_{peak} decreases with pressure, roughly inversely proportional to pressure. From the expression given for f_e given in section 3.5,it is seen that for $t_s << \tau_e$, $\tau_{peak} \simeq$ 5/P(Torr) nsec. A best fit to the experimental data corresponded to $\tau_{peak} \simeq 5.94/P(Torr)$ nsec.With increase in pressure, corresponding to higher neutral gas density,the plasma density increases for a given ionisation mechanism (here it corresponds to electron impact ionisation by the primary beam electrons). So for a given value of t_s,the number of electrons removed from the system increases with pressure,thereby reducing the value of τ_{peak}.

At lower pressures,with increase in the magnetic field, the initial rate of rise of the charge stored in the probe capacitor was seen to be faster.This can be due to decrease in f_e with B_o and here avalanche,discussed in section 3.5 does not seem to be contributing in the early time scales (< 20 nsec). But for time greater than 30 nsec,the rate of increase of the stored charge decreases for B_o > 200 gauss, possibly corresponding to the setting in of electron avalanche.

In the experiments reported so far,the REB transmission efficiency was found to increase with pressure for pressures less than a few hundred mTorr.In the experiments of Genuario et al (1974), oscillations were seen in the

transmitted current, believed to be Langmuir oscillations. Andrews et al [1971(b)] had observed periodicities in the light intensity of the beam, in the microwave activity and in the net beam current. The wavelength of these periodicities was found to be inversely proportional to the gas pressure. These have been considered to be due to some instabilities in the ionisation-neutralisation of the beam in the gas. The beam potential was found to be oscillatory in the experiments of Arutyunyan et al (1983). In the present study also oscillations were seen in the beam potential for pressures above 150 mTorr, with the amplitude of oscillation decreasing in time roughly inversely proportional to time. Similar time behaviour was reported in the numerical simulation by Godfrey (1977 and 1979).

Various possibilities exist for the oscillations seen in the present study. Essentially this has to be due to some perturbations in the beam and plasma densities. One of the possibilities is that of the perturbation propagating with the beam velocity ($\sim 10^8$ m sec^{-1}). This would give rise to a period of oscillation of the order of 0.1 nsec. (Probe dimension = 1.5 cm and axial resolution is of the order of the probe dimension). But the observed period is much more ($\simeq$ 40 nsec). This indicates an axial velocity for the perturbations of the order of 10^6 m sec^{-1}. So a time of flight measurement using the wall probes should have given a delay of the order of 1 μsec over a distance of 1 m. But the time of flight measurements did not yield any appreciable delay within the experimental error ($\simeq$ 4 nsec).

Another possibility is an axially independent perturbation. This can arise due to some coherent radial oscillation of the charge density.But it has not been possible to identify the exact cause leading to the observed potential oscillations.

In the experiments of Smith et al (1986),optimum beam transport was observed at about 80 mTorr for Nitrogen and Argon gases used by them. Here, as well as in other experiments reported so far,the charge neutralisation time is more than the beam rise time for low pressures (a few tens of mTorr).For the case where the plasma electrons are confined against radial loss by the external field or self B_θ field of the beam,the inductive axial electric field has been seen, in the present study, to influence the charge neutralisation process. So for beams with charge neutralisation time greater than the beam current rise time, the charge neutralisation process become complicated due to the change in the direction of inductive electric field.

CHAPTER IV

EFFECT OF SELF MAGNETIC FIELDS ON REB DYNAMICS

4.1 Introduction

Based on single particle description, an electron beam approaching a cusp magnetic field with velocity in the axial direction will have electrons encircling the axis after crossing the cusp [Schmidt, 1962]. The parallel and perpendicular component of the velocity for an electron after crossing the cusp are, $v_z = (v_o^2 - r_c^2 \omega_c^2)^{1/2}$ and $v_\theta = r_c \omega_c$. r_c = cathode radius, $\omega_c = eB_o/(m_o \gamma)$, cyclotron frequency. So essentially, after crossing the cusp, the axial velocity of the electron reduces, being converted into azimuthal. So here one can define a threshold velocity for cusp cut off given by $V_{ocrit} = r_c \omega_c$. An electron injected with velocity below V_{ocrit} will get reflected at the cusp.

The azimuthal current contributed by the rotating beam emerging out of the cusp field will produce axial self-magnetic field. For an intense electron beam, this self field can be of the order of external field and will modify the external cusp field. So after the beam self magnetic fields have reached the peak value, the electrons that come in will see a modified cusp. Therefore the beam dynamics in the cusp modified by the self fields will be quite

different from the single particle description.The beam dynamics will also be influenced by the strong self azimuthal magnetic field. This chapter reports a study on the effect of self magnetic fields on the beam dynamics in a cusp field.

4.2 Experimental Arrangement

The schematic of the experimental system is as given in Chapter 2. The diagnostics used were Rogowskii coils for beam current,miniature Faraday cup for beam radial profile, 3 cm. diameter Faraday cup for cusp loss,miniature Faraday cup array for axial profile of the cusp loss,diamagnetic loop and magnetic probes for beam self magnetic fields.Two beams of peak energy 200 KeV and of different durations were used for the purpose.The first beam corresponded to a duration of 800 nsec, and the second one to a duration of about 350 nsec. The low duration was due to flashover problem in the diode region.But the shots were reproducible enough for the set of measurements done using this beam.

4.3.Numerical Model

A fully self-consistent calculation would involve solution of the Maxwell's equations using the beam current and charge densities to get the fields at any instant of time and use of these fields to push the representative electron in time as per the equation of motion. This

involves lengthy computer time.A much simpler calculation involves following the trajectories of a representative set of electrons using an approximate model for the self-fields based on actual measurements of the same. This has the disadvantage in that the calculation can be done only for those parameters used in the experiment.But this simple simulation aids in providing a better understanding of the experimental results and so was carried out.The study is centred over timescale greater than 200 nsec,where the electrostatic fields are zero - i.e. charge neutralised beam. A representative set of electrons were injected into the system near the anode wall with total energy = 100 KeV for beam 1 and 40 KeV for beam 2,corresponding to the time in which the self magnetic fields produced by these beams are maximum. These electrons were then followed till they reach the walls - axial or radial.The time involved was less than 10 nsec and so the magnetic fields can be assumed to be constant over the duration of the numerical run.In the experiment B_z and J_z were measured as a function of r and z for an external field of 300 gauss.From this,assuming axisymmetry,

$$A_\theta = 1/r \int B_z r dr$$

$$B_r = - \frac{\partial A_\theta}{\partial z}$$

$$B_\theta = \mu_0/r \int J_z r dr$$

$$E_r = 0 \quad ; \quad E_\theta = 0 \quad ; \quad E_z = 0$$

The external field was modelled by,

$$B_{ze} = -B_o \tan h(z/\xi), \quad \xi = 3 \text{ cm.}$$

B_o = value of external field in the uniform field region.

This model is different from that used in chapter III for the beam dynamics in the following respects. In chapter III, the interest was on the radial oscillations of the beam in the postcusp side, where axial dependence can be ignored. The evaluation of the electron trajectory through the cusp magnetic field, done here, requires axial and radial variations to be kept. Also the functional form of the self fields used here, corresponds to an actual fit for the observed field values at the time scale of interest.

The angular distribution for the electron beam injected through the Aluminium foil anode is given by,

$P(\theta)d\theta = 2/\bar{\theta}^2 \; \theta \; \exp(-\theta^2/\bar{\theta}^2)d\theta$ [Birkhoff, 1958]

$\bar{\theta}$ = mean scattering angle ($\simeq 44.5^\circ$ for 100 KeV electrons and $\simeq 106^\circ$ for 40 KeV electrons, injected through 6 μm Aluminium foil anode).

The electron beam was represented by superparticles with scattering angle ranging from 10° to 80° in step of 10°. For each value of θ, the perpendicular components of the velocity are given by,

$$v_\theta = v_o \sin\theta \sin\phi \; ; \; v_r = v_o \sin\theta \cos\phi \; ,$$

v_o = total velocity, ϕ = phase angle and was chosen between 0° and 90° in step of 15°. Both positive and negative values were taken. This gave 24 superparticles for each θ value giving a total number of 192 superparticles. All the superparticles were injected at the same spatial location carrying a current given by $I(n) = I_o W(n)/\sum_n W(n)$, n =particle number, I_o = total beam current. W(n) = weightage function given by the angular

distribution. The equation of motion was solved using fourth order Runge-Kutta method. Since the net magnetic field was nearly a constant over the duration of the numerical run, all the electrons injected with a given initial condition can be assumed to follow the same trajectory. So the trajectories of the given set of superparticles superimposed over one another would give the beam profile. The runs were made as a funtion of B_o. The self magnetic fields were included only for B_o = 300 gauss, where they were measured. From the positions and velocities of the superparticles, the radial profile of the beam current density, the cusp loss and the beam diamagnetism were computed as given below and compared with the experimental results. The current density J_z and J_θ were computed as,

$$J_z(r) = \sum_n [I(n)/(2\pi r(n)\Delta r)]$$

$$\& \quad J_\theta(r) = \sum_n [I(n)v_\theta/(2\pi r(n)\Delta r v_z)]$$

Δr is the radial resolution. Summation was done for electrons with r between $r - \Delta r/2$ and $r + \Delta r/2$. The computation was done for different value of z.

In the uniform field region, the axial dependence can be ignored and this gives, $\frac{\partial B_z}{\partial r} = -\mu_o J_\theta$.

This along with the flux conservation, $\int_0^{r_w} B_z r dr = 0$

gives, $B_z(0) = -2\mu_o/r_w^2 \int_0^{r_w} (\int_0^{r_2} J_\theta(r_1)dr_1)r_2 dr_2$

$B_z(0)$ is the beam axial magnetic field. The cusp loss was obtained by counting the number of electrons lost at the cusp.

4.4. Calculation regarding particle orbits in the uniform field region

The individual electrons of the REB injected in through the anode foil will not have straight trajectories due to the large transverse energy, arising out of anode foil scattering. So the beam will consist of electrons executing Larmor motion about the net magnetic field present. Based on the orbits, two categories of electrons can be defined - (1) axis encircling, and (2) axis non encircling. The axis encircling electrons will give axial beam diamagnetism, whereas the axis non encircling ones will give axial beam paramagnetism as seen from figure 4.1. This section deals with the conditions leading to these two categories of electrons. The radial extent of the beam for a given magnetic field is also examined.

Consider the case where the self fields are not present. Here, the radial equation of motion is given by,

$$\ddot{r} = r\dot{\theta}^2 - er\dot{\theta}B_{ze}/m_o\gamma \qquad -(1)$$

$$\gamma = (1-v^2/c^2)^{-1/2}$$

B_{ze} is the external magnetic field and is equal to $+B_o$ in the precusp region and $-B_o$ in the postcusp region. The canonical angular momentum, a constant for axisymmetric system, is given by,

$$P_\theta = m_o\gamma r^2\dot{\theta} - erA_\theta \qquad -(2)$$

A_θ is the vector potential $= \pm rB_o/2$, positive sign refers to precusp and negative sign refers to postcusp.

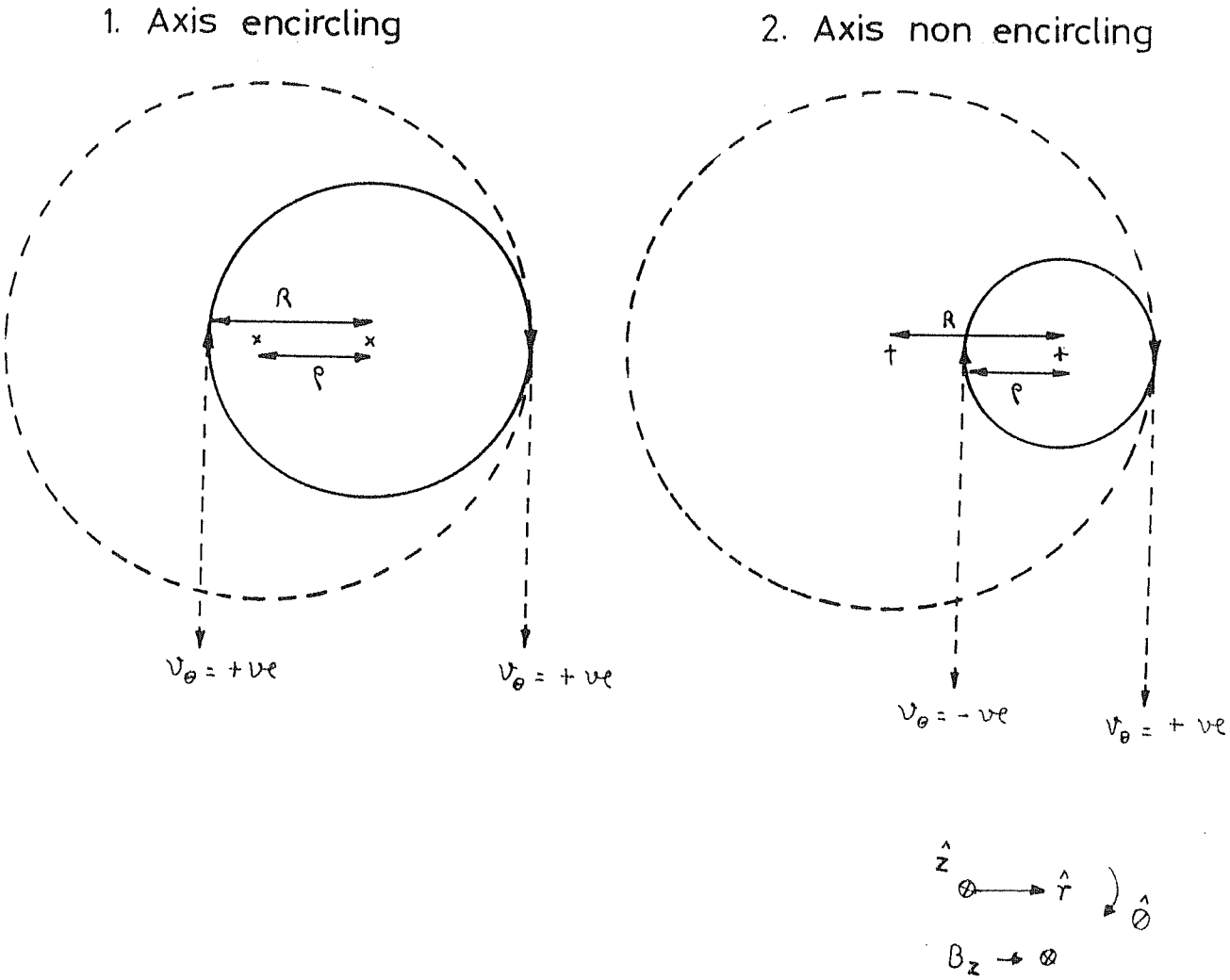

4.1 Electron orbits in the uniform field region.

(1) and (2) gives $\ddot{r} = (P_\theta/m_o\gamma)^2/r^3 - \omega_c^2 r/4$ .valid for both precusp and postcusp regions, $\omega_c = eB_o/(m_o\gamma)$ is the beam cyclotron frequency. Writing $\ddot{r}$ as $v_r\, dv_r/dr$ and integrating,

$$v_r^2/2 = -1/2(P_\theta/m_o\gamma)^2/r^2 - \omega_c^2 r^2/8 + \text{const.} \qquad -(3)$$

Let r_M and r_m denote the maximum and minimum radial points for an electron.At these two points,$v_r = 0$.This gives,

$$r_m r_M = 2|P_\theta|/eB_o \qquad -(4)$$

From figure 4.1,$r_m = |R - \rho|$ & $r_M = R + \rho$ $\qquad -(5)$

$$R^2 = (v_\perp^2/\omega_c \pm 2|P_\theta|/m_o\gamma)/\omega_c, \qquad -(6)$$

with $\rho = v_\perp/\omega_c$. So axis encircling orbit ($R < \rho$) will not be possible for $2|P_\theta|/m_o\gamma > v_\perp^2/\omega_c$ $\qquad -(7)$

From Figure 4.1, it is seen that with B_z positive (precusp region), an electron with initial v_θ negative,will execute axis non encircling orbit.An electron with initial v_θ positive, will not execute axis encircling orbit if (7) is satisfied.

From (7), $|2|v_\theta| - r_o\omega_c| > v_\perp^2/r_o\omega_c$,for axis non enircling. Now the equality sign gives,$2|v_\theta| = r_o\omega_c \pm v_\perp^2/r_o\omega_c$

For $2|v_\theta| = r_o\omega_c - v_\perp^2/r_o\omega_c$, $2|v_\theta| < r_o\omega_c$ and any value of $2|v_\theta| < r_o\omega_c - v_\perp^2/r_o\omega_c$ will make $|2|v_\theta| - r_o\omega_c| > v_\perp^2/r_o\omega_c$. Similiarly, any value of $2|v_\theta| > r_o\omega_c + v_\perp^2/r_o\omega_c$ will make $|2|v_\theta| - r_o\omega_c| > v_\perp^2/r_o\omega_c$. Now it can be shown that $2|v_\theta| > r_o\omega_c + v_\perp^2/r_o\omega_c$ is not possible,maximum value of v_θ being $v_\perp$. So this gives a maximum value on v_θ for axis non encircling orbits and is given by,

$$2v_{\theta max} = r_o\omega_c - v_\perp^2/r_o\omega_c$$

$$v_{\theta max} = 0 \text{ for } r_o\omega_c < v_\perp^2/r_o\omega_c$$

The effect of external magnetic field and the self magnetic fields on $v_{\theta max}$ will be examined in the following subsection.

The radial extent of the beam can now be evaluated. In terms of R and ρ, $r_m r_M = R^2 - \rho^2$. Also it has been shown that $r_m r_M = 2|P_\theta|/eB_o$. This gives,

$$|R^2 - \rho^2| = 2|P_\theta|/eB_o$$

i.e. $R^2 = \rho^2 \pm |2r_o v_\theta/\omega_c - r_o^2|$. Positive sign for axis non encircling orbit ($R > \rho$) and negative sign for axis encircling orbit ($R < \rho$). Maximum value of R occurs for $v_o = -\rho\omega_c$, and it corresponds to axis non encircling orbit.

$$\text{i.e. } R_{max} = (\rho^2 + 2r_o\rho + r_o^2)^{1/2}.$$

The maximum radial extent of the beam (maximum value of r_M) will be $R_{max} + \rho = \rho + (\rho^2 + 2r_o\rho + r_o^2)^{1/2}$. So for the beam to be radially confined,

$$(\rho^2 + 2r_o\rho + r_o^2)^{1/2} + \rho \leq r_W$$

For our case $r_W = 15$ cm, $r_o = 2$ cm. This gives the maximum value of ρ for an electron to be just radially confined as 6.5 cm. This corresponds to a magnetic field of about 145 gauss for a perpendicular velocity of 0.55 c (100 KeV electron). So an external field above 145 gauss is sufficient to provide radial confinement for the 100 KeV beam, even for those suffering 90^o scattering at the foil. For 40 KeV beam, this corresponds to about 100 gauss.

4.4.1. Effect of external and self-magnetic fields

From the expression of $v_{\theta max}$ given in the last subsection, it can be seen that $v_{\theta max}$ increases with

external field (B_o).So this will lead to an enhancement in the number of axis non encircling electrons.Physically,with increase in B_o,the Larmor radius, ρ ,decreases.So this will make an electron, which was encircling the axis at lower values of B_o, to execute axis non encircling orbit.The effect of self magnetic fields can also be seen qualitatively. Self diamagnetic field will cause the net axial magnetic field to decrease.This gives a reduction in the value of $v_{\theta max}$, thereby enhancing the number of axis encircling electrons. So the axial component of the self magnetic field will enhance the number of axis encircling electrons leading to enhancement in the beam axial diamagnetism.

4.5 Results and Discussion

4.5.1.Precusp region

The net beam current (beam current and axial plasma current induced by the beam fields) measurement was done at z = -8 cm from the cusp (7 cm from the anode) using Rogowski coil. (negative distance from the cusp refers to precusp region and positive distance refers to postcusp region, with the cusp plane of the external field at z = 0). Typical oscilloscope trace is shown in figure 4.2.The maximum value of the net current was about 3 KA.The decay time of the net current was seen to be about 2 μsec.By integrating the beam current density, obtained using miniature Faraday cup (discussed later), over the beam

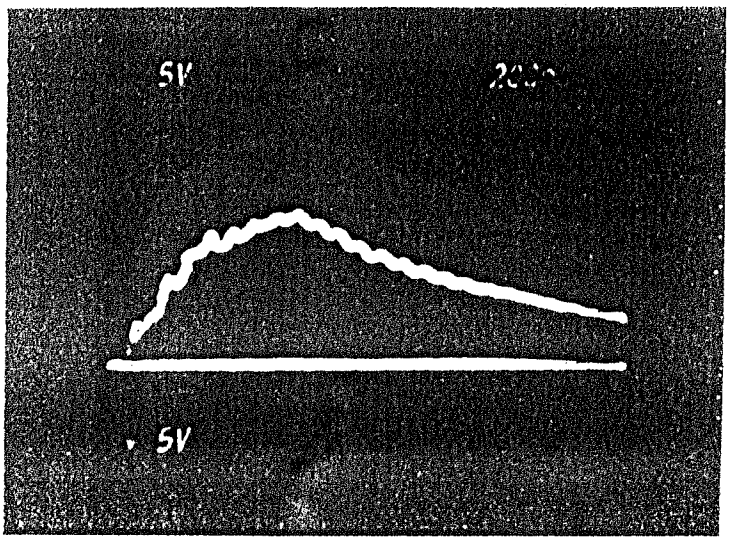

4.2 Oscilloscope trace of the net beam current.

cross-section, the total beam current was evaluated.It was seen to be about 3.5 KA.So this corresponds to a peak axial return current of about 0.5 KA.

Plasma heating by return currents can be estimated in terms of a resistivity.A crude estimate can be obtained by using the value of return current obtained as above.The power density input to the plasma electrons, $\dot{Q}$ is given by $j^2\eta$, where j=return current density and η = resistivity.The return current decay time is given by $4\pi a^2/(\eta c^2)$, a = beam radius. The observed decay time of 2 μsec gives $\eta \simeq 5.65 \times 10^{-4}$ ohm.m. The average return current density $\simeq 1.8 \times 10^5$ amp m^{-2}, decaying exponentially. This gives $\dot{Q} \simeq 1.8\, e^{-2t/\tau_D}$. τ_D = decay time. Equating the power density input to plasma internal energy density,

$$3/2 n_e K T_e = \dot{Q}$$

This gives a plasma electron temperature (T_e) of about 7.5 eV. for plasma density (n_e) of about 10^{13} cm^{-3}.The corresponding diamagnetism for an external field of 300 gauss will be only about 2 %.

Information regarding azimuthal symmetry of the beam was obtained by examining the damage pattern on a perspex plate placed in the path of the beam.This is given in figure 4.3 for an external field of 300 gauss and a background pressure of 225 mTorr for different axial locations. The beam was seen to be non hollow,more or less azimuthally symmetric.

At the time of injection,the beam is annular of mean radius $\simeq$ 2 cm.The filling in,making the beam non hollow,is

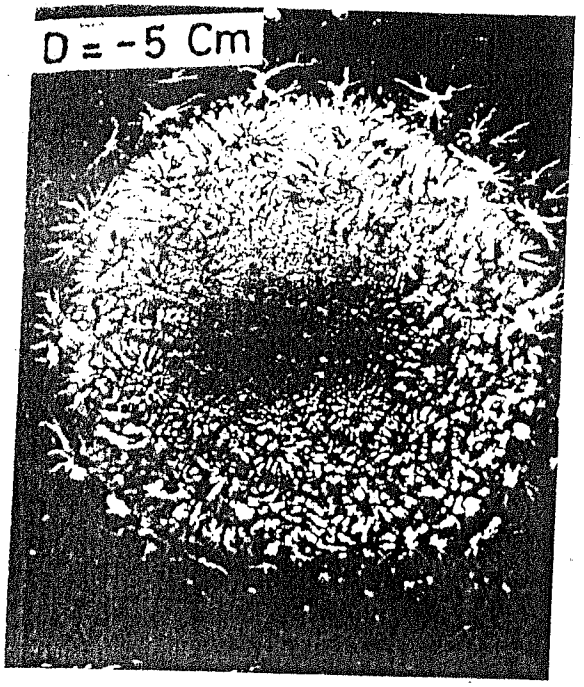

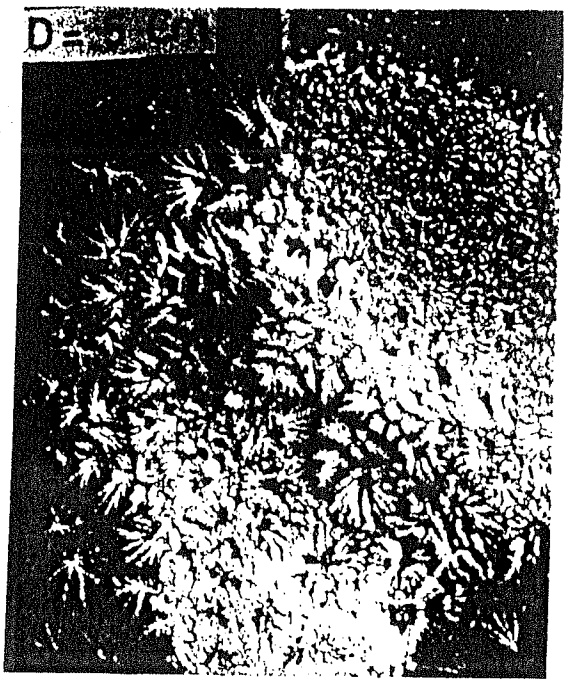

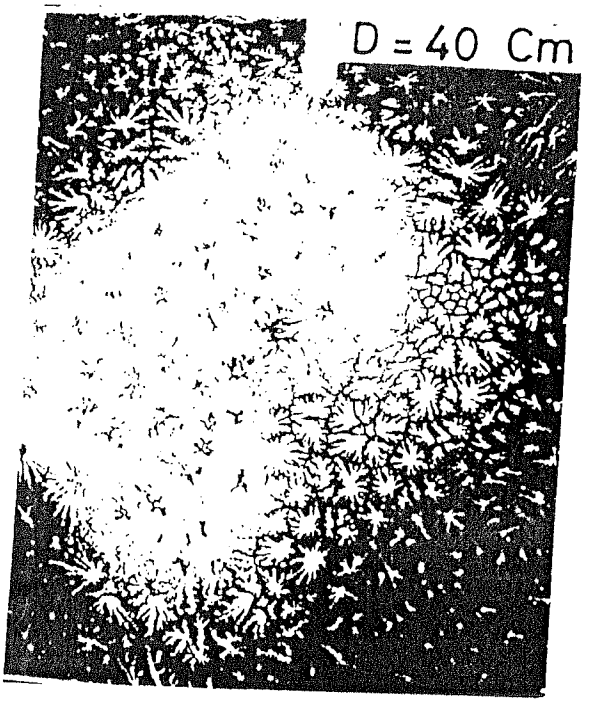

(D refers to axial distance with the cusp point as the origin).

4.3 Damage pattern on perspex plates.

due to the large scattering at the anode foil.For beam with $\omega_{pb}^2\beta^2/\omega_{cb}^2 > 1$,filamentation instability is usually seen [Kapetanakos, 1974]. ω_{pb} = beam plasma frequency, ω_{cb} = beam cyclotron frequency and β = beam velocity/c.For our case, $\omega_{pb}^2\beta^2/\omega_{cb}^2 \simeq 3$ for B_o = 300 gauss.But filamentation was not seen in the damage pattern taken upto 55 cm from the anode. The growth rate for the instability $\sim \omega_{pb} \simeq 1.7 \times 10^{10}$ sec^{-1}, and so the instability should have developed over a distance of a few cm.Davidson et al (1975) had shown the stabilizing effect of self magnetic fields on filamentation instability. Their calculation gives the threshold value of magnetic neutralisation for the filamentation instability to occur as,

$f_M > (1+ \omega_{pb}^2\beta^2/\omega_{cb}^2)/(2\,\omega_{pb}^2\beta^2/\omega_{cb}^2)$

f_M = current neutralisation factor.This gives,for our case, $f_M > 0.66$ for filamentation. But f_M in our case < 0.15 as seen from the total beam current ($\simeq$ 3.5 KA using Faraday cups) and net beam current ($\simeq$ 3 KA using Rogowski coil) measurements.

The radial extent of the beam evaluated numerically is given in figure 4.4 for an external field of 300 gauss. Figure 4.4(a) corresponds to calculation without the self fields included. Due to the large scattering at the anode foil, the beam spreads out.The maximum radial extent of the beam in the precusp region was seen to be about 9 cm.From the calculation done with the self fields included,it was seen that the maximum radial extent of the beam in the precusp region got reduced to about 7.5 cm.(Figure 4.4(b)).

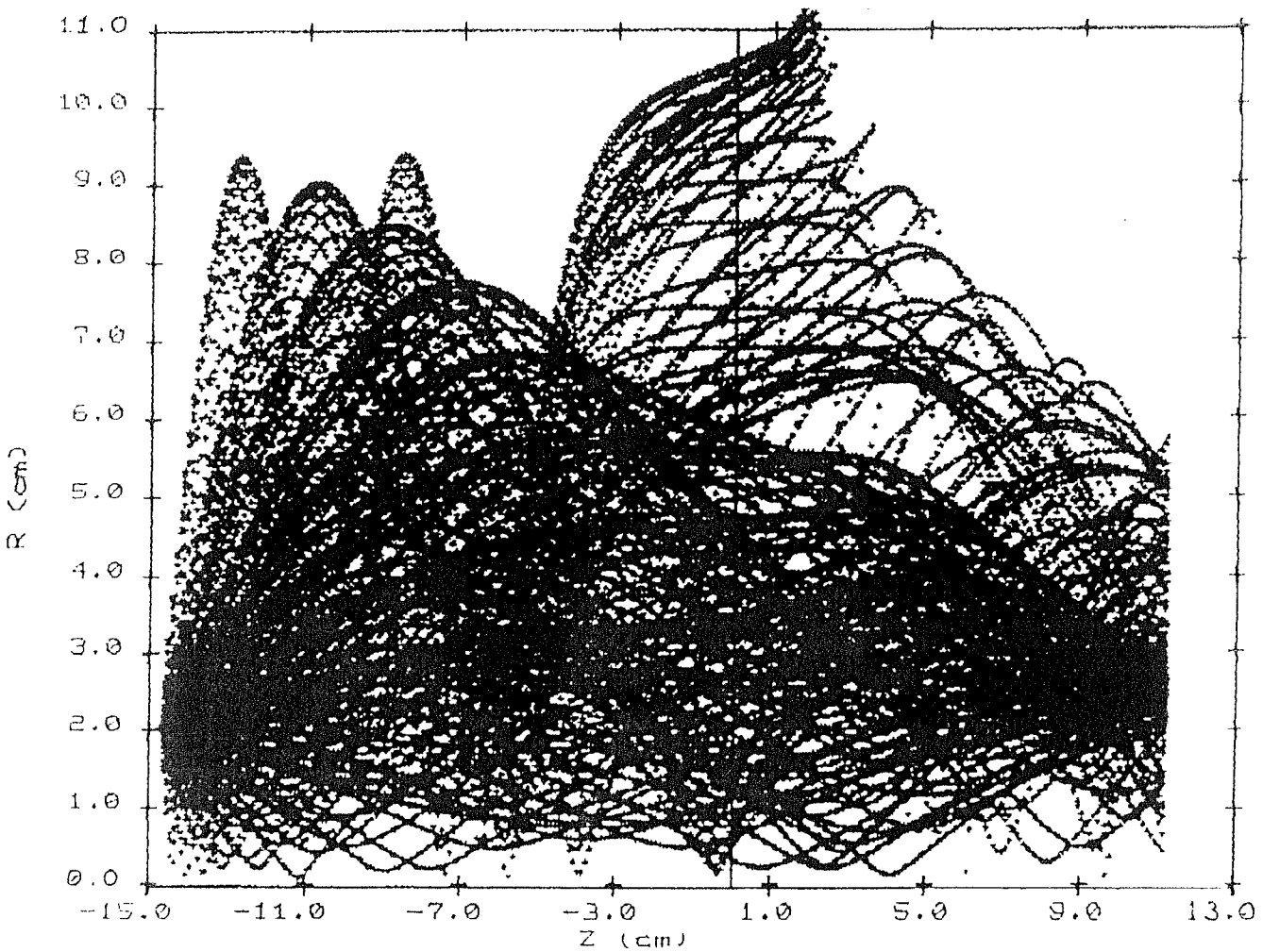

4.4(a) Beam profile with external fields alone present.

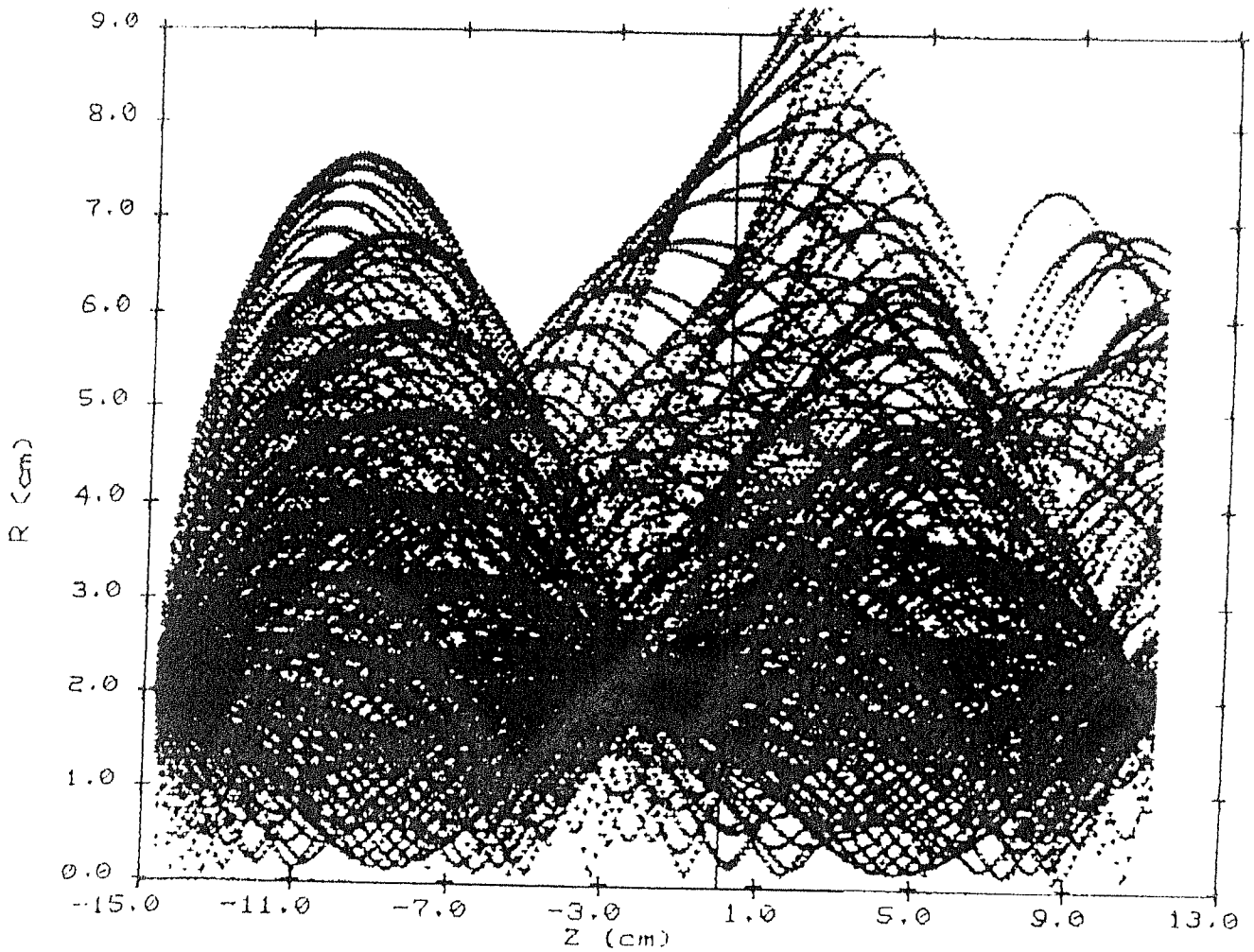

4.4(b) Beam profile with external fields and self fields.

The radial profile of the beam current density was measured using miniature Faraday cup for different axial locations and it is shown in figure 4.5. Figure 4.5(a) and 4.5(b) correspond to the precusp region. The results of the numerical calculation, with the self fields included, are also shown. The peak beam current density was seen to occur within a radial distance of 3 cm. The density was seen to decay off to zero over a radial distance of about 6 cm.

Beam axial diamagnetism was observed in the precusp region using diamagnetic loop and magnetic probes. Typical oscilloscope traces are given in figure 4.6. It was seen that the signal rises in about 500 nsec and decays off in about 1 μsec. The rise time of the diamagnetic signal matches with the current rise time shown in figure 4.2. The larger decay time of the net beam current is due to the plasma return current.

The contribution to the beam axial diamagnetism comes from the axis encircling electrons. The axis non encircling electrons will give a net axial paramagnetism as mentioned in section 4. The dependence of $v_{\phi max}$ for axis non encircling electrons on B_o is given in table 4.1. The nature of the beam axial magnetic field for higher beam energy and higher magnetic field can be seen from this table. It is seen that with increase in the beam energy, $v_{\phi max}$ approaches $v_\perp$ for lower values of B_o giving lesser number of axis encircling electrons. So for a higher energy beam and a higher magnetic field, beam axial diamagnetism will not be seen.

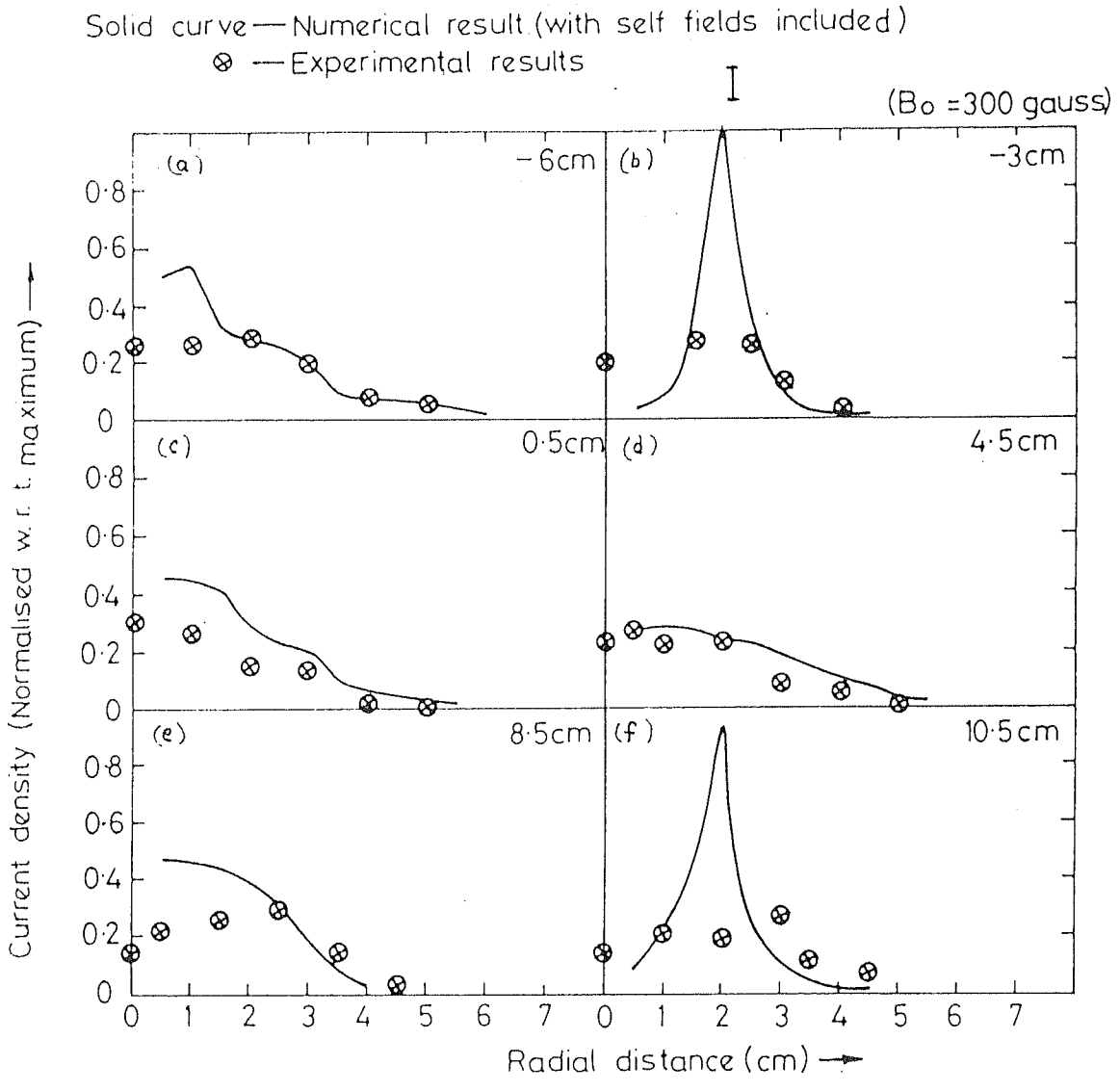

4.5 Radial profile of the beam current density.

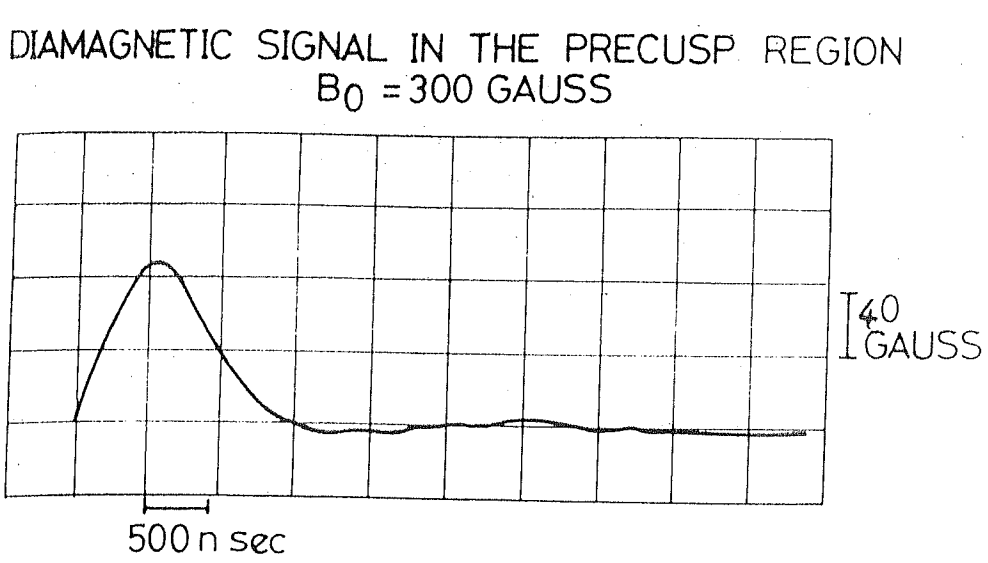

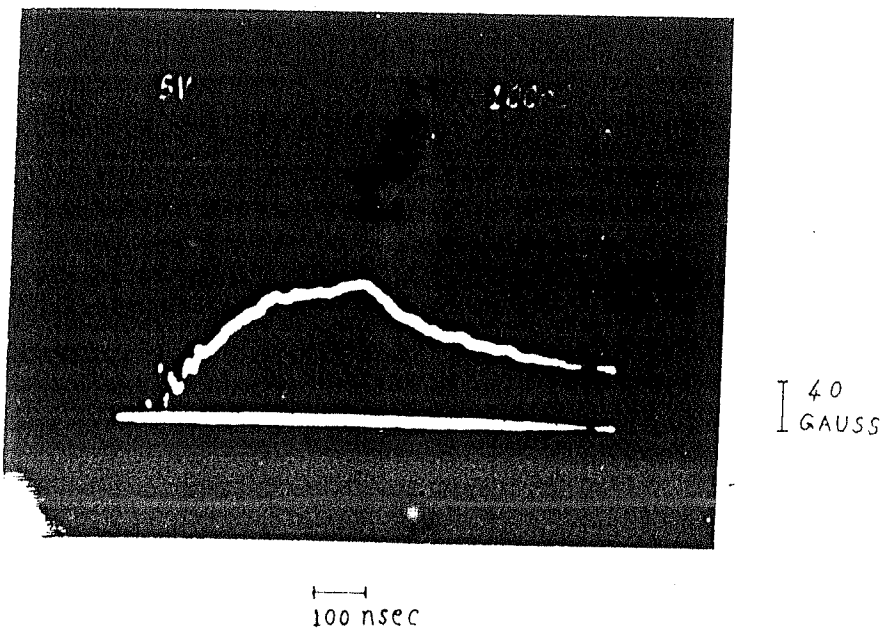

4.6 Traces of precusp diamagnetic signal.

TABLE 4.1

Beam energy (KeV)	Average scattering angle($\bar{\theta}$)	$v_\perp/c$ for this $\bar{\theta}$	B_o (gauss)	$v_{\theta max}/c$ for r_o = 2cm
100	44.5	0.38	100	-
			200	-
			300	-
			400	0.08
			500	0.17
			600	0.25
500	10.0	0.15	100	-
			200	0.07
			300	0.15

The dependence of beam axial magnetic field (ΔB_z) on external field (B_o) is given in figure 4.7.Here $\Delta B_z/B_o$, which gives the strength of the beam self field compared to the external field vs. external field is plotted.The curve based on single particle description,obtained numerically, is also shown. In the single particle description,it was seen that $\Delta B_z/B_o$ decreases slowly with increase in B_o upto 400 gauss and thereafter it decreases at a faster rate.The lower value at 100 gauss is because fields below 145 gauss is insufficient to prevent radial loss in the precusp region.

Based on the calculation of particle orbits given in section 4,the typical variations of r_M and r_m (farthest and closest distances from the axis respectively) with B_o are shown graphically in figure 4.8.It was seen that for both axis encircling and axis non-encircling orbits, the variation of r_M with B_o is more or less hyperbolic.In both cases, a decrease of r_M gives an increase in the axial diamagnetism. Since the rate of decrease of r_M decreases with increase in B_o, the rate of increase in the axial diamagnetism also decreases. For axis non encircling electrons, r_m increases with B_o, and for axis encircling electrons, r_m decreases with increase in B_o,both leading to a net increase in axial diamagnetism with B_o.Again the rate of increase of the beam axial diamagnetism reduces for higher values of B_o.Also plotted in figure 4.8 is the ratio of axis encircling electrons to the axis non encircling electrons. It was seen that the ratio decreases more or less

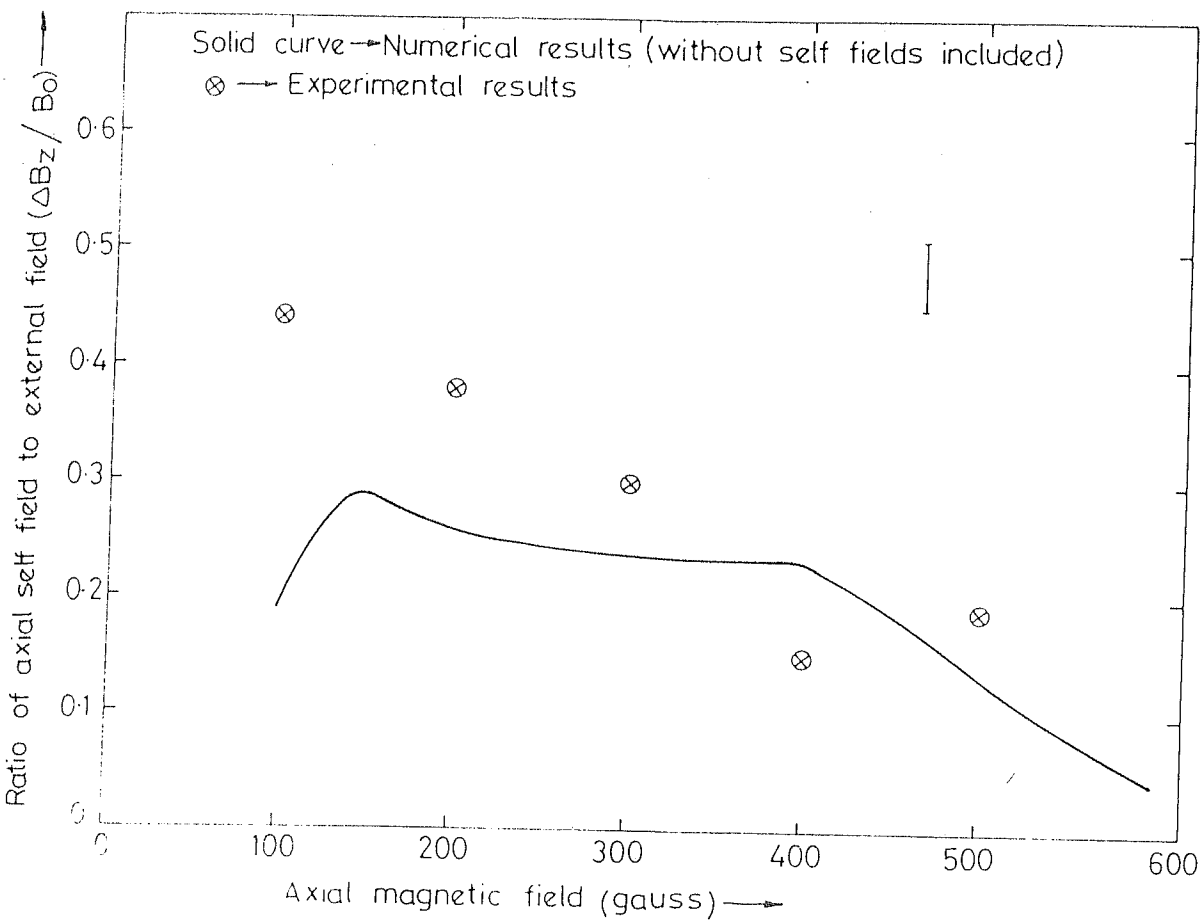

4.7 Axial self magnetic field (in the precusp)/external field vs. external field.

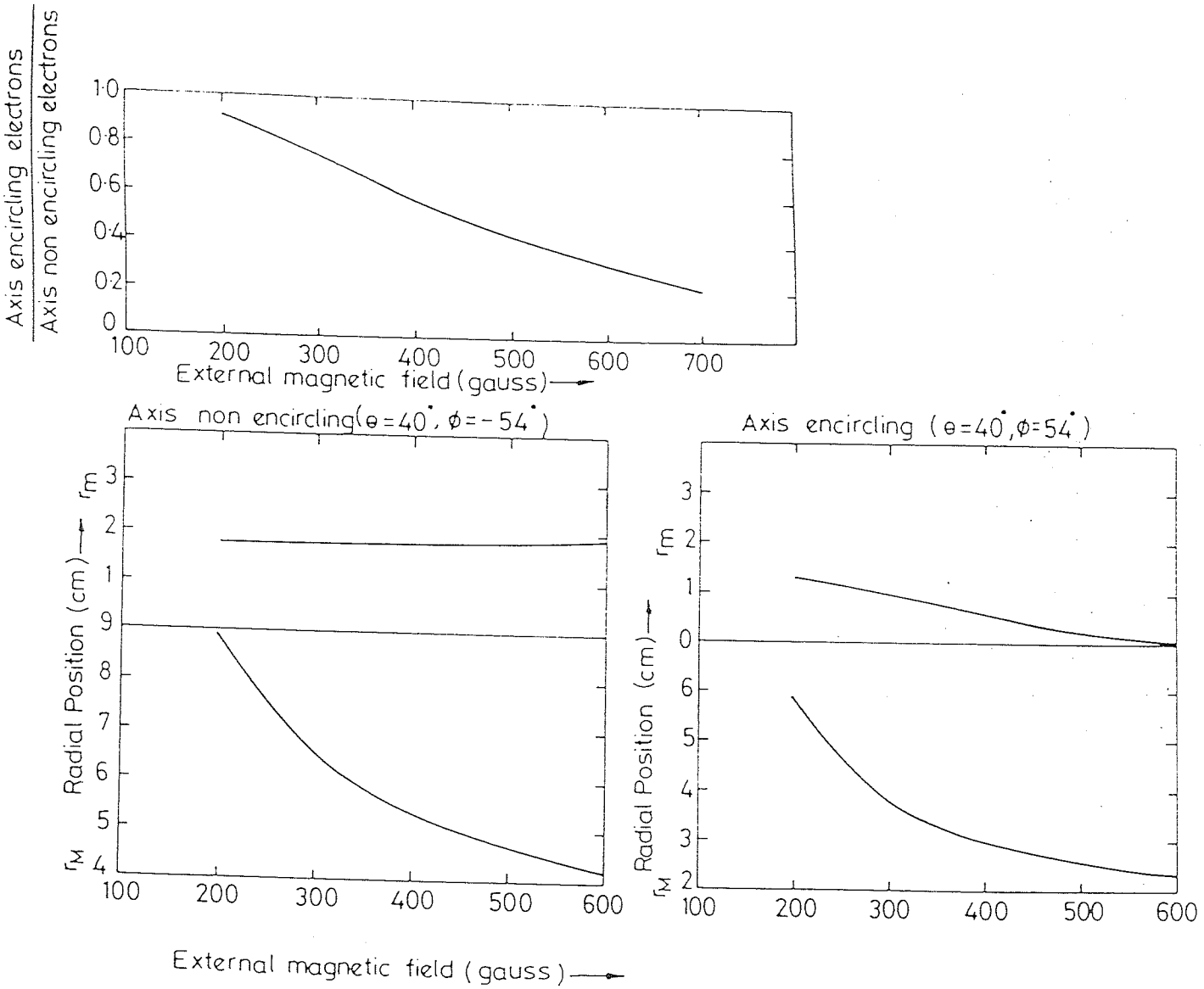

4.8 Features of the electron orbits in the uniform field region.

linearly with increase in B_o. Now, with increase in B_o, we have decrease in the ratio of axis encircling electrons to the axis non encircling electrons and a decrease in the rate of increase of axial diamagnetism for a given category of electron orbit. As a result, the ratio of axial diamagnetism to the external field decreases at a faster rate for higher values of B_o as seen in the numerical curve in figure 4.7.

Experimentally also it was seen that $\Delta B_z/B_o$ decreases with increase in B_o. But for lower values of B_o, the experimental values were seen to be more than that predicted by the single particle description. At low values of B_o, the decrease in the net axial magnetic field is significant. So the electrons that come in around 500 nsec (time in which the self magnetic field is maximum) see a reduced value of axial magnetic field. So the resultant value of $\Delta B_z/B_o$ is more than that predicted by the single particle description.

The beam axial diamagnetism was found to vary with distance from the anode and is shown in figure 4.9. Upto 500 nsec, the peak diamagnetism was seen to occur at about 5 cm from the anode. At about 600 nsec, it becomes more or less constant over the axial distance. Above 700 nsec, it decays off with the rate of decay increasing with the distance from the anode. The reduction in the diamagnetism near the anode upto 500 nsec can be due to eddy currents generated on the anode wall.

In summary, the electrons approaching the cusp were seen

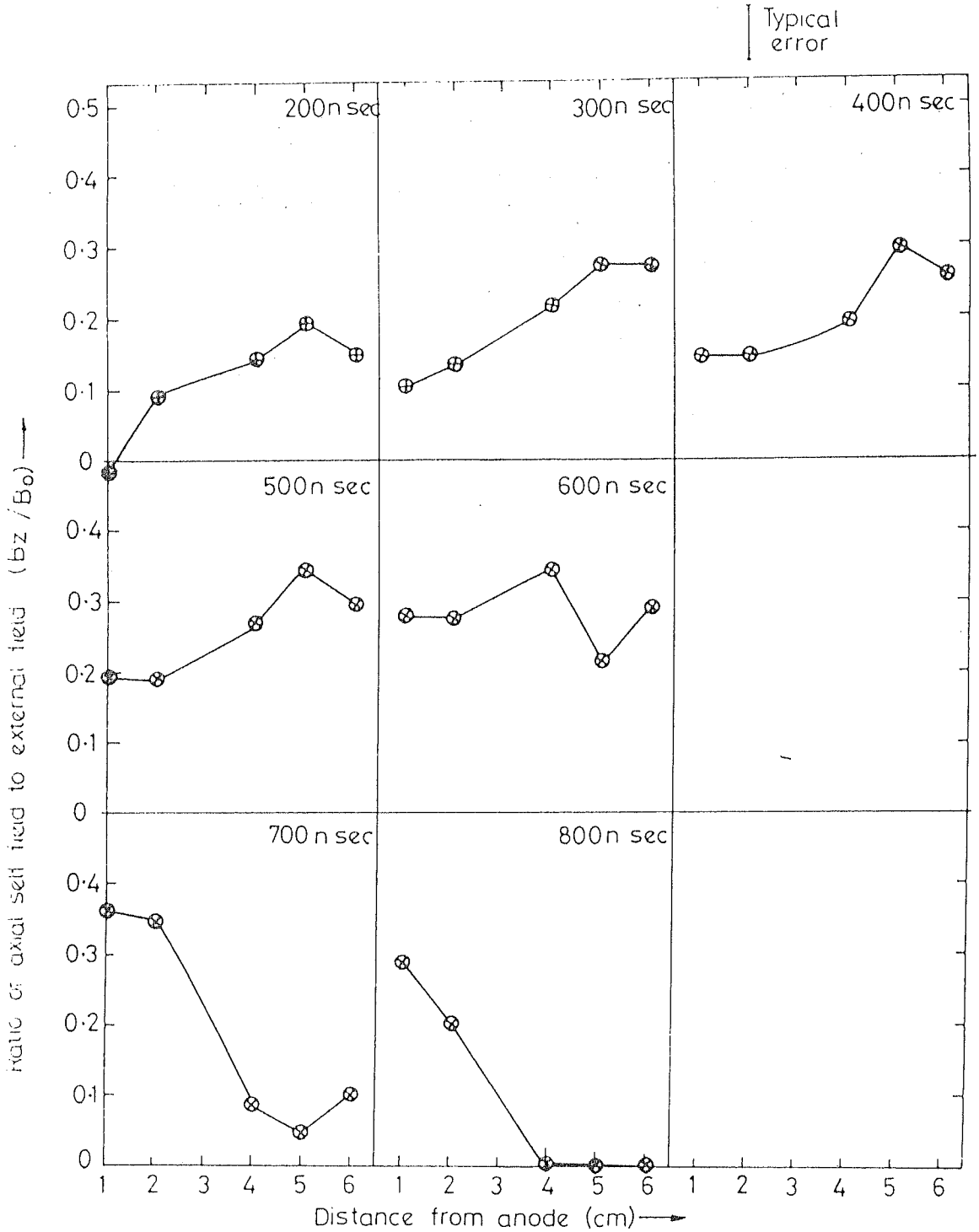

4.9 Variation of precusp axial self magnetic field with dstance from the anode.

to have large transverse energy due to scattering at the anode foil. Based on the orbits, two categories of electrons were seen to be present - (1) those encircling the axis giving an axial diamagnetism and (2) those that do not encircle the axis giving an axial paramagnetism. A net axial diamagnetism was observed in the precusp indicating the contribution of axial paramagnetism from the axis non encircling electrons to be less dominant compared to the contribution of axial diamagnetism from the axis encircling and axis non encircling electrons.

4.5.2. Cusp region

The beam self magnetic field reaches a maximum in about 500 nsec for the higher energy beam and in about 200 nsec for the lower energy beam, the total duration of the beam being about 800 nsec for the higher energy beam and about 350 nsec for the lower energy beam. The transit time for a electron from the injection point to the exit of the experimental chamber is less than 10 nsec. So the electrons that enter the system around the time in which the self magnetic fields have peaked, will see a cusp magnetic field, modified by the self magnetic fields.

The extent of modification of the external cusp was obtained by using an array of magnetic probes, movable radially. The magnetic probes give the beam self magnetic field (ΔB_z) as a function of z for different values of r. A best fit to the data was obtained using Simplex scheme. The fit gave ΔB_z as a function of r and z. The net magnetic

field $B_z(r, z)$ was obtained by adding $\Delta B_z(r, z)$ to the external field $B_{ze}(r, z)$. Using this, contours of constant flux were plotted to get the field configuration seen by the electrons as a function of time.

The time evolution of the axial component of the beam self magnetic field is plotted in figure 4.10 and 4.11. These correspond to beams of duration 800 nsec and 350 nsec respectively. For the beam of 800 nsec duration, it was seen that the self field (diamagnetic) in the postcusp region increases in time reaching a maximum around 600 nsec and decays off to zero in about 1.6 μsec. In the precusp region, the axial self field was seen to be diamagnetic during the beam duration and paramagnetic thereafter. (The external field is positive in the precusp region and negative in the postcusp region).

For the beam of 350 nsec duration, the axial self field was diamagnetic in the postcusp region and paramagnetic in the precusp region at all times. In the postcusp region, the fields peaked at about 200 nsec and decayed off to zero in about 1.5 μsec. In the precusp region, it was seen to peak in about 900 nsec and decay in about 2 μsec. In the postcusp region, the fields were also seen to be oscillatory. This can be due to some coherent radial oscillations of the electrons similar to the type described by Rhee and Destler (1974).

The rotation imparted to the beam after crossing the cusp, results in the observed postcusp axial diamagnetic field. The field in the precusp region produced by this

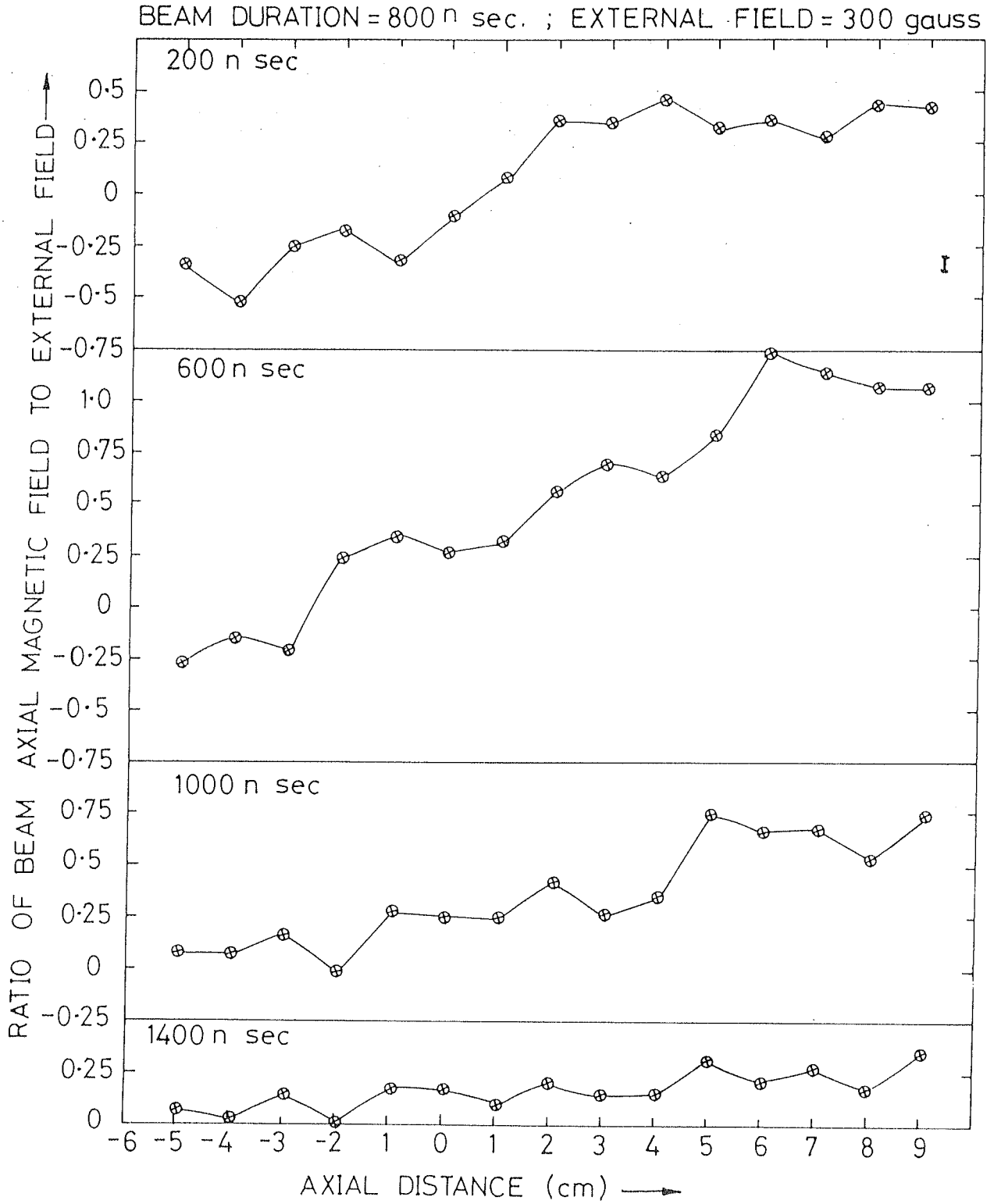

4.10 Time evolution of the axial self magnetic field for different axial locations (beam duration = 800 nsec).

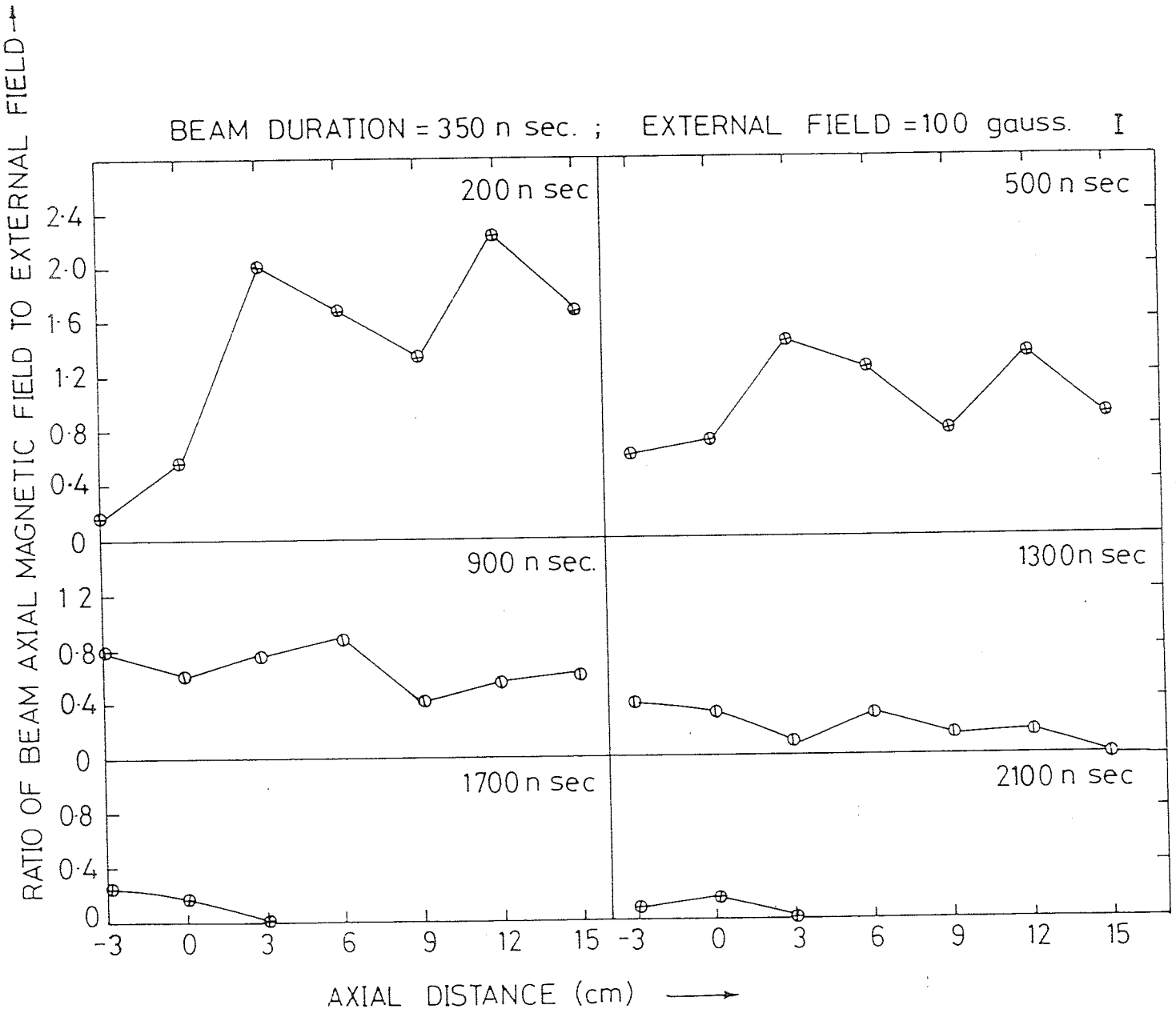

4.11 Time evolution of the axial self magnetic field for different axial locations (beam duration = 350 nsec).

rotating beam, will be paramagnetic. The large transverse energy of the beam due to anode foil scattering has been shown to result in beam axial diamagnetism.For the 800 nsec beam, the self field produced by the rotating beam of the postcusp being small,the observed net field in the precusp is diamagnetic. For the 350 nsec beam,the effect of self field produced by the rotating beam of the postcusp is dominant in the precusp region.The self fields produced by the beam are sustained by the plasma currents induced by the beam fields. The observed paramagnetic signal in the precusp region after the beam duration for the 800 nsec beam shows that significant azimuthal plasma currents are not induced in the precusp region.The maximum modification of the cusp field occurs around 200 nsec.After 200 nsec,the field configuration relaxes back to the original value,with the cusp plane moving back to its original position.This causes an axial compression of the azimuthal return current layer in the cusp region producing an enhancement in the diamagnetic field over there.This results in the observed rise time of 900 nsec for the diamagnetic field in the cusp region. The self fields finally resistively decay off to zero. The observed field decay time matches with the net beam current decay time.

Figure 4.12 and 4.13 give the field configuration as a function of time for the two beams. Figure 4.12(a) to 4.12(e) correspond to the beam of higher energy.The beam diamagnetic field pushes the field lines out as is seen in the field plots. The diamagnetic field increases in time

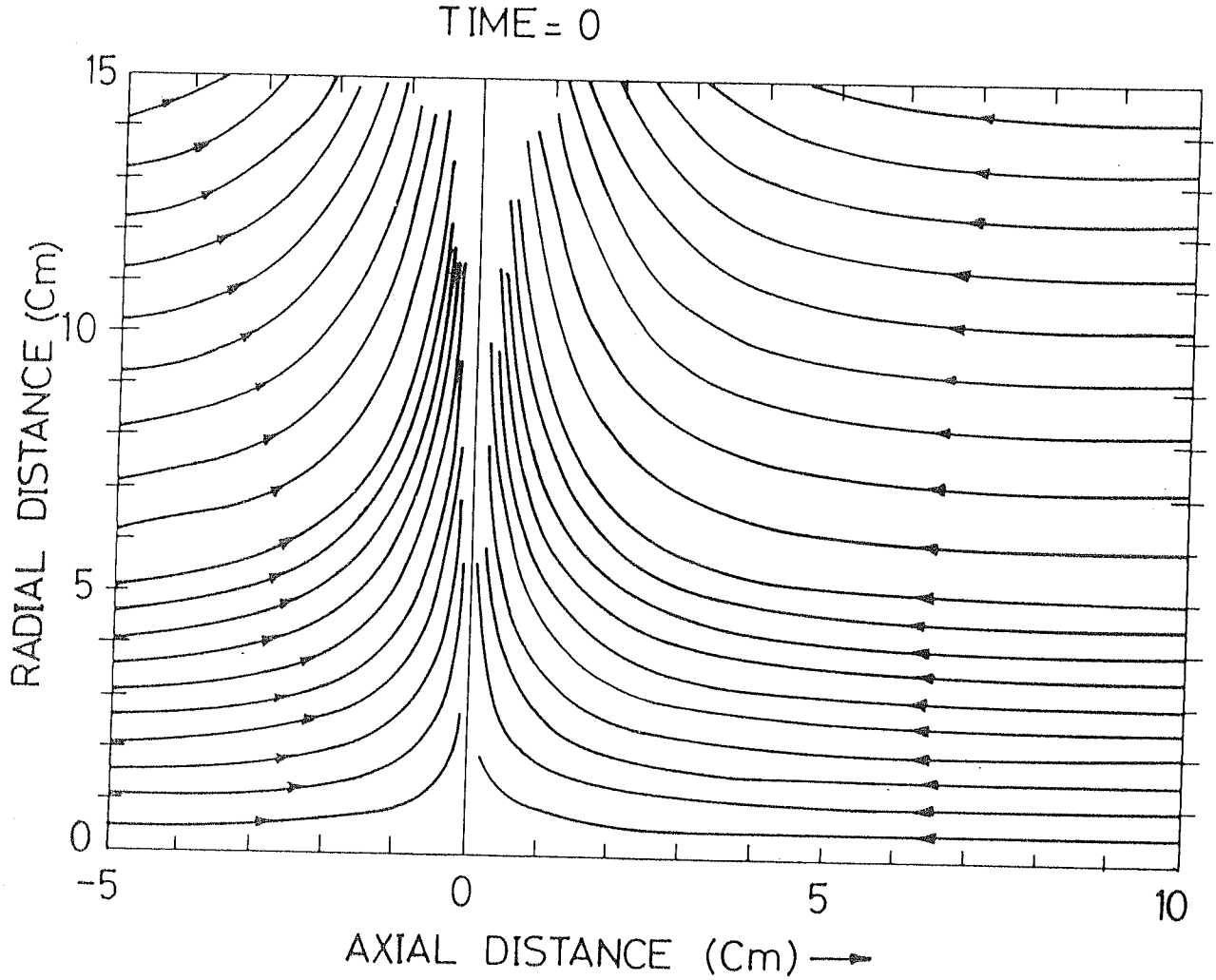

4.12(a) Constant flux plot.

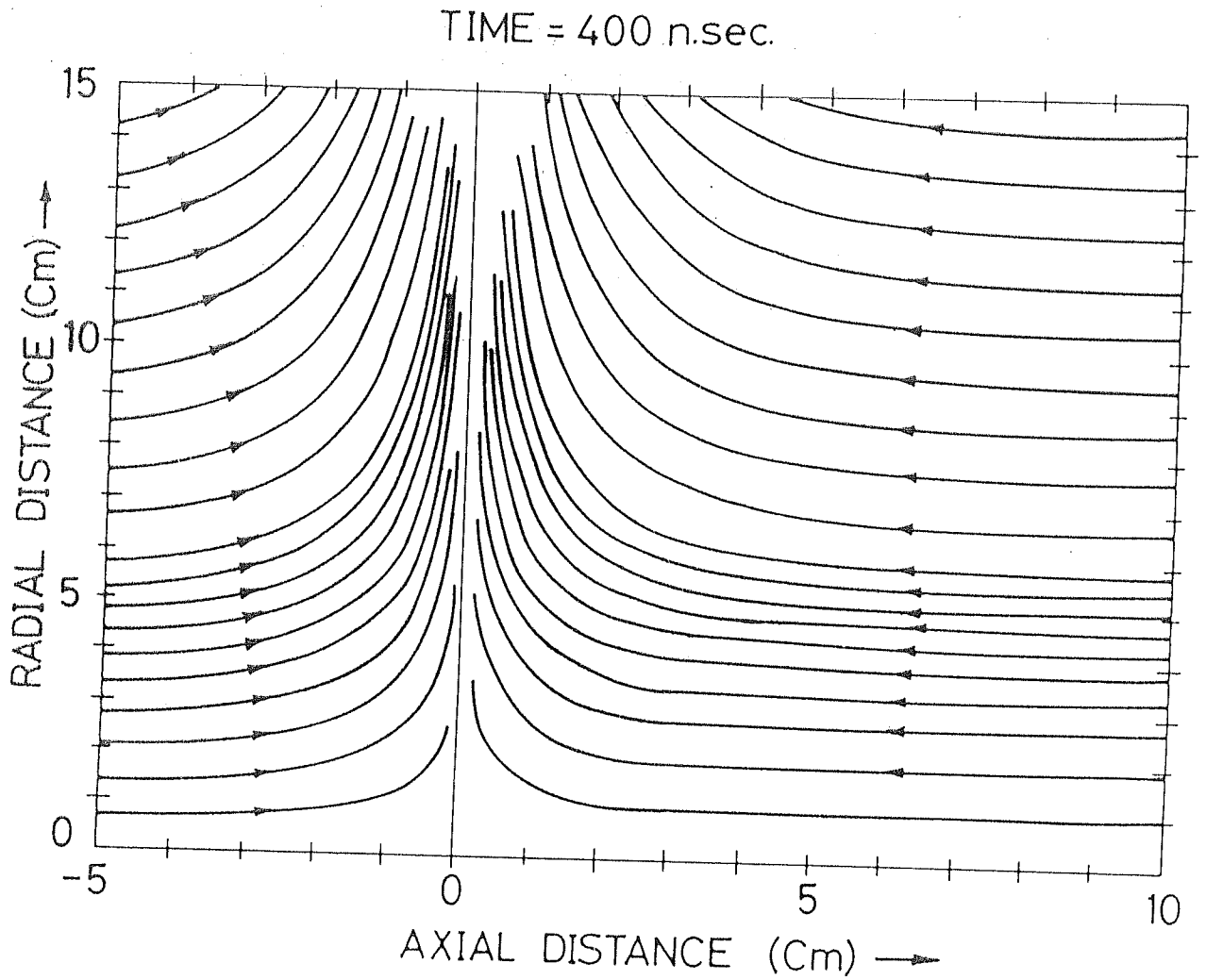

4.12(b) Constant flux plot.

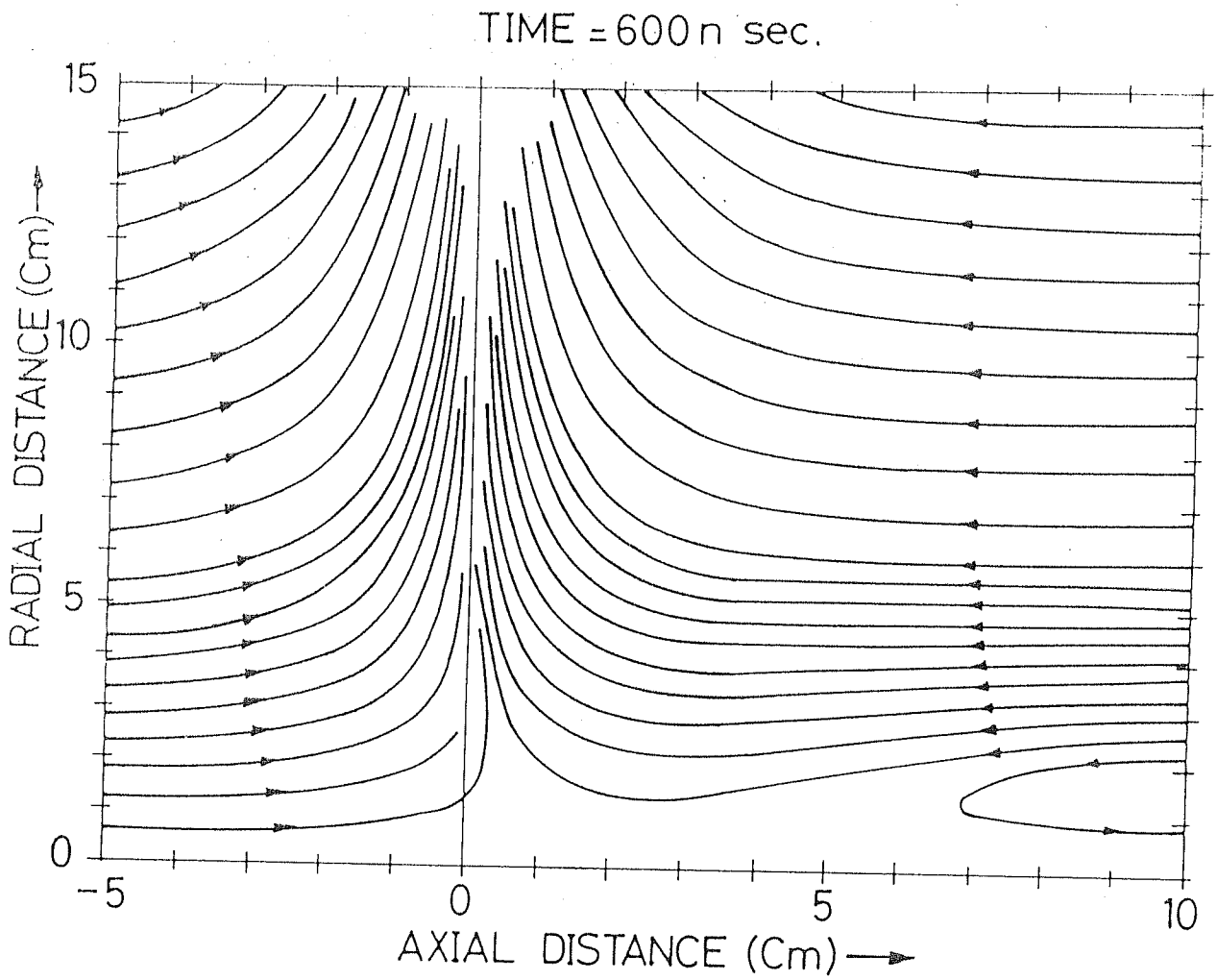

4.12(c) Constant flux plot.

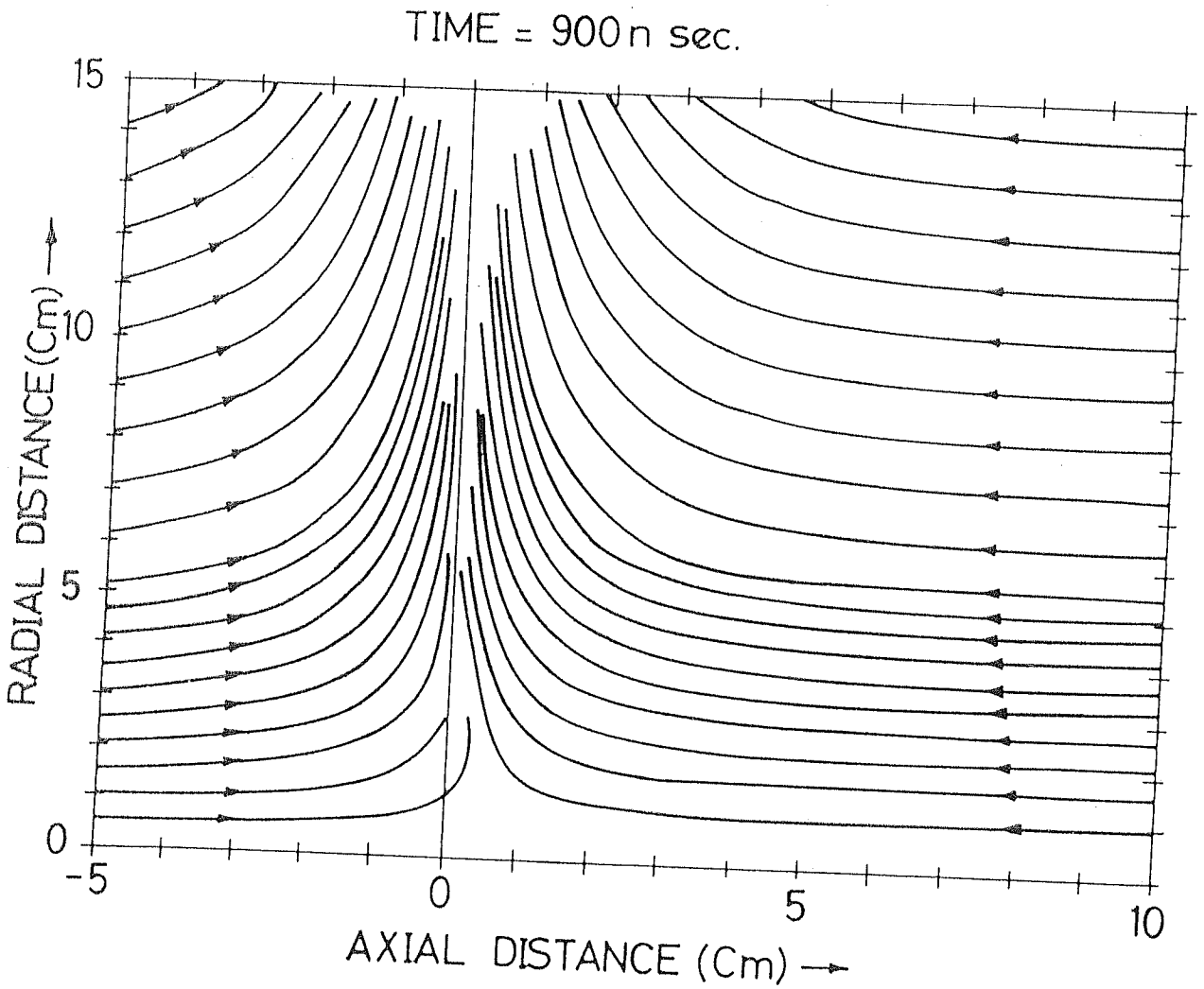

4.12(d) Constant flux plot.

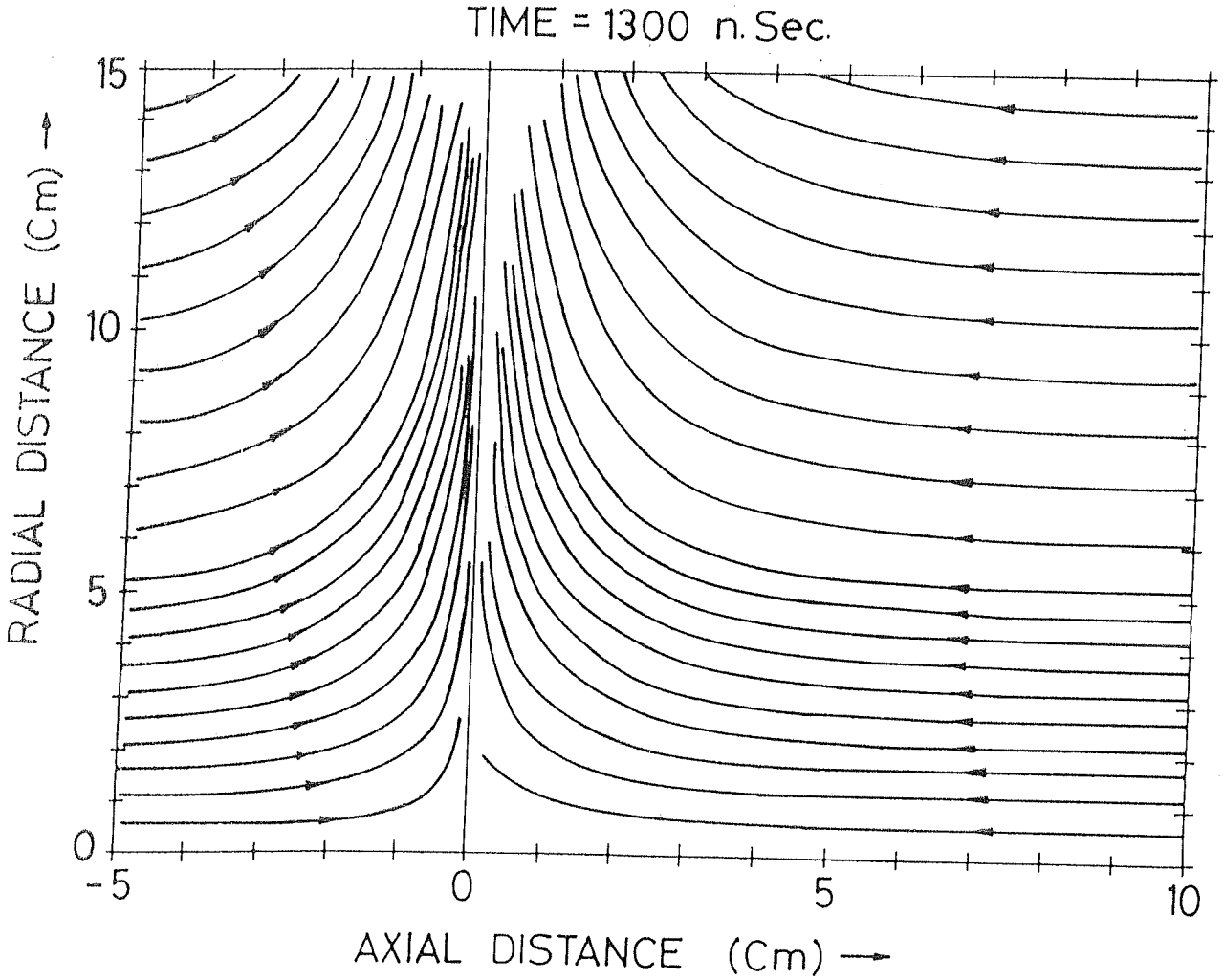

4.12(e) Constant flux plot.

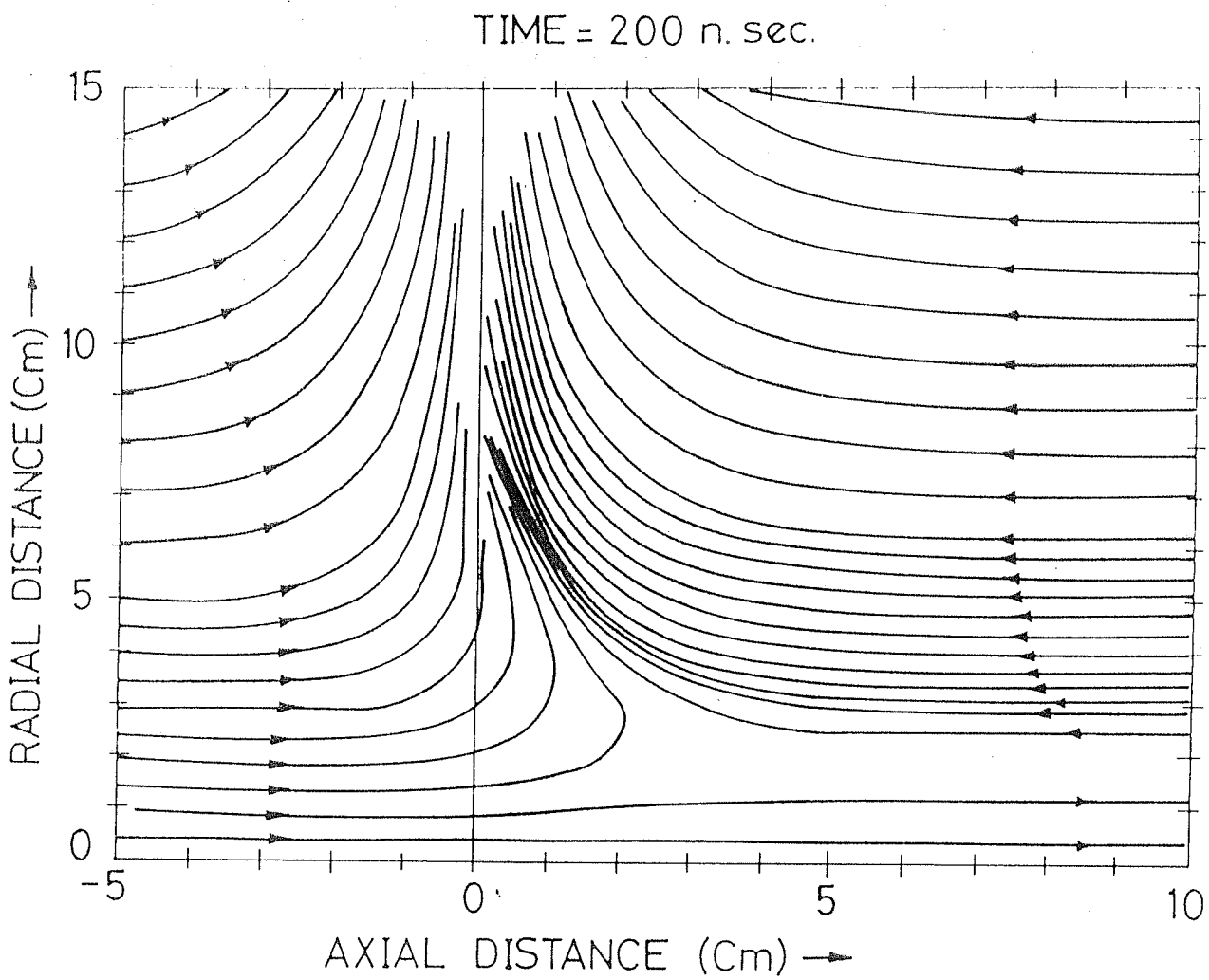

4.13 Constant flux plot.

upto 500 nsec. The beam diamagnetism is more in the region after z = 0 (the cusp plane of the external field) compared to that in the precusp region, because of the additional conversion of axial velocity to azimuthal velocity by the cusp magnetic field. This causes the cusp to shift towards the region after z = 0. The maximum shift of about 1 cm was seen around 600 nsec. Also here the beam diamagnetic field is greater than the external field reversing the direction of the net field within the beam forming field reversed configuration. It consists of antiparallel field lines with a neutral region in between. The field lines on either sides of the neutral region having the same flux value merge at the shifted cusp plane to form closed field line structure as seen in figure 4.13(c). Above 600 nsec, the diamagnetic field decreases and the cusp relaxes back to the initial state.

For the lower energy beam (40 KeV at 200 nsec), the field mapping done for an external field of 100 gauss (figure 4.13) showed the cusp to be drastically modified. At about 200 nsec, corresponding to the peak of the self fields, the net field lines were seen to be more or less axial for $r < 1$ cm. The cusp plane was seen to be shifted by about 3 cm. The ratio of the axial beam self field to the external field measured as a function of the external field (B_o) was found to decrease with increase in B_o (discussed later). So this corresponds to a reduction in the modification of the external magnetic field configuration, with increase in B_o.

The deviation of the beam dynamics from the single

particle picture due to the modification of the external cusp field configuration can be qualitatively understood by first looking at the single particle description. Based on single particle description, Rhee and Destler (1974) have given a critical value of external magnetic field for cusp cut off as $B_o^{cr} = m_o \gamma v_o / e r_c$, r_c = cathode radius, v_o = total beam velocity. So here, for a given beam energy (given value of v_o), when the value of B_o is increased above B_o^{cr}, the electrons get reflected back from the cusp. For a beam with part of its velocity in the transverse direction, Kapetanakos (1974) has shown that the expression for B_o^{cr} gets modified as, $B_o^{cr} = m_o \gamma ((v_o^2 + v_{\theta o}^2)^{1/2} + v_{\theta o})/e r_c$, for a cusp with the uniform field value positive on the precusp and negative on the postcusp side, with respect to the z axis. ($v_{\theta o}$ = initial beam velocity in the azimuthal direction). So far a precusp electron with negative $v_{\theta o}$ (axis non encircling) the value of B_o^{cr} decreases. But for an axis encircling electron, with positive $v_{\theta o}$, the value of B_o^{cr} increases. So for a given value of external field, the refelcted electrons will consist of mostly axis non encricling electrons of the precusp.

The effect of self fields can now be examined qualitatively. Beam axial diamagnetic field will produce a decrease in the net axial magnetic field resulting in a decrease in the number of electrons reflected. For the low energy beam (40 KeV at 200 nsec) at B_o = 100 gauss, electrons in the region R < 1 cm will not suffer reflection, the net field lines in this region being more or less axial.

But with increase in the value of B_o, giving a reduction in the beam self field, more and more axis non encircling electrons will get reflected around z=0. This will have consequence on the diamagnetic field in the postcusp region and will be discussed along with the experimental results - measurement of postcusp beam diamagnetism vs. external field.

The effect of self magnetic fields on the cusp loss was obtained by measuring the radial loss at the cusp using a Faraday cup of 3 cm diameter mounted with centre at r=7 cm and z=0. Measurements were done as a function of the external magnetic field, varied upto 600 gauss. Typical oscilloscope trace is shown in figure 4.14.There is a D.C. shift of the zero level corresponding to the external magnetic field signal (constant over the time scale) added on to the Faraday cup signal.It was seen that the current pulse shows a sharp rise in the first 50 nsec, then decreases nearly to half the initial peak and then rises slowly in about 400 nsec.In the first 50 nsec,the beam is not fully charge neutralised as has been seen in earlier measurement (Chapter 3).So the initial sharp rise is due to the effect of the self electric fields. High frequency oscillations of period less than 50 nsec were also seen between 200 nsec and 400 nsec.The total duration of the signal was about 800 nsec and is consistent with the beam duration (time in which the beam energy is below 20 KeV,the cutoff for the 6 μm aluminium foil anode).

The magnitude of the Faraday cup signal measured as a

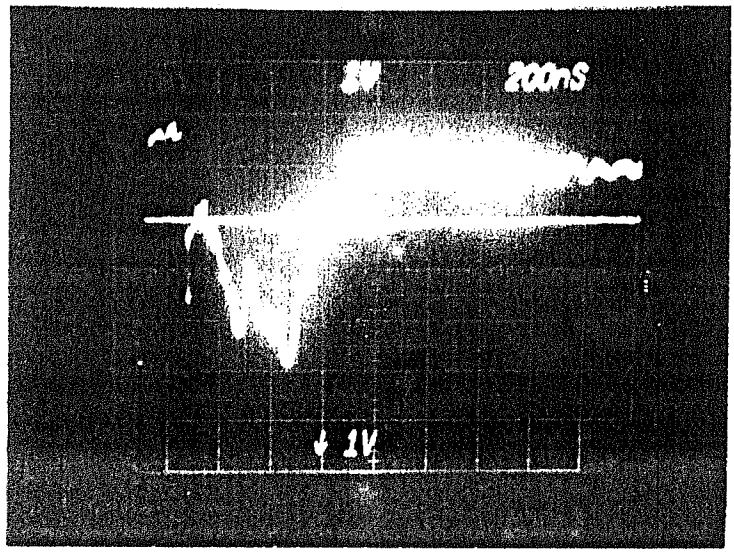

4.14 Oscilloscope trace of the Faraday cup signal.

function of the external field was seen to reach a constant value at around 600 gauss. The maximum value of the cup output normalised with respect to the value at 600 gauss is plotted in figure 4.15. The fraction of electrons getting lost radially at the cusp (-3cm < z < 3cm) as a function of B_o, normalised with respect to the value at 600 gauss, based on single particle description (numerical calculation) is also plotted in the figure. The experimental points were seen to occur more or less on the curve based on single particle description for values of external field above 200 gauss. Below 200 gauss, the single particle description gave larger loss increasing with decrease in B_o. This is because fields below 145 gauss is insufficient to provide radial confinement to the 100 KeV electrons. The experimentally observed cusp loss below 200 gauss was less compared to that given by single particle description. This comes as a result of additional confinement by the beam B_θ field. The maximum B_θ field is about 100 gauss (for a beam current of 3 KA) and its effect will be more dominant at lower values of B_o.

The axial profile of the cusp loss for an external field of 300 gauss was obtained using miniature Faraday cup array mounted at r = 7cm and is plotted in figure 4.16. The profile obtained numerically with the self fields included is also plotted in the figure. The cusp loss was seen to be extended over an axial distance of 5 cm on either sides of the external cusp plane (z=0). The peak value of the loss was seen to occur around 1 cm.

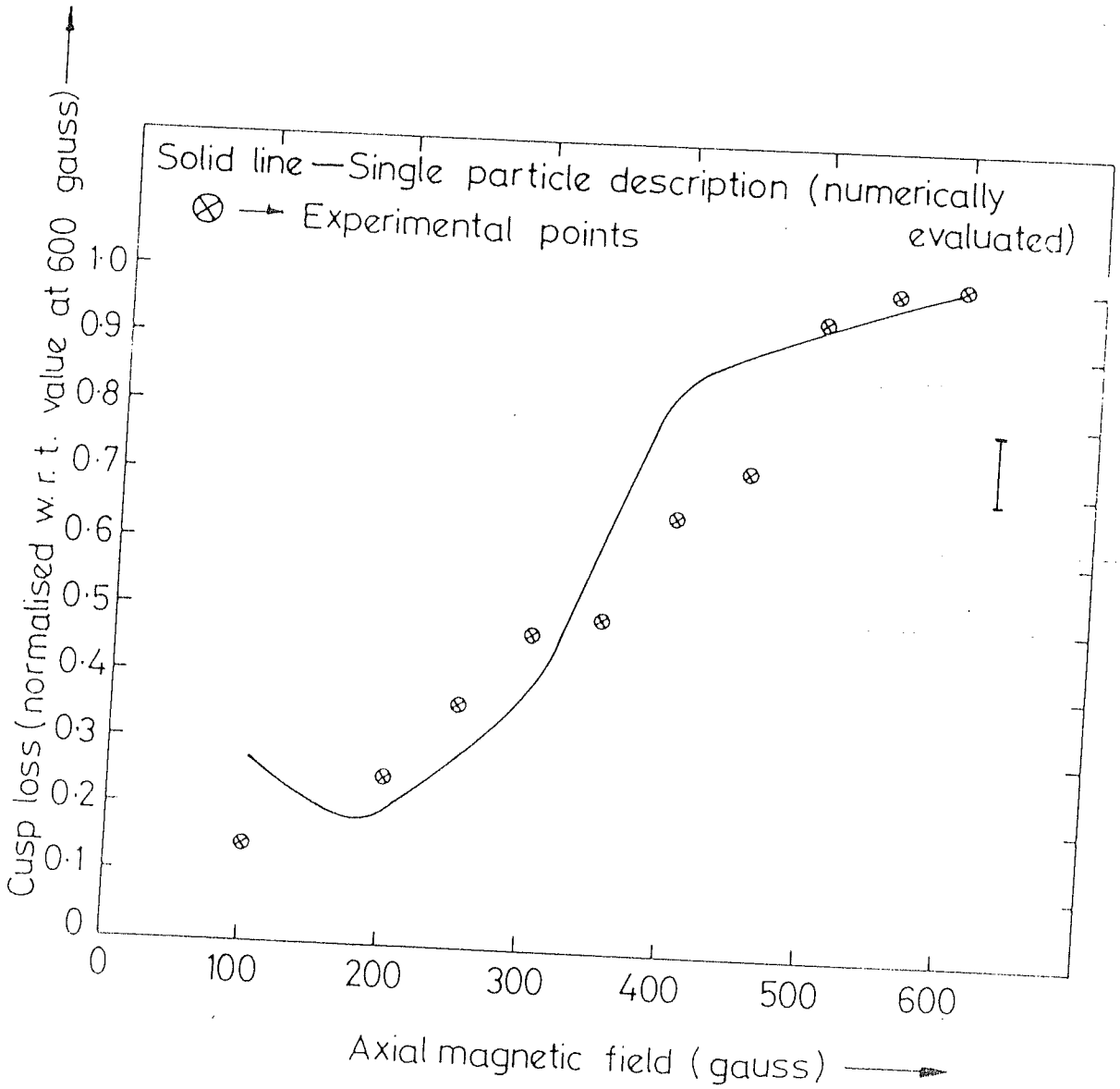

4.15 Variation of cusp loss with external magnetic field.

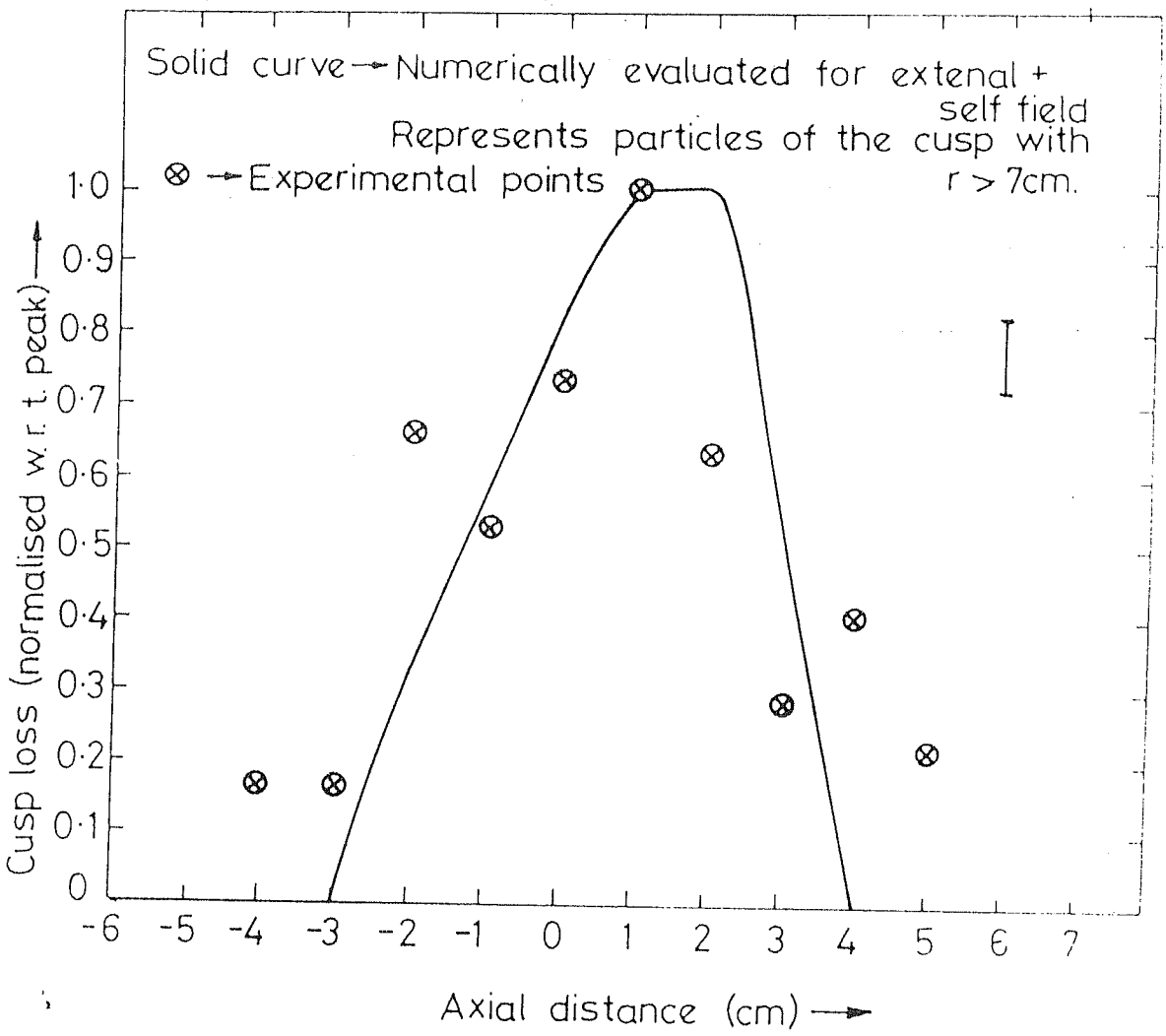

4.16 Axial profile of the cusp loss.

The electrons having a velocity below the critical velocity for cusp cut off will get reflected from the cusp. Out of these reflected electrons, those having large transverse velocity, such that the corresponding Larmor radius is greater than or of the order of the wall radius, will get lost from the system. The Larmor radius of the reflected electrons will increase as the cusp plane is approached. So the maximum cusp loss will occur at the cusp plane. Self fields were seen to shift the cusp plane by about 1 cm.The observed axial position of 1 cm for the peak cusp loss thus corresponds to the shift in the cusp plane.

Measurement of the net beam current transmitted through the cusp as a function of the net beam current in the precusp region was done using Rogowskii coils positioned at about 5 cm. on either sides of the cusp. When these measurements were done, the annular opening in the cusp region was about 5 cm. diameter.(The annular opening in the cusp region was about 14 cm. diameter for the other measurements). The results are shown in figure 4.17.It was seen that the net beam current after the cusp (I_z) increases more or less linearly with that before the cusp (I_o) for I_o upto about 2.5 KA.For I_o above 2.5 KA,I_z was seen to have a steady value of about 1.5 KA.

The cusp opening of about 5 cm. diameter is larger compared to the initial beam diameter of 4 cm.Because of the transverse energy due to scattering at the anode foil, some of the electrons will hit the cusp wall (annular mild steel disc) and get lost from the system.Self magnetic

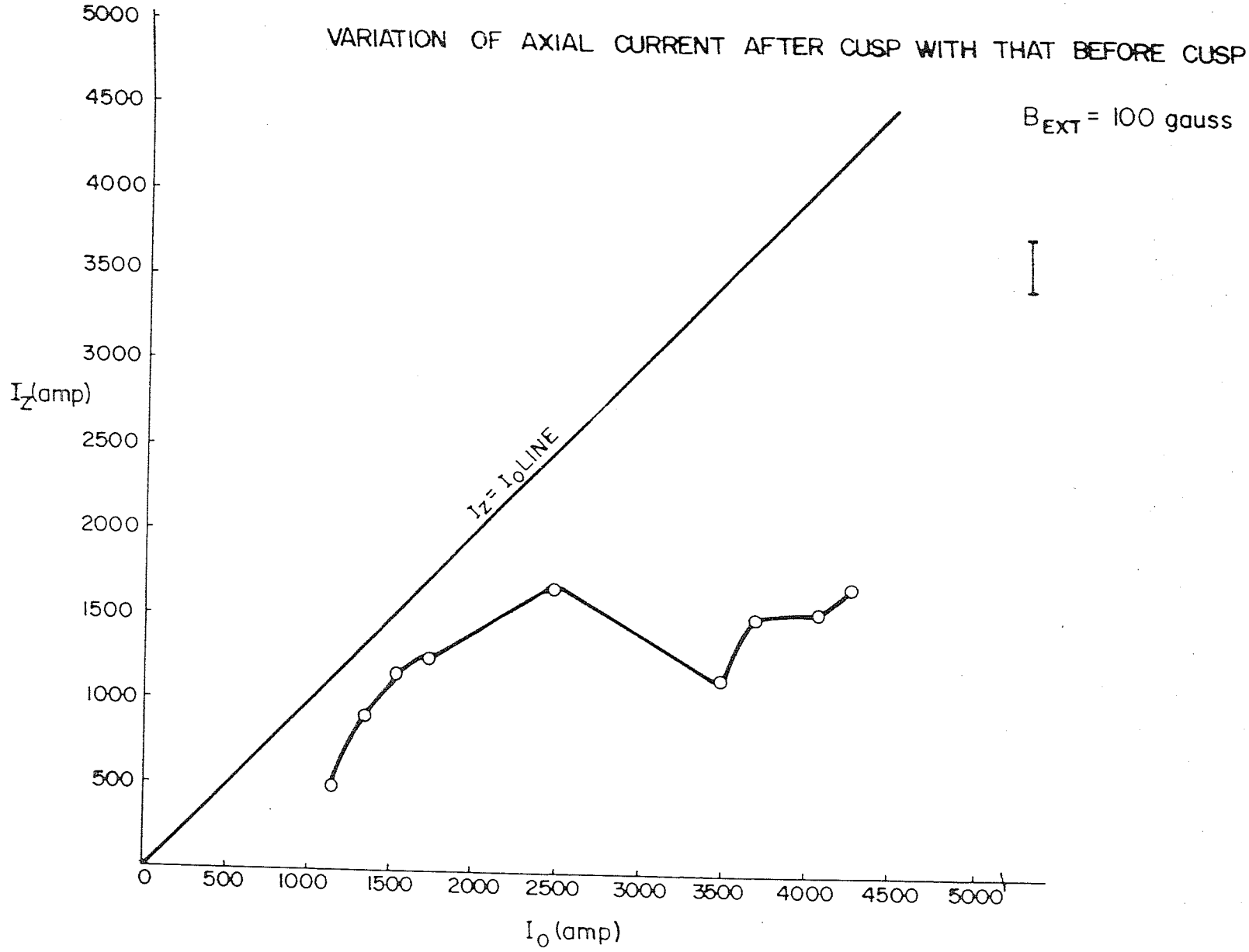

4.17 Variation of axial current after cusp with that before cusp.

fields have been seen to provide additional confinement in the cusp loss measurements. But for higher beam current corresponding to higher B_ϕ field, The radius of gyration (in the r-z plane) about the B_ϕ field decreases. The radius of gyration becomes about 3 cm., comparable to the axial width of the annular mild steel disc at the cusp, for a beam current of about 2.5 KA and for an electron positioned at the average beam radius of about 3 cm. So here an electron of mean beam radius remains within the axial extent of the cusp wall during a Larmor gyration and so is likely to hit the cusp wall. Therefore the observed attenuation of the beam current is essentially due to the smaller aperture of the cusp wall and does not correspond to any physical limiting currents.

Beam diamagnetism in the region after the external cusp plane was measured as a function of external field and beam current using magnetic probe and diamagnetic loop. Measurements were done for the lower energy beam (40 KeV at 200 nsec).

The ratio of axial self magnetic field to the external field ($\Delta B_z/B_o$) is plotted as a function of beam current (I_o) in figure 4.18. The curve based on single particle description is also shown in the figure. In the experiment, the transmitted beam current was varied by using brass grids of varying transmittivity in the path of the beam, just after the anode. The beam current was measured using Rogowski coil placed after the grids. The observed current neutralisation factor, discussed earlier, is less than 15%. So

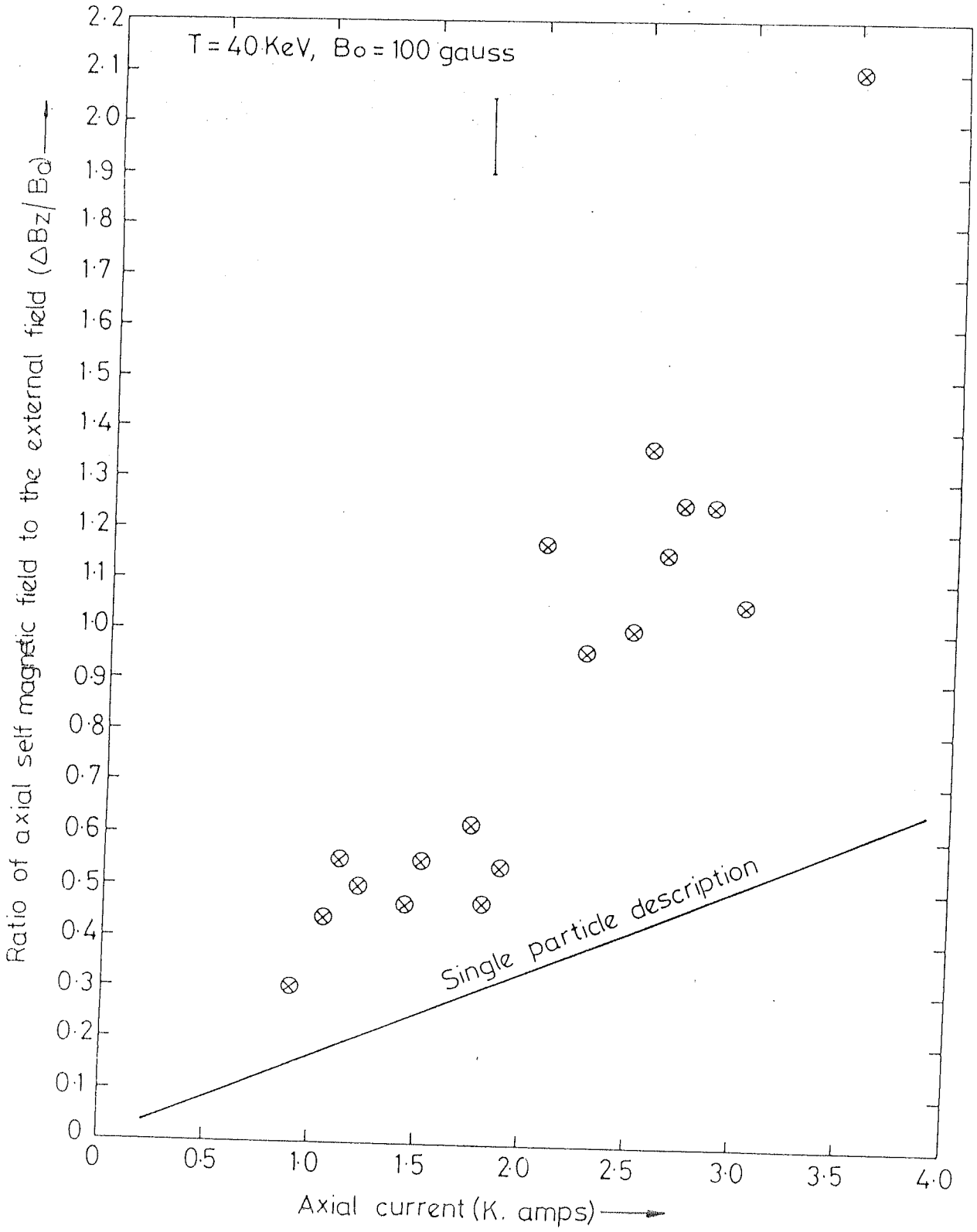

4.18 Variation of postcusp axial self magnetic field with beam current.

the net beam current given by the Rogowski coil is nearly equal to the total beam current. Higher values of I_o, corresponding to higher self fields, were seen to enhance the ratio $\Delta B_z/B_o$ over that given by single particle description.

The variation of $\Delta B_z/B_o$ as a function of B_o is shown in figure 4.19 for two values of I_o. It was seen that the ratio $\Delta B_z/B_o$ peaks at about 100 gauss and decreases thereafter with increase in B_o. The maximum value was about 2 for I_o = 3.5 KA and about 0.5 for I_o = 1.8 KA. Also plotted are the curves, based on single particle description. The deviation of the experimental points from the single particle description for I_o = 3.5 KA was found to be more compared to that for I_o = 1.8 KA, corresponding to the enhancement of ΔB_z due to self magnetic fields. Also the ratio of $\Delta B_z/B_o$ for I_o = 3.5 KA to that for I_o = 1.8 KA was found to decrease with increase in B_o. This shows the self magnetic field effect to be more dominant at lower values of B_o.

It can be seen that the beam looses part of its energy in setting up the self magnetic fields. This causes an additional slowing down of the beam as given by the power balance equation given by (Sethian et al, 1980),

$$E\ I \simeq 1/2\ L\ I^2\ \bar{v}_z + E'\ I$$

E, E′ = initial and final average energy of an electron. I = beam current, $\bar{v}_z$ = beam average axial velocity. L = inductance and is given by,

$$1/2\ LI^2 = \int_o^{r_w} (\Delta B_z^{\,2} + B_\theta^{\,2})/(2\mu_o).2\pi\, r\, dr$$

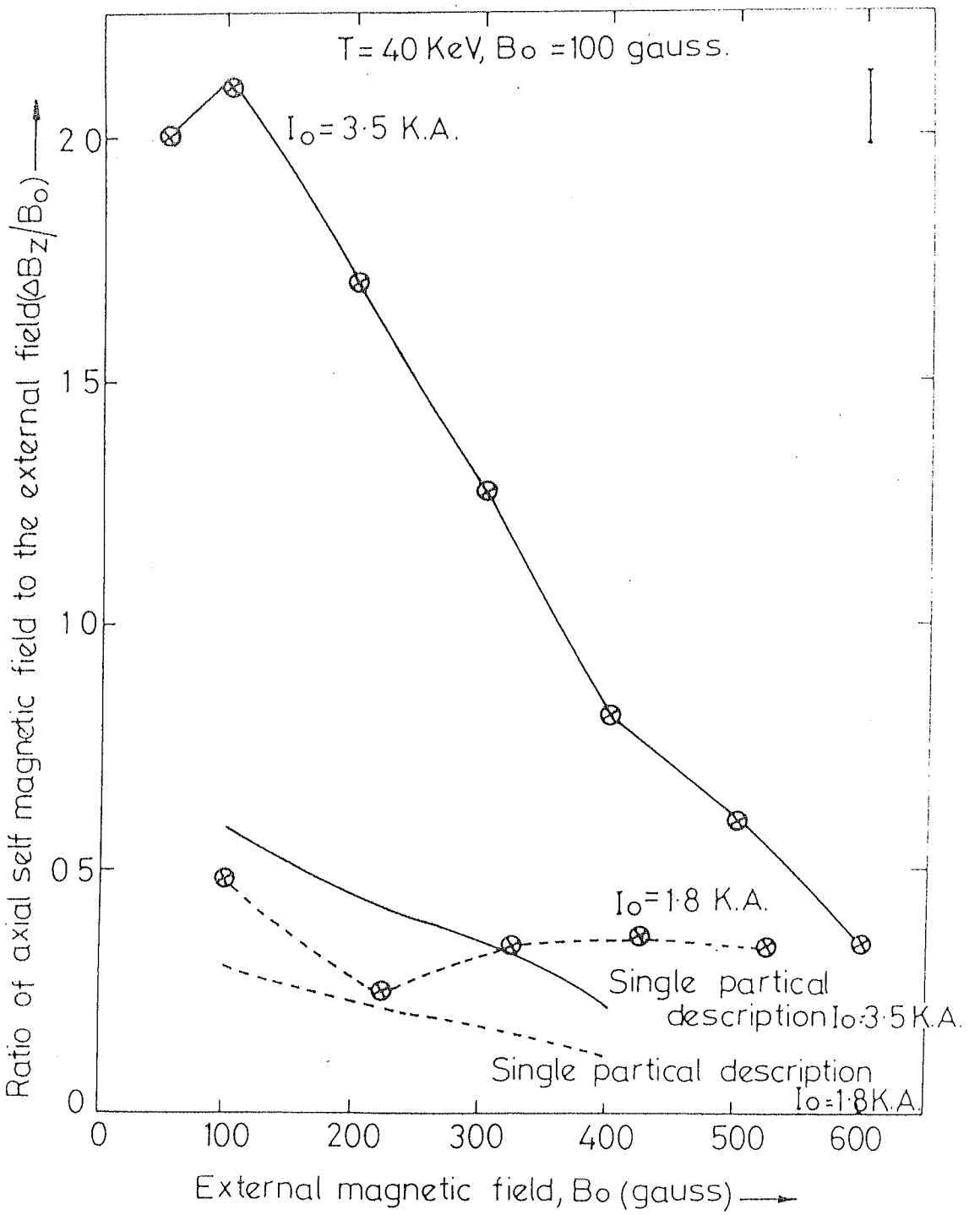

4.19 Variation of postcusp axial self magnetic field with external magnetic field.

A lower beam axial velocity would result in a higher beam axial self magnetic field, which is given by, $\Delta B_z \simeq \mu_0 I \bar{v}_\theta / (\pi r_o \bar{v}_z)$ for an infinitely long solid beam. r_o = beam radius and $\bar{v}_\theta$ = average beam azimuthal velocity. The average beam axial velocity has been measured by the time of flight measurement using beam probes.This gave $\bar{v}_z \simeq 5 \times 10^7$ m sec^{-1} for B_o = 100 gauss and for a beam current of about 3 KA.The beam axial velocity corresponding to 40 KeV (beam energy at 200 nsec for the beam of 350 nsec duration) is about 1.12×10^8 m sec^{-1}. So the enhancement factor for ΔB_z due to slowing down of the beam is about 2.24.The measured enhancement factor for ΔB_z was about 3.5. So the contribution from the slowing down of the beam is inadequate to explain the observed enhancement factor.Other factors that can lead to an enhancement are given below.

Higher values of I_o,corresponding to higher self fields has the following consequences -

(1) reduction of the cusp field by the beam diamagnetic field causes an enhancement in the number of electrons transmitted through the cusp. Essentially number of electrons with initial v_θ negative (axis non encircling) getting transmitted increases. The value of v_θ (from conservation of canonical angular momentum) in the region after the cusp is given by,

$$v_{\theta f} = v_{\theta i} r_c / r - e(B_{zi} r_c^2 + B_{zf} r^2)/(2 m_o \gamma r)$$

$v_{\theta i}$, $v_{\theta f}$ = values of v_θ in the precusp and postcusp regions respectively. B_{zi}, B_{zf} refers to precusp and postcusp axial magnetic fields respectively. r_c = cathode radius (initial

beam radius). A reduction in the value of the cusp fields would have resulted in a reduction in the value of $v_{\theta f}$, if $v_{\theta i}$ was zero and this would have resulted in a lesser diamagnetic contribution by the electrons seeing the modified cusp. Now, with decrease in the cusp field, since electrons with higher negative $v_{\theta i}$ get transmitted, the average value of $v_{\theta f}$ will more or less remain constant. But since the number of electrons transmitted increases, this will lead to an enhancement in the beam diamagnetic field. This will happen only if there exist electrons with large negative $v_{\theta i}$ such that

$$v_{\theta i}\, r_c/r + eB_o(r_c^2 + r^2)/(2m_o \gamma r) \gtrsim v_o$$

(2) In the postcusp region, higher beam axial diamagnetic field produces an increase in the number of axis encircling electrons. This will lead to an enhancement in the beam axial diamagnetic field. Also the B_θ field causes an effective reduction in the Larmor radius. This will lead to an enhancement in the beam diamagnetic field for the axis encircling electrons.

The observed reduction in the diamagnetic signal with increase in B_o can be related to the following reason. As discussed earlier, with increase in the value of B_o, the extent of modification of the cusp decreases. So essentially, the number of electrons with initial v_θ negative getting transmitted will decrease with increase in B_o, leading to the observed reduction in the diamagnetic signal.

4.6. Comparison with Other Experiments

The first experimental study on the dynamics of charged particles in a cusp field has been made by Sinnis and Schmidt (1963). The study has been extended to relativistic electron and ion beams by others [Rhee and Destler,1974; Destler et al, 1975; Golden et al,1981].The experiments of Sinnis and Schmidt involved the use of low current non relativistic electron beam.Their experiments confirmed the single particle theory regarding the conversion of axial velocity to azimuthal by the cusp,the critical field for cusp cut off etc.In the relativistic extension made by Rhee and Destler, the self magnetic fields were only 10% of the applied fields and their results were in reasonable agreement with the results predicted based on single particle description. Measurement of beam width as a function of external field made by Destler et al showed good agreement only for the case where self fields were small compared to the external field.Explanation for the deviation has not been given.The observed enhancement in the beam width for the case where self fields were comparable to external field can be attributed to the reduction in the net field by the beam self fields.The experiment of Golden et al was on the dynamics of a rotating proton layer.The diamagnetic self field was found to increase with decrease in the electrode angle, corresponding to a decrease in the applied radial electric field. With lower value of applied radial electric field,the

protons move closer to the axis caused by the net pinching force due to the self fields. The enhancement in the diamagnetism here has been attributed to the reduction in the radius of the azimuthal current distribution as the protons move inward with the azimuthal current remaining the same. But it can also be seen that with decrease in the applied radial electric field, for a given value of self fields, the number of axis encircling protons increase. So as per the calculation given in section 4, this would essentially lead to an increase in the diamagnetic self field. In the numerical simulation done by Golden et al, the self fields were seen to produce a somersaulting, i.e., protons at the head of the beam are decelerated and protons at the tail are accelerated, resulting in a spreading of the distribution of particle energy. But this will not be seen for a long pulse beam, where rise time of the self fields is much longer than the beam transit time.

In the experiments of Kapetanakos (1974), filamentation instability has been seen to occur for a beam, not satisfying the stability criterion $\omega_{pb}^2 \beta^2 / \omega_{cb}^2 < 1$, injected into a preformed plasma with plasma density much more than the beam density. ω_{pb} = beam plasma frequency, ω_{cb} = beam cyclotron frequency and β = beam velocity/c. The beam for this case has been seen to be almost completely current neutralised from the magnetic probe signals. But for beam injected into neutral gas of several hundred mTorr pressure, filamentation was not seen to occur. In our case also, filamentation was not seen for the rotating beam injected

into neutral gas of about 225 mTorr.This is consistent with the calculation of Davidson et al (1975),already discussed earlier, where they have shown the stabilising effect of self magnetic field on filamentation instability.

There have not been many experiments,where the beam axial self magnetic field has been measured using magnetic probes, for a straight beam with partial energy in the transverse direction,resulting from scattering by the anode foil and/or plasma background. In the experiments of Dove et al (1976), the self magnetic field was seen to be diamagnetic within the beam and paramagnetic elsewhere.The beam self magnetic field along the beam axis was not measured. As per the calculations given in section 4,a paramagnetic field is expected along the beam axis for a higher energy beam and a higher external magnetic field.In the present experiment using low energy beam, an axial diamagnetism was seen consistent with the calculations given in section 4.

Measurements reported in this chapter, regarding the magnetic field lines in the cusp region using magnetic probes, show the extent of modification of the external cusp by the beam self fields. The observed pushing out of the cusp field lines by the beam self fields has close resemblance to the model given by Sethian et al (1980),for beam injected into a half cusp field.As per their model,the electrons on reaching the cusp are made to rotate by the radial field of the cusp,and the beam motion gets retarded by the need to supply the self field energy.Fresh electrons

are reflected by the radial field B_r at the beam front, transferring a small fraction of their energy to the induced field, and the cusp gets pushed out axially.These reflected electrons on reaching the diode get reflected back without loss of energy and return to the beam front. Thus the beam consists of reflexing electrons with the cusp moving outward with the arrival of the new bunch of electrons. The beam front velocity has been reported to be reduced by a factor of 10.Cusp distortion was also seen in the computer simulation of the NRL ion ring experiment [Golden et al,1981].

The existing measurements on cusp loss relate to the transmitted beam current and/or beam total energy [Friedman, 1970; Kapetanakos, 1974]. Friedman observed a drop in the transmitted beam energy for external field exceeding the critical field for cusp cut off. In the experiment of Kapetanakos, the maximum beam current and beam energy transmitted through the cusp was found to decrease when the magnetic field was exceeded above a value much below the critical field predicted for beams with initial velocity $v_\theta = 0$. This has been attributed to part of the beam energy in the azimuthal direction before entering the cusp.Direct measurement of the radial loss at the cusp and the axial profile of the cusp loss, done in the present study,show that the peak cusp loss was seen to take place along the shifted cusp plane. The beam B_θ field was found to provide additional confinement to the electrons in the cusp region for self fields comparable to the external field.

In the context of formation of field reversed configuration, in the experiment of Roberson et al [Roberson et al, 1978], the beam diamagnetic field has been seen to be greater than that predicted by the single particle description by a factor of 2.This has been attributed to a breaking of the beam and an increase in I_ϕ due to a pile up of the beam after the cusp.But they do not have any direct evidence for the same. In the results reported in this chapter also, the beam diamagnetic field was seen to be greater than that predicted, when the self fields were comparable to the external field.Higher self fields have been shown to cause deviation from the single particle description. Also in the experiments of Roberson et al,the fraction of the beam passing through the cusp was seen to decrease with increase in external field,measurement done for external field greater than 1 K gauss.This was seen to keep the beam self field independent of external field.The critical field for cusp cut off for their case is about 600 gauss. So the existence of field reversal for fields even above the critical field for cusp cut off can be due to the improved cusp transmission because of the self fields, demonstrated in this chapter.

CHAPTER V

CONCLUSIONS AND SCOPE FOR FURTHER STUDIES

Experimental studies on the effect of self fields on the propagation of relativistic electron beams have been carried out. A long pulse rotating relativistic electron beam, of current rise time much longer than the charge neutralisation time, injected through neutral gas has been used for the study. A cusp magnetic field was used for producing the rotating beam. Two distinct phases are investigated.

1. Charge neutralisaton phase,where the beam ionises the neutral gas and is being charge neutralised. Beam current rise time being long compared to the charge neutralisation time,the self magnetic field is smaller compared to external field in this phase.So this phase involves the effect of self electric fields on beam propagation and dynamics.

2. The phase when the beam self magnetic fields have peaked. Here, the beam is charge neutralised and so the beam dynamics is under the influence of the self magnetic fields.

Various diagnostics - wall probes for beam potential, voltage divider for beam energy,Rogowskii coils for beam

current, Faraday cups for beam current density and radial loss, magnetic probes and diamagnetic loops for self fields were used in the present study. Numerical trajectory calculations for the beam and plasma electrons, using simple models based on measurements, were also done. These gave useful information regarding plasma electron escape time (an useful parameter in the context of charge neutralisation process), beam dynamics with and without the self fields present, etc.

5.1 Conclusions

The conclusions drawn from the present investigation are given in the following subsections.

5.1.1 Beam characteristics and equilibrium:

The beam propagating through neutral gas has been seen to be more or less azimuthally symmetric. The beam has been shown to be stable against the microscopic instabilities like diocotron and filamentation.

The self fields have been shown to influence the equilibrium for the rotating relativistic electron beam. A charge neutralisation factor, $f_e > 1-(v_z/c)^2 - \omega_c^2/2\,\omega_p^2$ has been found essential for equilibrium, where ω_c is the beam cyclotron frequency, ω_p is the beam plasma frequency and v_z is the beam axial velocity. The value of f_e has been estimated from a measurement of the beam potential.

Beam electrons before approaching the cusp (in the precusp region), were seen to consist of two categories (1)

Axis encircling giving an axial diamagnetism,and (2) Axis non encircling giving an axial paramagnetism.A net axial diamagnetism was observed in the present study. The diamagnetism was seen to be influenced by the beam self fields. The beam electrons that are injected after the beam self fields have peaked, contribute a higher diamagnetism than that expected from single particle description due to an enhancement in the number of axis encircling electrons.

5.1.2 Effect of self fields on the charge neutralisation processes

Charge neutralisation of the beam,which involves the expulsion of plasma electrons,is influenced by the external axial magnetic field.A critical magnetic field was observed, fields above which, provide magnetic insulation for the plasma electrons against radial loss.Charge neutralisation factor was seen to decrease with increase in external field till the critical field value.

For fields above the critical field for magnetic insulation, plasma electrons were seen to escape to the axial walls. The motion is directed away from the central region of the system,where the beam potential was observed to be minimum. Inductive axial electric field was seen to cause electron avalanche to set in. Electron avalanche increases the rate of production of plasma electrons and for a given plasma electron escape time to the walls,causes an enhancement in the charge neutralisation factor.The beam potential structure was seen to develop axial asymmetry with increase in time. In the region between the central

part of the system and the far end wall,avalanche process was enhanced by the inductive electric field,causing faster charge neutralisation in that region.

Higher background gas pressure was seen to provide faster charge neutralisation.The charge neutralisation time has been observed to decrease inversely proportional to pressure. The beam potential was seen to be oscillatory in time.

5.1.3 Cusp field modification by the beam:

The external cusp magnetic field was seen to be drastically modified by the beam self fields. The diamagnetism in the post cusp region produced by the rotating beam was seen to shift the cusp plane towards the post cusp side. The self fields produced by the beam are sustained by the plasma return currents.The presence of azimuthal plasma current in the precusp region was not seen in the diamagnetic signals.

5.1.4 Radial cusp loss:

The peak of the radial loss of beam electrons in the cusp region was seen to occur along the shifted cusp plane. The loss falls off to zero over a distance of the order of the cusp width.

The total radial loss in the cusp region was less compared to that given by single particle description,when the self fields were comparable to the external field.Self magnetic fields were seen to provide confinement against radial loss in the cusp region.The cusp loss was seen to increase with external field, saturating as the critical

field for cusp cut off is approached.

5.1.5 Post cusp field modification by the self magnetic fields:

The diamagnetic field produced by the rotating beam in the post cusp region was seen to deviate from the single particle value for beam self fields comparable to the external field. A maximum enhancement factor of about 3.5 was observed for the post cusp diamagnetic field. The enhancement factor for the diamagnetic field was seen to decrease with increase in the external field. The beam looses energy in setting up the self magnetic fields.This causes a reduction in the average beam velocity.A peak reduction by a factor of about 2 was observed in the present study, contributing to a part of the observed diamagnetic field enhancement. From the calculations done, the postcusp diamagnetism was found to depend on the ratio of the axis encircling electrons to the axis non encircling ones transmitted through the cusp.In the present study,this was seen to result in an enhancement.

5.2 Scope for Further Studies

The experimental results of the present investigation provides the basis to carry out further detailed experimental and theoretical work, in order to acquire a more complete and thorough understanding of the effect of self fields on the propagation and dynamics of relativistic electrons beams. The research work needed to be carried out

in the future are given below.

In the present study, an oscillatory behaviour in the beam potential was observed. These oscillations may be of importance in the context of collective ion acceleration, whereby ions trapped in the potential well get accelerated as it propagates.Exact cause of these oscillations couldn't be identified in the present study.Detail experiments need to be carried out to investigate this phenomenon, to ascertain the cause of the oscillatory behaviour.

An enhancement of beam diamagnetism produced by the rotating beam over that given by single particle description has been seen in the present study. The contribution coming from slowing down of the beam, in setting up the self magnetic fields, was found to be inadequate to explain the observed enhancement in diamagnetism. The diamagnetism has also been shown to depend on the particle orbits in the precusp region.But due to lack of proper time resolved diagnostics, a measurement regarding the particle orbits couldn't be carried out in the present study.A detail study need to be carried out in this direction to identify the causes leading to the enhancement in the diamagnetism.

The present numerical calculations were based on simple models. These were carried out to get useful information without having to spend too much of computer time. A detailed self consistent numerical calculation will be helpful in making a proper comparison of theory and experiment, especially in the context of enhancement of beam

generated diamagnetic field after it traverses through the cusp plane.

REFERENCES

1. Alfven H.,1939,Phys. Rev. 55,425.

2. Alston L.L. - ed., High Voltage Technology (Oxford University Press,1968),p.24.

3. Andrews M.L., Daviation H.,Fleischmann H.H.,Kusse B., Kribel R.E. and Nation J.A.,1971(a),Phys. Rev. Lett. 27,1482.

4. Andrews M.L.,Davitian H.,Fleischmann H.H.,Nation J.A., 1971(b),Phys. Fluids,14,2553

5. Arutyunyan S.G., Bogdankevich O.V., Bondar Iu.F., Zavarotni S.I., Ipatov A.Z.,Mcheidze G.P.,Ovchinnikov A.A. and Rukhadze A.A.,1983,Plasma Phys. 25,11.

6. Birkhoff R.D.,1958,Handbuch der Physik bd 34,p. 5388.

7. Bogdankevich L.S. and Rukhadze A.A.,1971,Sov. Phys. - Usp. 14,163.

8. Bora D. and John P.I., 1981,IEEE Trans. Plasma Sci. PS-9,80.

9. Briggs, R.J., Hester R.E., Law E.J., Lee E.P. and Spoerlein R.L.,1976,Phys. Fluids,19,1007.

10. Bruining H., Physics and Applications of Secondary Electron Emission (Pergamon,London,1954),p.47.

11. Buneman O., Levy R.H. and Linson L.M.,1966,J. Appl. Phys.,37,3203

12. Chen H.C.,1984,J. Appl. Phys.,56,101

13. Christofilos N.C.,1958,Proc. Second U.N. Int. Conf. on the Peaceful Uses of Atomic Energy (U.N.,Geneva) 32, 279.

14. Christofilos N.C.,1969,Phys. Rev. Lett. 22,830.

15. Cooperstein G. and Condon J.J.,1975,J. Appl. Phys.,46, 1535

16. Creedon J., Spence P. and Huff R.,1973,Bull. Am. Phys. Soc.,18,1310.

17. Davidson R.C.,Hui B.H. and Kapetanakos C.A.,1975,Phys. fluids,18,1040.

18. Davidson R.C. and Lebedev A.N.,1975,Physica Scripta,11, 330.

19. Davidson R.C. and Mahajan S.M.,1974,Phys. Fluids,17, 2090.

20. Destler W.W., Misra P.K. and Rhee M.J.,1975(a),Phys. fluids,18,1820.

21. Destler W.W., Hudgings D.W., Kehs R.A.,Misra P.K. and Rhee M.J.,1975(b),IEEE Trans. Nucl. Sci.,NS-22,995.

22. Destler W.W. and Rhee M.J.,1977,Phys. Fluids 13,182.

23. Dove W.F.,Gerber K.A. and Hammer D.A.,1976,Appl. Phys. Lett.,28,173.

24. Friedman M.,1970,Phys. Rev. Lett.,24,1098.

25. Friedman M. and Ury M.,1972,Rev. Sci. Instruments,43, 1659.

26. Genuario R. and Bromborsky A.,1974,IEEE Trans. Nucl. Sci.,NS-21,253.

27. Girgorev V.P.,Patashev A.G. and Shulaev N.S.,1979,Sov. J. Plasma Phys.,5,211.

28. Girgorev V.P.,Koryakin A.I. and Potashev A.G.,984,Sov. J. Plasma Phys.,10,454.

29. Godfrey B.B.,1977,IEEE Trans. Plasma Sci. PS-5,223.

30. Godfrey B.B.,1979,IEEE Trans. Plasma Sci. PS-7,53.

31. Golden J., Pasour J.A., Kapetanakos C.A., 1981,Naval Research Laboratory Memorandum Report 4699.

32. Graybill S.E.,1971,IEEE Trans. Nucl. Sci.,NS-18,438.

33. Jain K.K. and John P.I., 1981, Proc. of the Indian Academy of Sciences (Engg. Sci.),4,75.

34. Jain K.K. and John P.I.,1984,Pramana,23,1.

35. Kapetanakos C.A.,1974,Appl. Phys. Lett.,24,112.

36. Kapetanakos C.A., Hammer D.A., Striffer C.D. and Davidson R.C.,1973,Phys. Rev. Lett. 30,1303.

37. Kingsep S.S., Novobrantsev I.V., Rudakov L.I.,Smirnov V.P. and Spector A.M.,1973,Soviet Phys. JETP 36,1125.

38. Kirstein P.T., Kino G.S. and Waters W.E.,Space Charge Flow (McGraw Hill,New York,1967)

39. Kouichi Ono,1979,Jap. Journal Appl. Phys.,18,2263.

40. Lasslet L.J. and Sessler A.M.,1969,IEEE Trans. Nucl. Sci.,NS-16,1034.

41. McArthur D.A. and Poukey J.W.,1973,Phys. fluids,16, 1996.

42. Mikhailovskii A.B., Theory of Plasma Instabilities, (Consultants Bureau,New York,1974),Vol.I.

43. Miller P.A. and Gerado J.B.,1972,J. Appl. Phys.,43, 3008.

44. Miller P.A., Gerado J.B. and Poukey J.W.,1972,J. Appl. Phys.,43,3001.

45. Miller R.B., An Introduction to the Physics of Intense Charge Particle Beams,(Plenum Press,1982),p.24.

46. Olson C.L.,1975,Phys. Rev. A11,288.

47. Parker R.K., Anderson R.E. and Duncan C.V.,1974,J. Appl. Phys. 45,2463.

48. Poukey J.W. and Freeman J.R., 1974,Phys. Fluids,17, 1917.

49. Poukey J.W. and Rostoker N.,1971,Plasma Phys.,13,897.

50. Rieke F.F. and Prepejchal W.,1972,Phys. Rev. A6,1507.

51. Reiser M.P. (1971),IEEE Trans. Nucl. Sci. NS-18,460.

52. Rhee M.J. and Destler W.W.,1974,Phys. Fluids,17,1574.

53. Roberson C.W., Eckhouse S.,Fischer A.,Robertson R. and Rostoker N.,1976,Phys. Rev. Lett. 36,1457.

54. Roberson C.W., Tzach D. and Rostoker N.,1978,Appl. Phys. Lett.,32,214.

55. Rudakov L.I., Smirnov V.P. and Spector A.M.,1972,JETP Lett.,15,382.

56. Schmidt G.,1962,Phys. Fluids,5,994.

57. Sethian J.d.,Gerber K.A.,Spector D.N. and Robson A.E., 1978,Phys. Rev. Lett.,41,798.

58. Sinnis J. and Schmidt G.,1963,Phys. Fluids,5,841.

59. Sloan M.L. and Dummond W.e.,1973,Phys. Rev. Lett. 31, 1234.

60. Smith J.R., Schneider R.F., Rhee M.J., Uhm H.S. and Namkung W.,1986,J. Appl. Phys.,60,4119.

61. Striffler C.D. and Kim H.,1978,Phys. fluids,21,1428.

62. Suzuki Y. and Kato S.K.,1984,Proc. of Collaborating Research Meeting on Particle Beam Applications to Fusion Research,IPPJ-678,p.200.

63. Swain D.W.,1972,J. Appl. Phys.,43,396.

64. Tuszewski M., Rej D.J. and Fleischmann H.H.,1979,Phys. Rev. Lett.,43,449.

65. Vijaya Sankar M.K. and John P.I., Plasma Phys. and Controlled Fusion (In press).

66. Wachtel J.M. and Safran S.,1974,Phys. Rev. Lett.,32, 95.

67. Wiebel E.S.,1973,Phys. Rev. Lett.,13,1390.

68. Yonas G., Poukey J.W., Prestwich K.R., Freeman J.R., Toepfer A.J. and Clauser M.J.,1974,Nucl. Fusion 14, 731.